HYBRID IMAGING IN CONVENTIONAL NUCLEAR MEDICINE

A TECHNOLOGIST'S GUIDE

Produced with the kind support of

SIEMENS Healthineers

Table of contents

Foreword

Since the introduction of hybrid imaging, nuclear medicine has experienced a great development within its practices and conventional nuclear medicine has benefited greatly from the application of hybrid imaging.

The definition of hybrid being the product of combining two or more different things, it is evident that the purpose of any such combination is to extract the best qualities from them both and minimise their respective limitations. It is thus vitally important that both technologies are profoundly understood, not only in their individual characteristics but also in their combined use. The desired synergies can only be realised if the hybrid application makes optimum use of the respective technologies.

Nuclear medicine technologists interact directly with the patient in the imaging context, and are thus the professionals that bridge the gap between all the background science and engineering and the patient. These professionals are equipped with the skills necessary to use the imaging technology, for which they require a combination of theoretical and practical competencies. With this in mind, this book starts by outlining the basic concepts of physics, reconstruction methods and quality control procedures that allow image formation. This is followed by a discussion of clinical applications of hybrid conventional imaging, with a practical focus to facilitate implementation and develop good practice. The later chapters of the book address the topic of molecular therapy and outline hybrid imaging's contribution to this field.

It is with immense gratitude that I highlight the great contribution made by all the authors who gave their knowledge to this project. Here, special acknowledgment is due to the Physics, Paediatric and Cardiovascular Committees of the EANM, who have supported us throughout as well as furnishing their own contribution.

A special word of appreciation goes to the EANM-TC editorial group, who have dedicated their time to putting this publication together, and also to Angela Parker, for her editing, reviewing and support. Last but not least, I thank the EANM Board and Executive Office for their tireless efforts which have made this series of publications possible.

Hybrid Imaging in Conventional Nuclear Medicine was only possible thanks to the contribution of everyone mentioned before. Thank you all very much!

Andrea Santos
Chair, EANM Technologist Committee

Introduction

After nearly two decades since its first edition, the Technologist's Guide is an established tradition and a valuable product of the nuclear medicine technologists' community. We are all facing unprecedented challenges, both in our profession and in our homes. Seeing this Guide published in these circumstances is a tribute to our great colleagues, friends and our sponsor, who have dedicated time and other resources to ensure the tradition is kept alive.

Every year the Tech Guide, as we all know it, aims to bring together experts from the field and present concise opinion and guidance on a specific topic to support the workforce of technologists working in nuclear medicine. This year the topic is hybrid imaging in conventional nuclear medicine. When choosing the theme for the Tech Guide, the Technologists' Committee had in mind the impact of non-PET hybrid imaging on nuclear medicine practice. Moreover, SPECT-CT and the Tech Guide are of similar age, so we wanted to focus on collating conventional hybrid imaging practice in one concise and up-to-date guidance document.

The Tech Guide is a partnership between EANM committees, between physicians, scientists and technologists, and this year's edition is no different. We partnered with the Physics Committee to cover the technical aspects of the imaging modality, as well as with the Paediatric Committee for their chapter. We wanted to acknowledge the achievements of fellow technologists like Dr Sebastijan Rep, who is not only an ambassador for the technologist's role in quality assurance and quality control, but also a new PhD graduate. Other chapters were co-authored by technologists and physicians or scientists, such as those on myocardial perfusion imaging and the contribution of hybrid imaging to radionuclide therapy.

As ever, the Tech Guide has a practical content, with a focus on hands-on advice for technologists, showing the artefacts and pitfalls when imaging and the role of the technologist in achieving high standards of quality. The Technologists' Committee also plays an important role in defining our communication strategy with patients in nuclear medicine, and we have tried to include this new topic in this year's Tech Guide.

For us in the editorial team, publishing this Guide is a way of saying thank you to the nuclear medicine community for all your passion and dedication to patient care. We wanted to showcase the impact of our profession within the nuclear medicine community, as well as the high standard of quality delivered by technologists across Europe.

We trust that you will find the Tech Guide enjoyable reading, and would like to thank you all for taking part in the success of this project.

Marius Mada, MarieClaire Attard and Agata Pietrzak
Editorial team

1

PHYSICS AND RECONSTRUCTION METHODS FOR SPECT/CT

by Anne Larsson Strömvall

INTRODUCTION

In scintigraphy, the distribution of an administered gamma photon-emitting radiopharmaceutical in vivo is visualised using external detectors. The technique is sensitive and can image very small amounts of the injected radiopharmaceutical in the order of nanograms. Two-dimensional images can be acquired using a stationary detector, while three-dimensional images can be acquired using single-photon emission computed tomography (SPECT). The phrase "single photon" indicates that in SPECT, single photons emitted from the radionuclides are traced to their origin, in contrast to positron emission tomography (PET), where two simultaneous annihilation photons are detected by rings of detectors in a coincidence circuit. In most cases SPECT images are used for visual interpretation, but quantitative analyses are becoming increasingly popular.

SPECT is mostly used for diagnostic purposes but can also be used for planning and monitoring of radionuclide therapies. Radionuclides used for diagnostics are primarily chosen to have characteristics for high-quality imaging and low radiation dose to the patient, including a relatively short half-life. Therapy radionuclides, on the other hand, should provide the target organ or tumours with a high dose, enough to treat the disease, and emit most energy in the form of alpha or beta particles. Image quality is a secondary objective, but SPECT will of course benefit from at least some fraction of gamma photons that can be used for imaging. The most popular radionuclide used for diagnostics is [^{99m}Tc], with a half-life of 6 h and a relatively pure gamma photon emission of 140 keV. The most common radionuclide for therapy is [^{131}I] for treatment of thyroid diseases, with a half-life of 8 days and mostly beta radiation emission. Emitted gamma photons of relatively high energy, 364 keV, can however be used for imaging.

Hybrid imaging has revolutionised nuclear medicine with the addition of the structural component from X-ray computer tomography (CT) to SPECT/CT and PET/CT, or magnetic resonance (MR) imaging to PET/MR. The first commercial integrated SPECT/CT systems became available in the late 1990s, with the release of the Hawkeye (GE Healthcare, WI, USA). In the beginning, this low-dose, low-cost, and relatively slow CT provided 10 mm CT slices. Although somewhat rough, SPECT/CT image fusion then became an option for routine clinical work, as well as CT-based attenuation correction. The Hawkeye was later upgraded to a 4-slice system with 5.0 mm slices, which improved image quality and reduced CT acquisition time by a factor of 2. Nowadays there are several manufacturers providing fully diagnostic integrated CTs that can help to improve nuclear medicine diagnostics and therapy. For more information on the historical development of SPECT and SPECT/CT, a well-written review on the subject (1) can be recommended.

The SPECT/CT gantry consists of a CT bore and typically two gamma camera heads which are mounted on the front side. An example can be seen in Fig. 1.

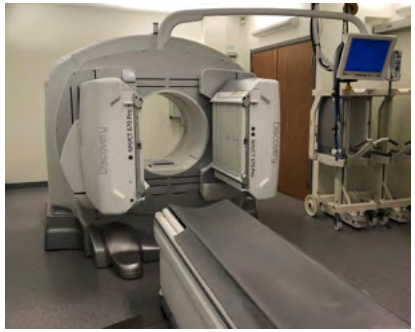

Figure 1: Example of SPECT/CT gantry and table

The position of the detectors can be adjusted to a certain number of fixed positions, for example with the detectors 180 degrees (H-mode, see Fig. 1) or 90 degrees (L-mode) apart. The detectors can usually also be flipped to point outwards from the gantry, or can be arranged side by side if needed. It is possible to select whether both detectors or only one should be used in the imaging protocol. For a high image resolution, it is important that the detectors are positioned as close to the patient as possible. Their position can be automatically adjusted using body contour detectors mounted on the side of the detectors.

The patient table can be adjusted in height for loading and unloading the patient, and to centre the patient in the scanner. Lasers can be used to help centre the patient correctly. Special solutions with cantilevered tables have been developed for a precise SPECT/CT registration in the axial direction, since the two examinations are performed sequentially with different table positions. The table is usually equipped with a low-attenuation top of carbon fibre, with an imaging range in the order of 200 cm to be used for SPECT and whole-body imaging. A soft mattress and straps are used for patient comfort and to prevent movements during the examination. The maximum permissible patient weight varies between scanners, and needs to be borne in mind when examining the heaviest patients.

THE SCINTILLATION CAMERA

The traditional detector used for SPECT imaging is known as a scintillation camera or a gamma camera. It was developed in the late 1950s by Hal Anger (2) and has been a standard imaging device in nuclear medicine for a long time. The major components of the scintillation camera today are in many cases similar to when it was invented, but its performance has of course improved over the years, especially through the introduction of digital electronics and multiple head systems. A schematic diagram of the intersection of a scintillation camera detector can be seen in Fig. 2.

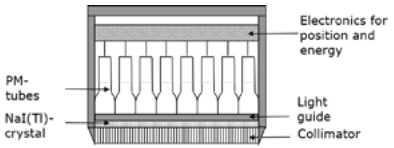

Figure 2: The scintillation camera

The collimator, which can be of different types, is closest to the patient and sets the acceptance angle for detection of the emitted gamma photons. The parallel-hole collimator is the most common type and consists of a lead plate with closely packed parallel holes, usually of hexagonal form like a honeycomb. The lead "walls" between the holes are called septa. The hole diameter, hole length (collimator thickness) and septal thickness depend on the resolution/sensitivity and the photon energy range for which the collimator is optimised. Collimators are crucial for identifying the point of emission. To illustrate this, an image of a point source acquired both with and without the collimator on can be seen in Fig. 3.

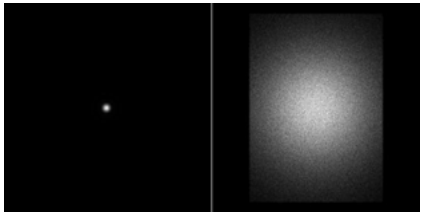

Figure 3: Left-hand side: point source image with collimator. Right-hand side: point source image without collimator.

High-resolution collimators have thinner holes compared to general-purpose or high-sensitivity collimators, and the reduced acceptance angle leads to a smaller number of detected photons per unit of time and activity, i.e. lower sensitivity. Collimators optimised for higher energies, known as medium-energy or high-energy collimators, have thicker septa to prevent septal penetration, which otherwise leads to reduced contrast and star patterns around hotspots in the image.

Another relatively common collimator is the multiple-pinhole collimator. It consists of a series of lead cones with a small hole at the apex, facing the imaged object. With these pinholes, the size of the image will depend on the distance from the object to the pinhole, which is not the case for parallel-hole collimators. The multiple-pinhole collimator is convenient when the imaged objects are small, for example small animals or small organs like the heart or the thyroid, since these objects can be magnified to produce a higher resolution. There are also other types of collimators, for example fan-beam, cone-beam and slant-hole collimators. For more information the collimator review by Van Audenhaege et al. (3) is recommended.

The detector material in the scintillation camera is typically a sodium-iodide (NaI) crystal doped with a small amount of thallium (Tl), which is needed in order for the crystal to generate scintillation light. It is coated with a thin protective layer on the front and edges to protect from outside light and moisture. A scintillation camera for diagnostic purposes usually has a crystal thickness of about 1 cm (3/8 inches), whereas a scintillation camera used mainly for radionuclides emitting higher energies may need a thicker crystal, for example 1.6 cm (5/8 inches) or even up to 2.5 cm (1 inch) in order to capture the majority of the photons. When a gamma photon interacts in the crystal, light photons are created, and their number is proportional to the energy deposited. The rear side of the crystal is optically coupled to a light guide made of glass, which directs the light onto an array of closely packed photomultiplier tubes (PM tubes). The PM tubes are relatively large, a few centimetres wide, and there can be 50–70 of them in a detector head of conventional size. The PM tubes first convert the light photons into electrons and then massively amplify their number. This results in measurable electrical pulses from those PM tubes that are hit by the light photons. The pulses are then processed to give information on the location of the gamma photon interaction in X and Y direction and the energy deposited in the crystal. Due to non-linearities, correction tables are used to improve the accuracy of both position and energy, and a uniformity matrix is used to correct for irregularities in detector response. The interactions in the crystal that are to contribute to the image are sorted out by logical processes, comparing the measured energy with the energy window settings.

THE CZT CAMERA

The NaI scintillation crystal is a sensitive detector material with many advantages which has been in use for several decades. Recently, however, CZT-based gamma cameras have become increasingly popular. CZT was first introduced in pre-

clinical and cardiac cameras but can now also be found in some multi-purpose SPECT/CT systems. Examples are the General Electric NM/CT 870 CZT, which is a dual-headed camera relatively similar to a conventional system, and the Spectrum Dynamics Medical Veriton SPECT/CT, which has a very special innovative design giving 360-degree coverage.

CZT is short for Cd, Zn and Te, that is, an alloy of cadmium, zinc and telluride which can serve as a semi-conductor detector. When the gamma photon deposits its energy in such a material, so-called electron-hole pairs are generated. A hole is the name given to a missing electron, and the combination serves as a pair of charge carriers. An electrical field over the detector will pull the electrons towards an anode and the holes to a cathode, which will result in the formation of an electrical pulse. In other words, the gamma photon energy is directly converted into an electrical signal. No PM tubes are therefore needed in a CZT gamma camera, which produces more compact camera heads with less dead space outside the field of view (FOV). This is useful for brain SPECT/CT studies, for example, where a tight orbit around the patient´s head is of great importance for a high geometrical resolution. In a conventional SPECT/CT with PM tubes, the rotation radius can be limited by the patient's shoulders, but if the frame outside the FOV is only a few centimetres wide, it is easier to get a tight orbit around the patient's head. The removal of the PM tubes is also advantageous for dedicated cardiac cameras, which incorporate several detectors pointing at the heart from different directions, allowing stationary SPECT acquisition. This design would be very difficult to achieve if bulky PM tubes had to be connected to the detectors.

Another advantage with semi-conductor detectors is energy resolution, which is a measure of uncertainty of the measured gamma photon energy. In a NaI-based system the energy resolution is usually in the order of 9–10% for 140 keV (calculated as the full width at half maximum of the photopeak divided by the peak energy), but with a CZT camera it is usually better. Values in the order of 3% have been reported for pre-clinical systems, whereas many clinical systems seem to be closer to 6% in terms of energy resolution. A small percentage value (high energy resolution) is positive, since it means that a tighter energy window can be used when collecting the primary photons. Less scattered photons will be registered within the energy window, which means higher contrast and less need for scatter correction. The high energy resolution is also a key factor in some cases of dual- isotope imaging. If simultaneous imaging of [^{99m}Tc] and [^{123}I] is warranted (photon energy: 140 and 159 keV respectively) the peaks will be easier to separate with a CZT system than with a conventional one.

In contrast to NaI-based cameras, CZT cameras can be manufactured as pixelated systems, meaning that the detector surface is composed of a high number of small detectors. Each detector is mapped to a corresponding pixel in the image. This has been reported to be advantageous in terms of resolution and contrast-to-noise, but it can also have disadvantages. For a parallel-hole collimator, the collimator holes need to be matched exactly to the detector locations, and this means less flexibility when it comes to resolution/sensitivity considerations. If the system includes a fixed collimator optimised for low-energy imaging, it is also difficult to perform imaging with radionuclides emitting higher energies such as [^{111}In], [^{177}Lu] or [^{131}I].

COMPUTED TOMOGRAPHY (CT)

CT is a technique which originated in the early 1970s, and its developers, Cormack and Hounsfield, were awarded the Nobel Prize in 1979. It is not difficult to imagine what the introduction of 3D imaging meant for radiology at the time, and the explosion in research and development that followed. In CT, a motorised X-ray tube rotates rapidly around the patient in a circular orbit, while the patient table moves through the gantry. The detectors on the opposite side of the tube measure the X-ray photons that are not attenuated in the patient. Collimators are used to limit the X-ray field to the detectors, defining the slice thickness. Bowtie filters are needed to shape the X-ray beam by removing more of the low-energy photons from the peripheral parts of the field, thereby reducing the radiation dose to the patient. The signals from the detectors are converted into digital information, and the tomographic images can then be calculated from the measured projections. A complete scan can be acquired in a just a few seconds.

CT technology has evolved rapidly during the last decades, and advanced multi-slice models have been developed in order to improve image quality, reduce scanning times, reduce the dose to the patient, and freeze cardiac and respiratory motion. Top-of-the-range models are able to acquire up to 640 slices per rotation with a rotation time of about 0.3 s. Dual-energy imaging has also been introduced, viewing the patient at two different kV energies simultaneously, which allows better classification of anatomical features and reduction of artefacts. However, the top-of-the-range models are not typically found in SPECT/CT systems, which are usually based on conventional 16–64 slice CT systems. Advanced and expensive

equipment needs a high patient throughput to be economically justifiable, and for most SPECT/CT systems the CT is only used for a small fraction of the total scanning time.

The CT scanner measures a number of attenuated profiles around the patient, which can be reconstructed with methods that are relatively similar to those used in SPECT (to be described later). The images can have less than 1 mm resolution and are usually reconstructed into 512x512 pixel matrices. The image information, which is based on attenuation, is recalculated to a standard scale, Hounsfield numbers (H), using the following equation:

$$H = 1000\frac{\mu - \mu_w}{\mu_w} \quad (1)$$

where μ is the attenuation coefficient in the voxel of interest and μ_w is the average attenuation coefficient of water for the X-ray photons (4). Air has a standard H of -1000 and the H of water is 0. The scale continues on the positive side for tissues with higher attenuation, and bone can have H-values of 1000 or more. The acquired tomographic images build up a three-dimensional image volume that can be sliced in any direction.

For CT acquisition it is important that the patient is centred correctly in the scanner, to ensure optimal image quality and radiation dose to the patient. This is because of the bowtie filters, which filter the X-ray photons in proportion to the attenuation characteristics of the exposed region of the patient. The patient's midline needs to be on the centre of the table, and the table has to be adjusted so that the centre of mass of the scanned part of the patient's body corresponds to the centre point of the FOV. Lasers can aid the technologist when positioning the patient. It has been shown that mispositioning of about 2 cm can result in a dose increase of about 20% and an image noise increase of about 5–6% (5).

SPECT ACQUISITION

In SPECT, 2D projections are acquired at different angles around the patient. A complete acquisition measures projections over a 360° rotation, but a restricted acquisition of 180° is usually used for cardiac imaging or for other lateralised uptakes. The projections are used for reconstruction of a 3D image volume, which ideally should correspond to the activity distribution in the patient. A continuous acquisition of data is possible but requires complicated data management, and in most cases a "step and shoot" technique is used instead, with no data collected during the detector movements. The projection images are acquired in an elliptical, or sometimes circular, orbit around the patient, and the number of projections usually varies between 60 and 128, equally distributed in space.

Early SPECT systems were based on a single gamma camera head rotating around the patient, but dual-headed, triple-headed and even four-headed systems became available during the 1990s. These systems lead to an n-fold increase in sensitivity, where n is the number of gamma camera detectors, hence enabling higher image quality. Today, dual-headed systems are by far the most common systems used for clinical work.

SPECT using traditional equipment is often relatively slow, with examination times in the order of 10–30 min. Some studies require several sequential SPECT scans (FOVs) to cover a larger part of the patient, which can make the examinations even longer. The time per view will be 20 s for a 20 min acquisition using a dual-headed camera measuring 120 projections. The time required for analysis of the CT must also be added to the total time in the camera.

Resolution in clinical SPECT is relatively poor, and for traditional equipment it can be in the order of 8 –15 mm FWHM (full width at half maximum), mostly limited by the collimator. Using large image matrices with small pixels is therefore usually counterproductive, since image noise will increase without an increase in resolution. In SPECT, the most commonly used matrix size is 128x128 pixels for both projections and reconstructed images. If the whole FOV is used for imaging, i.e. if the zoom factor is set to 1, this usually means a pixel size in the order of 4–5 mm. In myocardial SPECT the matrix size used is typically 64x64 pixels, and together with a zoom factor of 1.3 this leads to a typical pixel size of 6–7 mm. It should, however, be noted that SPECT resolution can be significantly better in systems dedicated to specific tasks, for example the cardiac cameras on the market. For pre-clinical SPECT the resolution can even be at sub-mm level. In these cases, matrices and pixel sizes have to be adjusted to do justice to the higher resolution.

RECONSTRUCTION OF SPECT IMAGES

In SPECT, the acquired projection images measured at different angles around the patient are used to calculate the 3D activity distribution within the patient. On clinical work stations both analytical and iterative methods are implemented, the iterative methods being the most commonly used nowadays. In future, however, it is likely that reconstructions will increasingly rely on methods based on artificial intelligence (AI).

The classical analytical method of image reconstruction is the filtered back-projection (FBP) technique (6, 7), which is based on the inverse of a transform that was developed as early as 1917 (8). In this method, the measured projection data (each row of pixels in the acquired planar images) is filtered with a so-called ramp filter. The filtered projections are then added back from the acquired angles to give transaxial images. The ramp filter is used to remove blurring introduced by this back-projection step. This filter will also amplify noise, and the projection images are therefore usually filtered with a noise-reducing filter before reconstruction. Popular filters include, for example, Butterworth, Hamming and Hann filters (9). FBP is a linear method which is simple to implement but can give streak artefacts due to the limited number of projections. The calculated transaxial images build a 3D image volume that can be sliced in any direction.

Iterative techniques have long been known to possess some advantages over the filtered back-projection technique. Image noise is handled in a better way, and it is possible to incorporate corrections for image-degrading effects within the reconstruction. The methods are based on a probability matrix which describes the probability of a photon originating from a certain voxel in the patient being detected in a specific pixel in a projection image. The probability matrix is very large, and is not usually stored in computer memory but calculated on the fly during the reconstruction. The iterations start with an initial estimate of the activity distribution in the patient, which for example can be a blank image or a homogeneous phantom image. This estimate is then improved in repeated steps (iterations) by comparing calculated projections with the acquired ones. Usually, a pre-set number of iterations is used, which should have been optimised for the SPECT analysis in hand, and the estimated and measured projections should be well matched. The optimisation is important, since quantitative accuracy and image noise are dependent on the number of iterations. If the iterations are too few, the activity distribution has not yet converged, and contrast and quantitative accuracy will be poor. With a high number of iterations, the noise level may rise to unacceptable levels. As in FBP, a filter is usually used to reduce the noise level. However, for iterative techniques the filter is usually 3D and is applied after the iteration process is finished. It is therefore called post-filtering.

A well-known statistical iterative technique is the maximum likelihood expectation maximisation (MLEM) method (10, 11), which iteratively maximises a likelihood function and takes the Poisson noise structure of the acquired images into account. For each iteration it uses the whole amount of acquired images when calculating a new update, and it has been proven to be stable. The MLEM method is, however, relatively slow and is seldom used as it is. Hudson and Larkin (12) suggest a way of grouping the set of images into smaller subsets to reduce computing time. This method is called ordered-subsets expectation maximisation (OSEM) and it is widely used and included in clinical software today. The subsets are comprised of evenly spread projections around the patient, and two projections is the absolute minimum number per subset. In theory, however, it is much better to use at least four projections per subset, since the sum of counts in the projections forming each subset should ideally be equal for all subsets, and this requirement is more likely to be fulfilled with larger subset sizes. When using OSEM, an update of the activity distribution is calculated for each subset, but one iteration is defined as a pass through all the subsets. The reduction in computing time in comparison with the MLEM technique is roughly a factor of the number of subsets used, so if we have 120 projections and 12 projections/subset, the computing time decreases by a factor of 10. OSEM has been shown to result in images that are very similar to images using MLEM, using the same number of updates (which means fewer iterations).

An advantage of iterative methods like OSEM is that models for attenuation, scatter, resolution and septal penetration can be incorporated into the reconstruction, i.e. included in the probability matrix. This implies that these effects are indirectly corrected for, and this will be discussed further in later sections.

ATTENUATION CORRECTION

Attenuation correction is the correction for the loss of counts in the images due to attenuation in the patient and surrounding material in the field of view, such as the table top. For the photon energies used in SPECT, attenuation means either photoelectric absorption, where the photon ceases to exist, or Compton scattering, where the photon continues with a lower energy at a scattered angle. Most of the Compton-scattered photons will not be detected because of out-scattering from the patient, photoelectric absorption in the patient or the energy being outside the energy window. The scattered photons that are detected contain less useful information and can be corrected for using techniques described in the next section. An example of a phantom reconstructed with and without attenuation correction can be seen in Fig. 4.

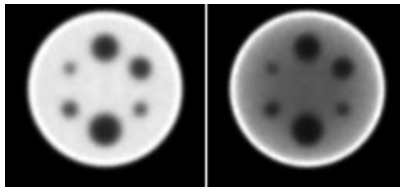

Figure 4: Left-hand image has been reconstructed with attenuation correction and right-hand image without.

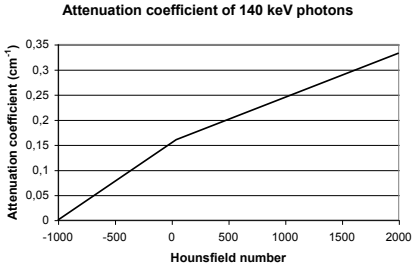

Figure 5: Calibration curve for a Somatom Plus 4 Power (Siemens, Germany) CT scanner.

CT images are based on attenuation of photons from an X-ray tube, and it is therefore natural to base SPECT attenuation correction on the CT information for SPECT/CT. The X-ray photon energies are, however, distributed in a spectrum whose average energy is considerably lower than the photon energies of most radionuclides used for SPECT. In order to be used for attenuation correction in SPECT, the Hounsfield numbers must be calibrated to the attenuation coefficients of the SPECT radionuclide. This conversion is not uniquely defined, since attenuation coefficients depend both on electron density and atomic number, but a reasonably accurate approximation can be achieved (13). For Hounsfield numbers below that of soft tissue, tissue can be assumed to be a mixture of soft tissue and air, and for higher Hounsfield numbers tissue can be seen as a mixture of soft tissue and bone. This gives a straightforward calibration for the Hounsfield numbers below that of soft tissue, since we have two fixed points on the scale, air and water, for which we know the Hounsfield numbers and their corresponding radionuclide attenuation coefficients. A linear relationship is usually assumed between these points. However, for most radionuclides this linear relationship is not valid for the attenuation coefficients of bone, since photoelectric absorption is more important for the X-ray photons than for the higher energy emission photons. A calibration for the Hounsfield numbers above that of soft tissue is therefore needed, and is implemented by the SPECT/CT manufacturer. The calibration curve is specific to each radionuclide and kV setting on the CT scanner, and each setting requires its own calibration. An example of a calibration curve for the 140 keV photons of ^{99m}Tc and for a 120 kVp CT protocol can be seen in Fig. 5. This calibration was created by the author many years ago using bone samples, before the introduction of SPECT/CT equipment.

For the attenuation correction to work properly, the CT image volume must correspond geometrically to the SPECT image volume. Each voxel in the CT image volume should point to the same piece of anatomy as the voxel with corresponding coordinates in the SPECT image volume. The patient therefore needs to stay on the table in exactly the same position throughout the two measurements. A mismatch due to patient movements or scanner problems can usually be dealt with in the reconstruction software, where the mismatch is manually adjusted. If the mismatch is not corrected, the CT images will introduce attenuation correction artefacts in the SPECT images, which could lead to faulty diagnostics and errors in quantitative analyses. It is therefore important that matching is carefully checked during reconstruction using the software tools available. Breathing motion is a well-known problem, since the SPECT, unlike the CT, is acquired during free breathing. It is therefore recommended to also save images without attenuation correction which can be used for comparison if attenuation correction artefacts are suspected.

A CT scanner is capable of delivering a relatively high dose to the patient, and the use of CT imaging for attenuation correction purposes only can, of course, be questioned as a routine basis for diagnostic imaging. If the CT images are not meant for diagnostics, it is therefore important to lower the CT dose so that the image quality fulfils the requirements of the analysis, but no more. A very low CT dose can usually be given if the images are meant for attenuation correction only. If used for image fusion, the CT image quality needs to be high enough to give the anatomical localisation of the functional information. A dialogue with radiologists and physicists is important in order to find the optimal level of CT image quality for all protocols used for SPECT/CT imaging.

SCATTER CORRECTION

Compton scattering is a common interaction process for the photon energies in SPECT. When scattered, the photon interacts with an electron, which leads to a loss of energy and a change in direction. Most scattered photons will not be detected, but due to the relatively poor energy resolution of the detector materials used for SPECT, some scattered photons will be registered within the energy window. For NaI detectors, the share of scattered registrations can be in the order of 30%. Scatter correction of SPECT images is used to remove these detections, in order to improve image quality and quantitative accuracy. Most of the detected scattered photons will have scattered in the patient,

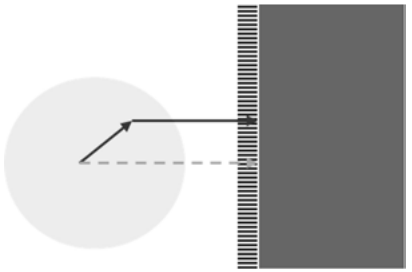

Figure 6: Registration of a scattered photon far from the projected point of emission.

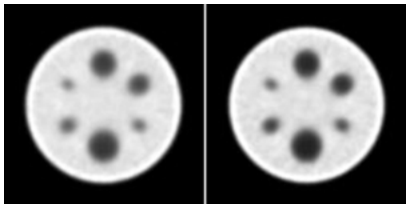

Figure 7: Contrast reduction due to scatter. Scatter is included in the left-hand image but not the right.

but scattering from other parts of the detector system and its environment can also be detected. The amount of scattered registrations depends on the size, density and composition of the part of the patient examined, and the distribution of the radiopharmaceutical within that part of the body. Furthermore, it depends on photon energy, the energy resolution of the gamma camera and the size of the energy window used. A smaller window, perhaps also centred asymmetrically, reduces the number of scattered registrations at the expense of reduced sensitivity. Most of the detected scattered photons have scattered only once, but photons that have scattered 2 or 3 times will also contribute to the number of scattered registrations (14).

Detected scattered photons carry false information about their emission sites, since their place of detection in the crystal does not correspond to the projected point of emission. This is illustrated in Fig. 6, where a scattered photon is detected relatively far from the expected perpendicular point (dashed arrow). Scatter will therefore reduce image contrast, but artefacts can also be induced, for example in cardiac imaging. These effects will also reduce the quantitative accuracy. The effect of scatter in SPECT is demonstrated in Fig. 7 for the same water phantom as shown in Fig. 4. For the left-hand image no scatter correction has been performed, but for the right-hand image scatter is not included. Both images are corrected for attenuation. The reduction in contrast in the image including scatter can clearly be seen in the spheres without activity.

A variety of scatter correction techniques have been developed and evaluated. Many methods are based on subtraction of scatter images, which, for example, can be estimated from measurements in separate energy windows. A more modern approach is to include scatter correction in the iterative reconstruction, to include 3D information when modelling scatter. It should, however, be noted that all scatter correction methods are based on approximations, and severe approximations may introduce image artefacts. Furthermore, corrections based on subtraction of scatter images increase image noise, and methods included in iterative reconstructions can demand a lot of computing time. Nevertheless, if implemented correctly, scatter correction has been shown to be beneficial for both quantitative evaluation and visual interpretation of the images.

ENERGY WINDOW TECHNIQUES

A variety of different energy window techniques for scatter correction have been developed. The most common one is the Compton window method (15), where images are acquired at the same time in the photopeak window and a Compton window, usually adjacent to the lower energy limit of the photopeak window. A fraction of the Compton window image is then subtracted from the photopeak image to give the corrected image. This fraction is constant, and is something that needs to be optimised before implementation. This method is often used for [^{99m}Tc] imaging.

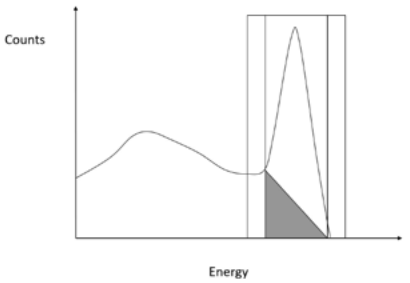

Figure 8: TEW window setting

Another popular method is the triple energy window technique (TEW) introduced by Ogawa et al. (16). The method is illustrated in Fig. 8. TEW is based on two smaller sub-windows adjacent to the photopeak window, one at either side of the photopeak. The scatter image to subtract is approximated by the triangular grey-shaded area in Fig. 8 and is calculated taking the widths of the different windows into account. The method can be recommended when higher energy photons contribute to the counts in the photopeak by scatter and septal penetration from the high-energy side. Examples of radionuclides with such characteristics are, for example, [^{123}I] and [^{131}I].

When using energy window techniques, scatter correction can be performed swiftly and without delay. Scatter from sources outside the field of view will be included, in contrast to many other methods. A disadvantage is the increased noise level resulting from the subtracted noisy scatter estimate. It should also be noted that these methods are based on the assumption of identical spatial distribution of scatter in the different windows, which is an approximation.

Scatter correction in an iterative reconstruction procedure

When scatter correction is included in the iterative reconstruction, it is possible to take 3D information from the patient into account. The scattered photon can actually be mapped back to the point of emission of the primary photon, which results in a lower noise level compared with energy window methods. This correction approach is usually used in PET image reconstruction, but it is less common in the SPECT clinical workflow. The modelling of scatter in iterative reconstruction techniques can be performed with different degrees of complexity. Methods relying on simple models based on point or line source measurements are in use, but it is also possible to simulate the scattering process with Monte Carlo simulations. This means that for each iteration, virtual photos are emitted from the most recent update of the calculated activity distribution and the resulting simulated projections are compared to the measured projections. However, Monte Carlo simulations are a relatively time-consuming method of scatter modelling.

COMPENSATION FOR COLLIMATOR-DETECTOR RESPONSE (CDR)

The poor spatial resolution in SPECT is a problem for accurate quantification, especially with small objects. However, it is possible to compensate for this to some degree if the spatial resolution as a function of the distance from the collimator is known (17). This is called "resolution recovery" or compensation for collimator-detector response (CDR) and can be implemented in the iterative reconstruction probability matrix. Manufacturers of reconstruction software offer different ingeniously named packages in which this type of correction is included.

In CDR compensation the projection of a voxel in the activity distribution can be seen as an "inverse cone" originating in the projection pixel, which describes the range of the detector response for a point in the projection data. Without CDR compensation a perpendicular projection is assumed, but when it is included a probability function is used for the point of origin of the emission photon. The technique is illustrated in Fig. 9.

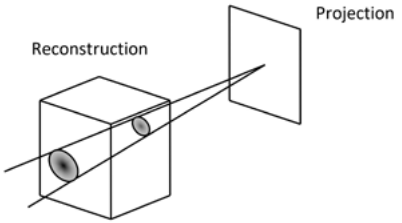

Figure 9: CDR viewed as a cone.

When using CDR compensation, an increase in resolution of several mm has been observed. If a resolution increase is desired, it is nevertheless important that other factors that may limit resolution are adjusted, like the reconstruction post-filter. Not much is gained if one uses the same smoothing post-filter as for conventional reconstructions. It should also be mentioned that the use of this technique has been debated, especially for quantitative analyses. Ringing artefacts (Gibbs artefacts) have been observed around sharp edges, resulting in disturbing patterns which also affect the quantitative accuracy. Another thing to take into account when implementing this technique is a clear increase in reconstruction time.

CORRECTION FOR PARTIAL VOLUME EFFECTS

The spatial resolution of SPECT can, as mentioned, be in the order of 8–15 mm, measured as the full width at half maximum (FWHM) of the point spread function. The poor resolution causes spill-over between regions of different activity concentrations, affecting the quantitative accuracy. Regions with high activity concentration will be underestimated due to spill-out of registrations, while regions with lower activities will be overestimated due to spill-in. CDR compensation increases spatial resolution, but for quantitative purposes it may be necessary to try to increase resolution even further, or to compensate for the quantitative effect of the limited resolution. This is called correction for partial volume effects (PVE). Many such techniques rely on an accurate definition of the organ or tumour contour that is of interest for quantification. Some applications try to find these contours from the CT in the SPECT/CT hybrid equipment, but other segmentation techniques are also in use. PVE is often quantified with the recovery coefficient (RC), which is the ratio between the activity concentration measured in the image and the true activity concentration. Approximate RC values can be calibrated in volumes of interest (VOIs) using phantom measurements or Monte Carlo simulations and can then be applied to the measured quantitative values.

Theoretical calculations of RC values can also be performed, for example by using convolution methods (18).

IMAGE FUSION

Image fusion means that the two sets of images, SPECT and CT, are brought together in an operation called registering to make them correspond geometrically. The images can then be displayed as an overlap, with different colour scales. CT is usually displayed in grey scale, whereas a colour scale is used for SPECT. Different window settings are used for CT, such as soft tissue window, lung window or brain window, depending on type of examination. The degree of transparency can usually be adjusted to make it possible to cross-fade between SPECT and CT.

Image fusion can be used for images from different scanners with the patient in different positions, but this involves complicated geometrical transformations of the image data to make it correspond. In hybrid equipment such as SPECT/CT the patient is usually positioned in the same way on the two sets of images, and this means that the image registration is just a factor of calibration. Factors that the software needs to handle are differences in matrix/pixel size, slice thickness, field of view and table positions. Patient movement can result in a misregistration, and this is usually checked for and if possible corrected as a compulsory step during image reconstruction.

ARTIFICIAL INTELLIGENCE IN SPECT

Artificial intelligence (AI) is a very broad topic that has been playing an increasing role in our daily lives, and the number of possible applications seems endless. In nuclear medicine, for example, AI has shown success in segmenting different structures for determining volume and other parameters of interest for organs and tumours (19,20). This is expected to evolve into efficient tools for diagnostics, staging of disease and prognostics, using advanced methods of machine learning (21) and preferably also taking the CT or MR into account. Promising results have also been presented showing that AI can be used to speed up image reconstruction and improve image quality and quantitative accuracy (22). This involves training a neural network on thousands of images that should be relatively similar to those of the planned application. It should then be possible to use the acquired projection images as input and get a high-quality SPECT image volume as output, without the need for the traditional reconstruction steps. AI also has the potential to speed up the acquisition of the images, since it can be used to compensate for missing data, thus permitting acquisition of a reduced number of SPECT or CT projections (23). If less data is needed for an equivalent image quality, this can also be used to reduce the dose to the patient, both in SPECT and CT. For all aspects of machine learning, validation is a key factor which requires intensive effort before an algorithm can be implemented in clinical work. We can surely expect a lot more from this field in the future.

REFERENCES

1. Hutton BF. The origins of SPECT and SPECT/CT, Eur J Nucl Med Mol Imaging 2014; 41:S3–S16
2. Anger HO. Scintillation camera, Rev Sci Instr 1958; 29:27-33
3. Van Audenhaege K, Van Holen R, Vandenberghe S, Vanhove C, Metzler SD, Moore SC. Review of SPECT collimator selection, optimization, and fabrication for clinical and preclinical imaging. Med Phys 2015; 42:4796-4813
4. Curry, III TS, Dowdey JE, Murry, Jr RC. Christensen's Physics of Diagnostic Radiology. Lea & Febiger Philadelphia 1990
5. Habibzadeh MA, Ay MR, Asl AR, Ghadiri H, Zaidi H. Impact of miscentering on patient dose and image noise in x-ray CT imaging: phantom and clinical studies. Phys Med 2012; 28:191-9.
6. Cormack AM. Representation of a function by its line integrals with some radiological applications. J Appl Phys 1963; 34:2722-2727
7. Hounsfield GN. Computerized transverse axial scanning (tomography). Part I: Description of system. Part II: Clinical applications. Br J Radiol 1973; 46:1016-1022
8. Radon J. Uber die bestimmung von funktionen durch ihre integral-werte längs gewisser mannigfaltigkeiten. Ber Verh Sächs Akad Wiss Leipzig, Math Phys 1917; 69:262-277
9. Van Laere K, Koole M, Lemahieu I, Dierckx R. Image filtering in single-photon emission computed tomography: principles and applications. Comput Med Imaging Graph 2001;25: 127-133
10. Shepp LA, Vardi Y. Maximum likelihood reconstruction for emission tomography. IEEE Trans Med Imaging 1982; 1:113-22.
11. Lange K, Carson R. EM reconstruction algorithms for emission tomography. J Comput Assist Tomogr 1984; 8:306-331
12. Hudson HM, Larkin RS. Accelerated image reconstruction using ordered subsets of projection data. IEEE Trans Med Imaging 1994; 13:601-609
13. Fleming JS. A technique for using CT images in attenuation correction and quantification in SPECT. Nucl Med Commun 1989; 10:83-97

14. Zaidi H, Koral KF. Scatter modelling and compensation in emission tomography. Eur J Nucl Med Mol Imaging 2004; 31:761-782
15. Jaszczak RJ, Greer KL, Floyd CE, Harris CG, Coleman RE. Improved SPECT quantitation using compensation for scattered photons. J Nucl Med 1984; 25:893-900.
16. Ogawa K, Harata Y, Ichihara T, Kubo A, Hashimoto S. A practical method for position-dependent Compton-scatter correction in single photon emission CT. IEEE Trans Med Imaging 1991; 10:408-412
17. Pretorius PH, King MA, Pan TS, de Vries DJ, Glick SJ, Byrne CL. Reducing the influence of the partial volume effect on SPECT activity quantitation with 3D modelling of spatial resolution in iterative reconstruction. Phys Med Biol 1998; 43:407-420
18. Soret M, Bacharach SL, Buvat I. Partial-Volume Effect in PET Tumor Imaging. J Nucl Med 2007; 48:932–945
19. Wang T, Lei Y, Tang H, He Z, Castillo R, Wang C, Li D, Higgins K, Liu T, Curran WJ, Zhou W, Yang X. A learning-based automatic segmentation and quantification method on left ventricle in gated myocardial perfusion SPECT imaging: A feasibility study. J Nucl Cardiol 2019; Jan 28. doi: 10.1007/s12350-019-01594-2.
20. Anita S, Priya PA. Three Dimensional Analysis of SPECT Images for Diagnosing Early Parkinson's Disease using Radial Basis Function Kernel - Extreme Learning Machine. Curr Med Imaging Rev. 2019;15(5):461-470.
21. LeCun Y, Bengio Y, Hinton G. Deep learning. Nature 2015; 521(7553):436-444
22. Häggström I, Schmidtlein CR, Campanella G, Fuchs TJ. DeepPET: A deep encoder-decoder network for directly solving the PET image reconstruction inverse problem. Med Image Anal 2019; 54:253-262.
23. Ryden T, Marin I, van Essen M, Svensson J, Bernhardt P. Deep learning generation of intermediate projections and Monte Carlo based reconstruction improves 177Lu SPECT images reconstructed with sparse acquired projections. J Nucl Med 2019; 60 1: 44

2

QC OF HYBRID SYSTEMS

by Sebastijan Rep

INTRODUCTION

The image reproduced by the SPECT/CT gamma camera shows the distribution of radiopharmaceutical activity in the body. The basis of image quality is the ability to detect differences in the uptake of radiopharmaceuticals into the lesion and the surrounding tissue. A high-quality image is one that can reproduce this contrast in a way that enables the right diagnosis. However, there are several factors that affect image quality. Some of them are impossible to influence, such as the size of the patient and the overlap and movement of the organs. Factors which allow us to influence the quality of the image, on the other hand, include a number of parameters and properties of the camera and the choice of reconstruction algorithm. The user must have complete control over the properties of the gamma camera in order to optimise the image of activity distribution. Regular control of the quality of the gamma camera is critical to the reliability of the result. When the conditions are not optimal, misdiagnosis can occur, which means that the gamma camera can give false positive and false negative test results. Regular quality control is important in order to prevent such errors (1, 2).

The Quality Control Programme (QC) is designed to maintain the high performance of equipment regardless of age. QC begins with an initial acceptance test based on a QC programme to assess whether or not the equipment meets the specifications upon installation. The user (technologist or medical physicist) must subsequently perform routine QC measurements at regular intervals and also after major component changes, manufacturer updates or repairs. In order to maintain long-term overall stability of operation, these measurements need to be specified, performed, recorded and evaluated (Table 1). QC programmes should follow international guidelines (IAEA, EANM, NEMA), taking into account national guidelines and legislation as well as the manufacturer's recommendations. The annual SPECT/CT QC tests and assessment should be performed by an independent medical physicist (1, 3).

TEST	RADIATION SOURCE	TOLERANCES	DAILY	MONTHLY	HALF-YEARLY
Physical inspection			X		
Background		In line with the initial benchmark. In a daily check, check the number on the monitor; take images in the annual test.	X		
Intrinsic uniformity	Point source ^{99m}Tc	Integral: CFOV ≤ 5%, UFOV ≤ 6% Differential: CFOV ≤ 2.5%, UFOV ≤ 3%		X	
Energy photo-peak	Point source ^{99m}Tc, or the appropriate isotope		X		
Extrinsic uniformity	Line source ^{153}Gd	Integral: CFOV ≤ 5%, UFOV ≤ 6% Differential: CFOV ≤ 3.5%, UFOV ≤ 4%	X		
	Flat source ^{57}Co	Integral: CFOV ≤ 5%, UFOV ≤ 6% Differential: CFOV ≤ 3.5%, UFOV ≤ 4%	X		X
Sensitivity (for quantification)	The solution of ^{99m}Tc or the appropriate isotope	In accordance with the initial reference value		X	
	Reference sources; ^{75}Se in ^{57}Co	< 10%		X	
Spatial resolution and linearity	Bar phantom + Flat source ^{57}Co	In accordance with the initial reference value			X
	Micro capillary glass tubes filled with ^{99m}Tc	≤ 7.5 mm (@10cm)			X
Centre of rotation	Point source ^{99m}Tc	≤2 mm		X	
SPECT/CT alignment	Point source: Tc-99m + iodine contrast agent	<5 mm misalignment		X	
Jaszczak phantom	Solution of ^{99m}Tc in Jaszczak phantom	Homogeneity (homogeneous part) <10%, contrast (cold balls) and resolution (bar sectors) comparable to initial reference measurements and published research			X

Table 1: Recommended routine QC tests (daily, monthly and half-yearly tests)

CHAPTER 2

QC OF HYBRID SYSTEMS

1 Daily tests

The operator must perform a daily visual and physical inspection of SPECT/CT cameras to detect external mechanical or electrical defects or damage. If the detector collimator has a touch pad that stops all movement when contact is made, a touch pad test should be performed every day and after each change of column restraints. An operational check of the background count rates with or without collimators and within one or more energy windows should be performed daily to detect radiation caused by possible radioactive contamination of the scintillation camera, floor or walls, radiation from any neighbouring unshielded source (Fig. 1) or an excess of electronic noise. Before using the SPECT/CT cameras, the operator must check the setting of the energy windows to confirm that all the pre-set energy windows of the pulse height analyser are correctly oriented around the energy photo-peaks of the radionuclides, indicating that the system energy calibration is correct. The most sensitive parameter affecting changes to and performance of the system is the uniformity of the detector system. Factors potentially affecting uniformity are changes in the photomultiplier (PMT), energy and linear corrections, hygroscopicity of the crystal and damage to the collimator, which affect the evenness of the image (1, 3, 4).

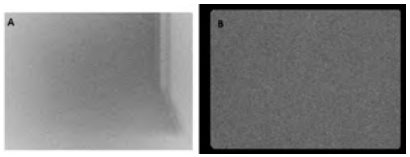

Figure 1: Poor intrinsic uniformity (A) due to contamination in the room (background) and normal uniformity (B).

1.1 Extrinsic uniformity

The system test evaluates the uniformity of the detector system with the collimator (Bolstad et al., 2011). A ^{57}Co flat source (Fig. 2) or a phantom flat filled with ^{99m}Tc mixed with water may be used for implementation. Newer gamma cameras use the ^{153}Gd line source for the automatic QC system consistency test, which is designed to perform the test automatically (5-8).

Figure 2: Implementation of extrinsic uniformity test with a 57Co flat source

1.2. Intrinsic uniformity

In an intrinsic uniformity test, the collimator is removed from the detector system. The most commonly used measurement is the ^{99m}Tc point source (Fig. 3), which is placed at a distance equal to four times the detector's field of view diameter to ensure uniform detection of the detector system. In the internal evenness test, the impact of the collimator is not evaluated (4, 9).

Extrinsic and intrinsic uniformity tests aim to verify the response of the gamma camera to the steady flow of incident photons into the field of view of the detector system using a symmetrical energy window, with and without collimators (4).

The scintillation gamma camera displays the uniform field of view of the system for all collimators used. If there are any significant differences in uniformity deviating from the reference values, an intrinsic (internal) uniformity test must be performed by calibrating and adjusting the PMT (3, 4).

Figure 3: Implementation of intrinsic uniformity test with ^{99m}Tc point source.

1.3 Assessment of uniformity

We use visual assessment to check changes in the distribution and density of pulses in the visual field of the image.

For quantitative assessment of the uniformity tests, the integral uniformity (IU) and differential uniformity (DU) in the usable field of view (UFOV) and the central field of view (CFOV) are calculated. The IU is calculated using the minimum and maximum counts/pixels, according to the following equation:

IE = 100 [(max - min) / max + min)]

For the DU the highest and lowest pixel values are identified every five consecutive pixels in X and Y direction.

Their differences are computed according to the following equation:

DE = 100 [(high - low) / (high / low)] (4)

Figure 4: Daily report on extrinsic uniformity

Figure 5: Report on intrinsic QC tests for a gamma camera

2. Spatial resolution and linearity with the bar phantom

The spatial resolution characterises the system's ability to resolve spatially separated sources of radioactivity. Extrinsic tests of spatial resolution are performed under clinical conditions and include the effects of the collimator. The quantitative measure of spatial resolution is given in millimetres as the full width at half maximum (FWHM) or full width at tenth maximum (FWTM) of the peak of the imaged point or line radioactive sources. This test must be performed for all low-energy parallel-hole collimators. To perform the test, we use a bar phantom, a line source and a point source. The bar phantom is mounted on the collimator head (Fig. 6) at a distance of 10 cm from the detector head. Align the phantoms with the X and Y axes of the detector head. The estimated FWHM values for each collimator must be compared with the manufacturer's worst-case values. If the lines on the surface of the collimator are straight and curved at a distance of 10 cm (Fig. 7), this indicates that the bars and collimator are not parallel, which will result in a decrease in resolution and contrast in the clinical images (3, 4, 10).

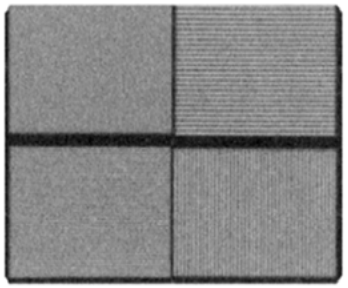

Figure 6: Test of spatial resolution and linearity performed with the bar phantom ^{57}Co flat source

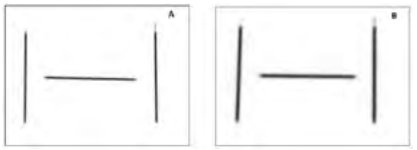

Figure 7: Test of spatial resolution (average FWHM = 4.26mm and FWTM = 7.76 mm) with line source on the head of collimator (A) at a distance of 10 cm (average FWHM = 7.44 mm and FWTM = 13.55 mm) (B).

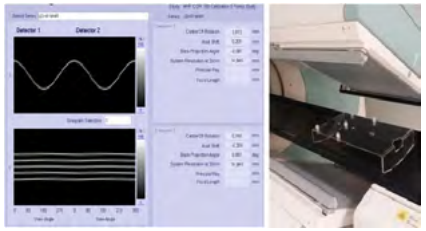

Figure 8: COR test results and phantom position for performance of the test

3. Centre of rotation (COR)

The aim of this test is to ensure the proper operation of the SPECT system and to ensure that the distance from the centre of rotation is minimal. The SPECT system must be precisely centred, since every deviation from the axis of rotation reduces the spatial resolution. The COR test must be performed in all angular configurations of the SPECT system and for all the collimators used. This test should be run as a reference test at weekly/monthly intervals, or if a problem is suspected. COR is measured by 360 degree coverage around one or more ^{99m}Tc point sources (Fig. 8). Most manufacturers have software that analyses the acquisition to determine if the COR is within acceptable limits. It is important not only to use the correct COR value, but also to keep this value constant as a function of angle. When measured on a gamma camera system at a radius of 20 cm, both X and Y values for COR must show less than 2 mm in a 360° orbit (3, 4, 10).

4. SPECT resolution and homogeneity test

The Jaszczak phantom test is designed to provide an assessment of the overall performance of the SPECT system. The Jaszczak phantom allows us to check whether the system works satisfactorily, even in a high-repetition study. Phantoms should have at least one area for homogeneity assessment and one area for cold lesions (Fig. 10). Place the phantom on a bed and align it with the axis of rotation, or use a special holder to align the phantom correctly with the centre of rotation. The acquired images should be carefully examined, paying particular attention to the appearance of any artefacts (Fig. 12). Adjust the profile of the phantom uniform region through the incisions and measure the ratio of pixel counts in the centre to pixel counts at the edge (Fig. 9). If attenuation correction is used, the profile across the uniform area of the phantom must be straight or flat. Using the appropriate ROI, measure the uniformity (Fig. 11) and contrast of all

visible spheres. Record acceptable values and compare with values when the test is performed routinely. The quality of the image is visually checked and the contrast of the detected lesions recorded (3, 4, 10).

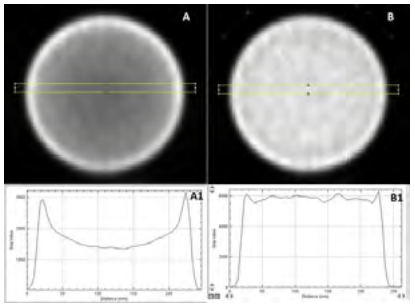

Figure 9: Profiles to check the accuracy of attenuation correction. A profile was drawn across one of the transverse slices. A and A1: no attenuation correction. B and B1: CT attenuation correction

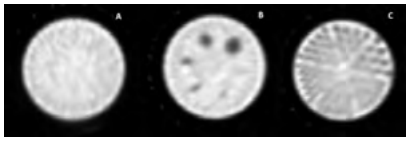

Figure 10: The Jaszczak phantom in three specific areas: homogeneous area (a), cold spheres (b) and cold bars (c).

RESULTS - JASZCZAK PHANTOM - UNIFORMITY	
Frames	10-15
Centre - Border ratio	1.037
Integral Uniformity (%)(CFOV)	8.016
Differential Uniformity (%)(CFOV)	4.136

RESULTS - JASZCZAK PHANTOM - CONTRAST	
Radius	Contrast
31.6	31.1
25.3	28.8
19.0	20.1
15.9	14.8
12.9	8.85

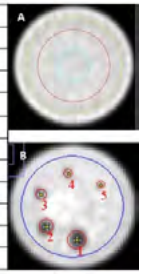

Figure 11: Calculated integral and differential uniformity in the homogeneous area and contrast in the cold spheres area of the Jaszczak phantom.

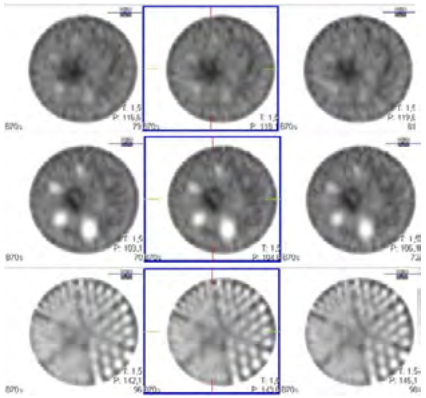

Figure 12: Seven transverse slices of the homogeneous and sphere sections of the Jaszczak phantom, imaged with a 360° total angle of rotation and corrected for attenuation. Distinct artefacts are seen in different slices.

5. SPECT/CT alignment

Accurate registration of SPECT and CT images is essential in order to achieve accurate attenuation correction and merging of SPECT/CT images. After the SPECT/CT system has been installed and calibrated, the match between the SPECT and CT fields needs to be checked at regular intervals. The frequency of testing depends on the stability of the system (EANM suggests that this be done monthly). The test can be performed using hollow spheres, which can be filled with a solution of ^{99m}Tc (visible on SPECT) and iodine contrast medium (visible on CT). A SPECT/CT scan is then performed and image fusion software is used for accurate alignment (Fig. 13).

When matching between SPECT and CT images, attenuation correction is appropriate, and an image with accurate reproduction of the radionuclide distribution will be generated. This is especially important when SPECT/CT quantification of uptake is required (6, 11).

6. CT tests

Daily routine QC tests and phantoms for CT scanners are recommended and provided by the manufacturers. The daily measurement of quality is based on three parameters. Measure the voltage in the tubes directly in the x-ray tubes. Test the uniformity of a CT image of a homogeneous object by measuring the CT numbers (Hounsfield units - HU) across the image of homogenous phantom, and calculate pixel noise as a standard deviation. The aim of the test is to ensure that the relative calibration of all CT numbers to water remains within acceptable limits and that quantum noise and electronic system noise do not increase. Too much image noise degrades low-contrast detectability (3, 6, 11).

Figure 13: Spatial registration phantom used in SPECT/CT. Reconstruction in sagittal, coronary and sagittal direction on ten-point source vial filled with a solution of ^{99m}Tc and iodine contrast medium.

THE INFLUENCE OF RECONSTRUCTION ALGORITHMS ON IMAGE QUALITY

Image reconstruction allows the provision of diagnostic information based on the distribution of activity in different tissues. There are two reconstruction methods used in practice: analytical filtered back-projection (FBP) and the iterative reconstruction method. The FBP method is simple, fast and easy to implement in research and clinical practice. However, there are some disadvantages that can be eliminated through iterative techniques. Images reconstructed with iterative techniques have been shown to have better qualitative features, including more accurate estimates of concentration and improved image contrast, spatial resolution and noise characteristics compared with analytical methods. Advanced SPECT/CT reconstruction algorithms include techniques to correct for photon attenuation and scattering (Fig. 14) (12-14).

ABSOLUTE QUANTIFICATION IN SPECT/CT

The accuracy of SPECT/CT quantification depends on many factors, including the need for scatter correction and attenuation correction. In addition, absolute quantification is influenced by both the reconstruction algorithm and the settings. Recent developments in corrections for attenuation and scatter of photons, collimator modelling and 3D reconstruction with resolution recovery and noise regulation have improved reconstruction techniques, thereby enabling absolute SPECT quantification. The addition of an integrated computed tomography (CT) system not only provides anatomical reference, but also enables accurate attenuation and scatter correction and improves quantification. Hybrid SPECT/CT cameras have now become standard clinical practice and absolute quantification has thus become a reality (15, 16).

In order to calibrate the sensitivity of the calculation of absolute quantification, use of a standardised point source of a clinically

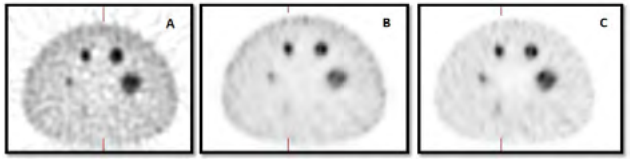

Figure 14: NEMA body phantom reconstructions with FBP (A), iterative reconstruction (B), and iterative reconstruction corrected by photon attenuation and scatter (C).

used isotope is the preferred method. Two point sources are available: ^{57}Co and ^{75}Se. The sensitivity calibration test with ^{57}Co and ^{75}Se sources is performed at monthly intervals (Fig. 15) (21).

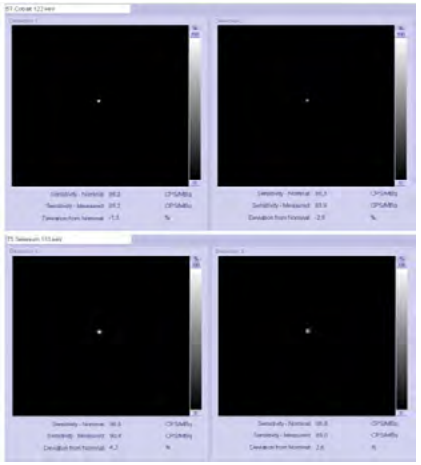

Figure 15: Monthly test; sensitivity of ^{57}Co and ^{75}Se point sources, which are used for absolute quantification in SPECT/CT.

THE ROLE OF THE TECHNOLOGIST

Nuclear medicine technologists are health professionals who cover a wide range of tasks including radiopharmaceutical dispensing and administration, patient care, image acquisition and processing, image evaluation to exclude artefacts and quality control of SPECT/CT. In most cases, technologists are responsible for the routine tests which are performed daily and monthly. They may also be responsible for conducting annual tests in collaboration with a medical physicist.

The technologist's basic daily task is to evaluate images to exclude possible artefacts. Low-dose CT (10-40 mA) is used to make images of appropriate quality for their intended purpose (16). CT imaging is used to obtain transmission folders that serve to correct attenuation in SPECT data (17).

Common artefacts that are generated in the reconstructed images are the result of a misalignment of CT data and emission data. The reason for the formation of artefacts is the movement of organs due to breathing, which gives rise to major changes in attenuation coefficients. Metal implants and patient movement during CT acquisition are another cause of poor image quality. The misalignment between emission and transmission imaging, in addition to patient movement and breathing, also causes the table to bend as it enters the gantry. CT imaging takes much less time than SPECT, resulting in a time mismatch. This is a problem, especially when chest scanning, because the heart and lungs are moving organs. This temporal mismatch can produce unwanted artefacts on attenuation-corrected images, which can lead to

misinterpretation of results (16, 17, 18, 19).

To exclude artefacts due to attenuation correction, it is important always to check uncorrected images as well. The anatomical accuracy of image fusion must be verified before interpreting the corrected scans. The responsibility of the technologist includes the regular performance of quality control tests and the evaluation of scans to exclude potential artefacts (16, 20).

SUMMARY

This chapter has included examples to give an insight into some of the procedures and practices associated with SPECT/CT cameras. Local practice and recommendations from the manufacturer, technologists and physicists will determine how and when QC tests are performed. Performance of tests may vary between different departments depending on the clinical practices undertaken.

REFERENCES

1. Murph PH. Acceptance testing and quality control of gamma cameras, including SPECT. J Nucl Med. 1987, 1221-1227.
2. Zanzonico P. Routine quality control of clinical nuclear medicine instrumentation: a brief review. J Nucl Med. 2008 Jul;49(7):1114-31. doi: 10.2967/jnumed.107.050203.
3. Busemann Sokole E1, Płachcínska A, Britten A; EANM Physics Committee. Acceptance testing for nuclear medicine instrumentation. Eur J Nucl Med Mol Imaging. 2010 Mar;37(3):672-81. doi: 10.1007/s00259-009-1348-x.
4. National Electrical Manufacturers Association (NEMA). Performance Measurements of Scintillation Cameras: Rosslyn, NU-1 NEMA. 2012.
5. Bolstad R, Brown J, Grantham V. Extrinsic Versus Intrinsic Uniformity Correction for γ-cameras. J Nucl Med Technol. 2011. 39(3):208-12.
6. Siemens Operating Instructions Symbia System T16/T6/T2/T Series, Version VA60A. Quality Control and Assurance. 2010. 251-323.
7. Busemann Sokole E, Kugi A, Bergmann H. High count rates cause non-uniformities in cobalt-57 flood images. Eur J Nucl Med.1993. 20: 896.
8. English RJ, Polak JF, Holman BL. An iterative method for verifying systematic nonuniformities in refillable flood sources. J Nucl Med Technol.1984. 12: 7-9
9. Elkamhawy AA, Rothenbach JR, Damaraju S, Badruddin SM (2000). Intrinsic uniformity and relative sensitivity quality control tests for single-head gamma cameras. J Nucl Med Technol.; 28(4):252-6.
10. International Atomic Energy Agency. Quality assurance for SPECT systems. Human Health Series No. 6.
11. Jones DW, Hogg P, Seeram E. Practical SPECT/CT in nuclear medicine. London: Springer; 2013.
12. Bruyant PP. Analytic and iterative reconstruction algorithms in SPECT. J Nucl Med. 2002 Oct;43(10):1343-58.
13. Zeraatkar N, Rahmim A, Sarkar S, Ay MR. Development and Evaluation of Image Reconstruction Algorithms for a Novel Desktop SPECT System. Asia Ocean J Nucl Med Biol. 2017 Spring;5(2):120-133. doi: 10.22038/aojnmb.2017.8708
14. Berker Y, Li Y. Attenuation correction in emission tomography using the emission data--A review. Med Phys. 2016 Feb;43(2):807-32. doi: 10.1118/1.4938264
15. Peters SMB, van der Werf NR, Segbers M, van Velden FHP, Wierts R, Blokland KJAK, Konijnenberg MW, Lazarenko SV, Visser EP, Gotthardt M. Towards standardization of absolute SPECT/CT quantification: a multi-center and multi-vendor phantom study. EJNMMI Phys. 2019 26. dec.; 6 (1): 29. doi: 10.1186 / s40658-019-0268-5
16. Ziegler SI, Dahlbom M, Sibylle I et al. Diagnostic Nuclear Medicine. 2nd ed. Berlin: Springer. 2006. 277-88.
17. Mariani G, Flotats A, Israel O, Kim E.E, Kuwert T. Clinical Applications of SPECT/CT: New Hybrid Nuclear Medicine Imaging System. Dunaj: Nuclear Medicine Section International Atomic Energy Agency. 2008.
18. Suzuki A, Koshida K, Matsubara K. Effects of Pacemaker, Implantable Cardioverter Defibrillator, and Left Ventricular Leads on CT-Based Attenuation Correction. J Nucl Med Technol. 2014. 42: 37–41.
19. Apostolopoulos D, Savvopoulos C. What is the benefit of CT-based attenuation correction in myocardial perfusion SPECT?. Hell J Nucl Med. 2016. 19 (2): 89-92.
20. Magdy M K Ed. Basic Sciences of Nuclear Medicine. London: Springer.2011.
21. www.siemens.com/healthcare

3

QUANTITATIVE SPECT

by John Dickson

INTRODUCTION

From its very early days, nuclear medicine has been a quantitative modality. From probes counting the levels of radioactivity in the neck, through to quantifying thyroid uptake in planar imaging or looking at changes in activity distributions in the kidneys in dynamic renogram studies, the quantitative capability of nuclear medicine has been key to its success. Similarly, in SPECT, we've been performing quantification for many years. In myocardial perfusion imaging we can quantify relative perfusion in territories of the heart and determine wall motion and ejection fractions, while in the brain SPECT can be used to determine striatal specific binding ratios in I-123 ioflupane imaging (Figure 1). What is noteworthy in all these SPECT examples is that this type of quantification is ***relative***, i.e. relative to other areas of uptake in space, such as areas of the occipital lobe in I-123 ioflupane SPECT, or relative over time, as in SPECT determination of left ventricle ejection fraction.

While relative quantitative SPECT has had its successes, because of its historical inability to perform ***absolute*** quantification in terms of e.g. activity concentration, SPECT has been considered quantitatively inferior to PET. This difference arose because of the long-established incorporation of corrections for physical factors such as scatter and attenuation in PET reconstruction, which until relatively recently were absent from routine SPECT imaging. However, with the introduction of SPECT/CT, together with improved reconstruction and correction algorithms, we now have the ability to perform absolute quantification in SPECT too (1). While this form of quantification was initially used to determine activity concentration, the technique has been extrapolated to normalised quantitative measures such as standardised uptake value (SUV) and used in a similar way to PET (2)(3). Absolute quantitative SPECT will be the focus for the rest of this chapter.

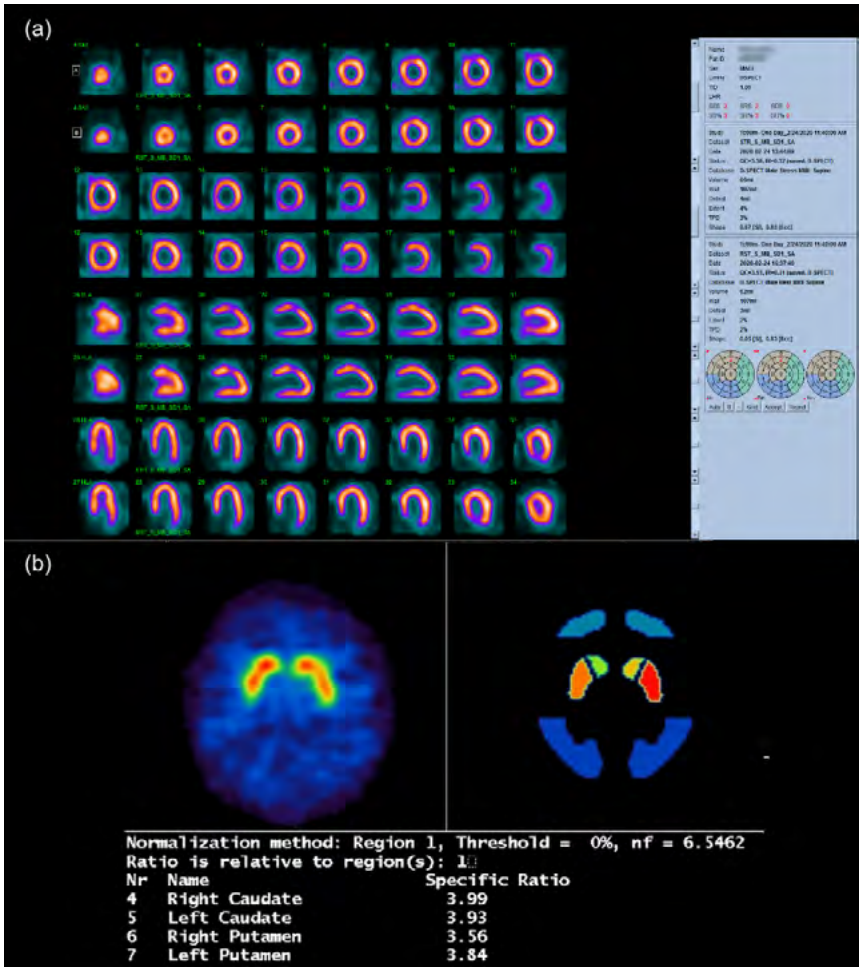

Figure 1: Examples of relative SPECT quantification in (a) myocardial perfusion imaging and (b) I-123 ioflupane SPECT.

THE CLINICAL NEED FOR QUANTITATIVE SPECT

The initial need for absolute quantification came with the growth of theranostics (4). With the expansion of molecular radiotherapies such as I-131 mIBG, Lu-177 dotatate and Lu-177 PSMA, together with the expansion of Y-90 microsphere therapy and its pre-assessment with Tc-99m MAA (5), there has been an increasing need to calculate organ dosimetry. This has happened because, as in external beam radiotherapy, effective, safe radiation treatments require the maximum possible dose to the tumour site while minimising the dose given to organs at risk.

For molecular radiotherapies using agents such as I-131, I-131 mIBG, Lu-177 dotatate and PSMA, dosimetry is typically performed using the MIRD scheme. Using this methodology, the time-activity curves of tumours and/or organs are calculated to help derive overall radiation exposure, before being combined with 'S' values which estimate the dose to the organ or tumour. Historically, the derivation of time-activity curves was based on anterior and posterior whole-body scans (6). By drawing regions of interest around relevant features on anterior and posterior views, the geometric mean of the counts in these regions is used to calculate attenuation-compensated time vs. count curves before translation into activity (MBq) using a known activity standard or sensitivity factor. Although this approach works, it does not have the accuracy of quantitative SPECT, where organs/tumours can be clearly defined in three

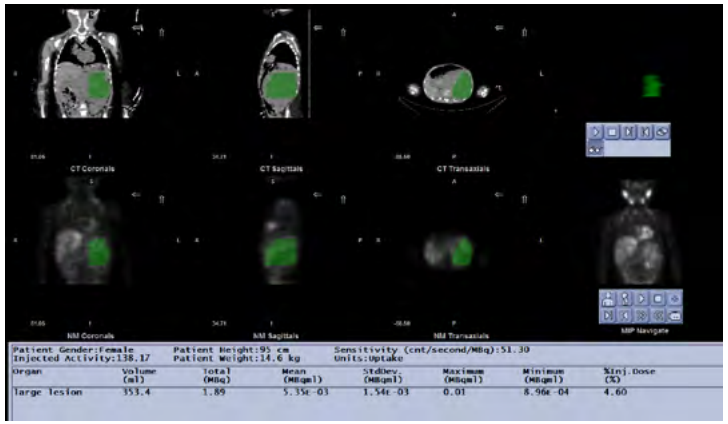

Figure 2. Quantitative SPECT screen directly showing activity concentration within regions of interest.

dimensions, and where the incorporation of corrections for attenuation, scatter, resolution losses and an inbuilt sensitivity factor can produce time-activity curves directly from an image (Figure 2). Because of this, incorporating quantitative SPECT into dosimetry calculations is now well established (7), and the direct derivation of voxel values of activity concentration is a clear benefit of this technique.

A second clinical use of absolute quantitative SPECT, again in theranostics, is in disease assessment. Typically for radiotherapeutic interventions using e.g. iodine-131 sodium iodide for thyroid cancer and I-131 mIBG for neuroendocrine tumours, initial staging or disease follow-up is performed with planar gamma camera and SPECT imaging using iodine-123-labelled diagnostic versions of these radiopharmaceuticals. Having a body habitus normalised uptake value such as SUV in these diagnostic studies can be incredibly helpful in determining disease extent and aggressiveness, and can be used in a similar way in which disease progression is assessed using PET. As can be seen in Figure 3, which shows a patient who has had imaging following multiple I-131 treatments for thyroid cancer, the SUVmax in the bone lesion has reduced slightly from 2.26 to 2.01 from June to December. This small change in SUV indicates that the last therapeutic

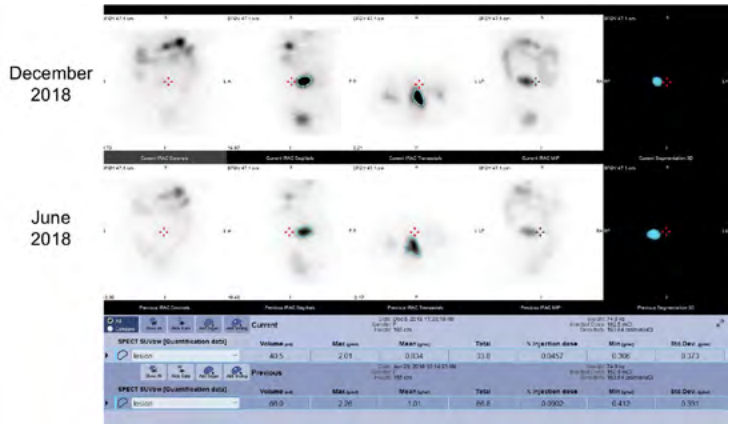

Figure 3. Quantitative SPECT on two occasions following Iodine-131 therapy for thyroid cancer. SUV_{max} in December 2018 (2.01) was only marginally lower than that measured in June 2018 (2.26), highlighting no significant change in the metabolic activity in the lesion following therapy.

intervention did not have the desired effect.

One final area where quantitative SPECT is gaining interest is in orthopaedic and oncological bone scanning (Figure 4). Having the ability to calculate an SUV in bone SPECT is becoming useful in characterising bone disease (8–10). However, an initial challenge with this technology is understanding the relevance of an SUV value where values relevant to normal and indeed diseased bone are still not well established, and where normal uptake depends on the location of that bone tissue (2,11). A further potential application of quantitative bone SPECT is combining uptake in the diseased bone in terms of activity and volume across the field of view in the form of a Bone Scan Index or total bone uptake (12,13). This is analogous to total lesion glycolysis in FDG-PET. Publications in this area are growing in number, so it is anticipated that this form of quantitative bone SPECT may become increasingly useful. While dosimetry, theranostic follow-up and bone scintigraphy are establishing themselves as areas where quantitative SPECT is becoming helpful, one can also envisage other areas where quantitative SPECT may be used. SPECT for parathyroid adenomas and cardiac innervation, or indeed I-123 ioflupane or regional cerebral blood flow SPECT have been suggested as areas where the technology could be applied (14).

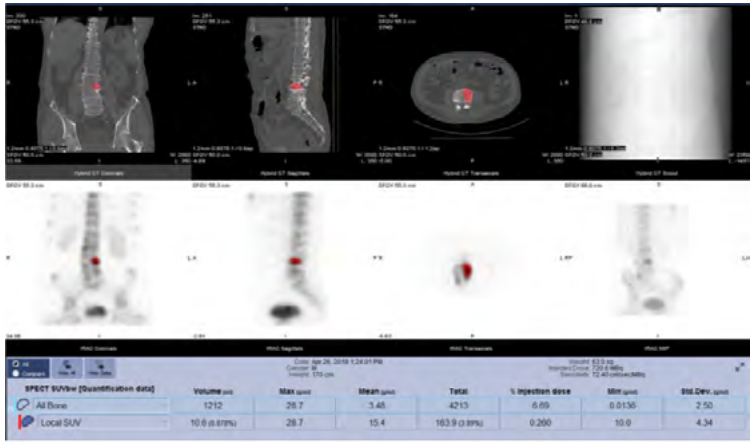

Figure 4. Bone SPECT quantification showing the uptake in a lumbar spine bone lesion in terms of SUV_{max} SUV_{mean} SUV_{min} together with the volume of the lesion. Also shown in the figure for reference is the SUV of the total segmented bone in the image data.

OPERATIONAL REQUIREMENTS

While quantitative SPECT has many potential advantages, there is also an overhead, and changes in practice are required to implement the technology operationally.

To calculate the activity or SUV in an image requires several input parameters. These input parameters work in much the same way as in PET (15). The first is the sensitivity factor required to translate counts in the SPECT image into activity concentration. This requires a sensitivity calibration to be performed, which should also be assessed periodically to ensure consistency between the calibrations. While this overhead is not onerous, it still requires some time on the scanner.

The second set of input parameters is related to the determination of SUV. SUV is calculated using the following equation:

SUV = (activity concentration in area of interest) / (available activity concentration)

where available activity concentration can be the injected activity normalised to body surface area, lean body mass, or, more commonly, body weight. The calculation of activity concentration or SUV therefore requires several input parameters to be known:

» The exact activity injected into the patient, i.e. the syringe activity pre and post injection

» The time of injection, to account for radioactive decay from the time of the activity measurement

» The body habitus, i.e. the weight and/or height of the patient depending on the type of SUV normalisation.

While this is frequently performed in PET, the availability of weighing scales or height measures may be an impediment for some, while the routine measurement of activity in a syringe pre and post injection may not be routine or indeed possible in some nuclear medicine clinics if a dose calibrator is not readily available. Introducing quantitative SPECT to a nuclear medicine practice also brings with it other overheads, such as the checking and quality control of weighing scales and height measures, and the availability and synchronisation of clocks in injection areas to the clock on the scanner.

A final factor that may not be as well appreciated in SPECT compared to PET is the pharmacokinetics of the SPECT radiopharmaceutical, and the patient status prior to injection. In non-quantitative SPECT, the interpretation of images is based on visual assessment of hot or cold features. With the introduction of quantification, the quantitative values may be dependent on drug interactions, fasting/hydration status, and whether the radiopharmaceutical status is in equilibrium. For the latter, when performing longitudinal comparisons it

may be necessary to scan at the same time post injection to ensure comparability. While the issue of scanning time is an inconvenience rather than a challenge, the pharmacokinetic status at the time of imaging and any possible drug interactions of established radiopharmaceuticals may need to be revisited. Figure 5 summarises the operational issues associated with quantitative SPECT.

LIMITATIONS OF QUANTITATIVE SPECT

With a calibrated SPECT system and knowledge of the injected activity and body habitus of the patient, it is possible to perform quantitative SPECT. However, there are some caveats. To perform quantitative SPECT, it is essential that the data is corrected for physical factors. Given that the corrections should work in all environments, it is important that measured rather than calculated attenuation correction is used, i.e. CT attenuation correction inside iterative reconstruction rather than Chang calculation using filtered back-projection (FBP). This is because Chang attenuation

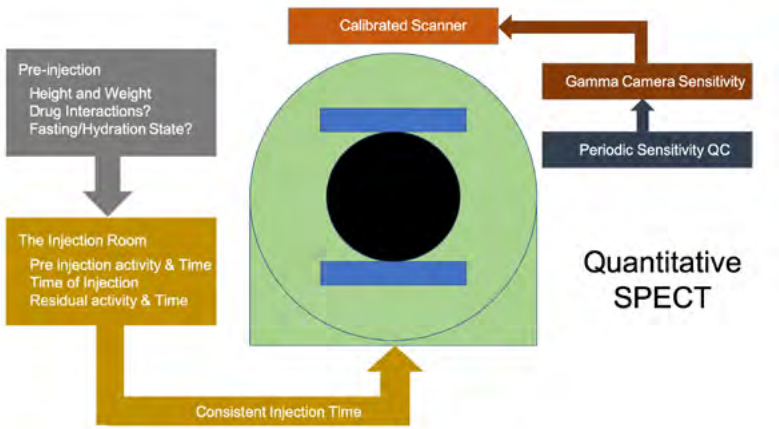

Figure 5. Operational steps required to perform quantitative SPECT.

correction assumes a uniform attenuation environment which does not work in mixed- attenuation parts of the body such as the chest, where soft tissue, lung and bone may be present. The use of CT entails a small radiation exposure burden, which may be an issue for some. Scatter and other corrections within the iterative loop are also valuable for the highest level of accuracy. However, unlike in PET, corrections are not routinely used in SPECT, and while attenuation correction in iterative correction is relatively common, corrections for scatter are not as well developed on most software platforms, nor are they frequently used. Additionally, corrections for resolution losses, known as point spread function or resolution modelling, are not available on some systems, or are not used. This correction is also prone to overshoot (Gibbs) artefacts, so should be used with care (16,17). As a consequence, not only will the value of uptake be different for users using different corrections, but there will also be a loss of accuracy unless all corrections are applied. This is not an issue when performing non-quantitative SPECT, where patterns or relative uptake are assessed. Also, in relative SPECT quantification, corrections are often not as relevant because they affect the different regions or time points in a similar manner. However, the choice of corrections is an issue in absolute SPECT quantification.

Figure 6 shows the value of uptake in a small feature (in this case the striata of a DaTSCAN™) with different corrections applied. As a comparison, FBP and iterative reconstruction with no corrections is also shown. On visual assessment, the image with resolution modelling (ACSCRM), as expected, shows better resolution of the separation of caudate and putamen, while the scatter-corrected data (ACSC and SC), which also corrects for septal penetration of high-energy photon emissions with iodine-123, demonstrates superior image contrast between the striata and non-specific uptake elsewhere in the brain. Visually, attenuation correction appears to have very little impact (AC vs. NC, ACSC vs. SC), while iterative reconstruction without corrections (NO) and filtered back-projection with no corrections (FBP(NO)) data have similar image appearance with the lowest definition and contrast. Quantitatively, concentrating on striatal uptake, if it is assumed that correction for all physical effects (ACSCRM) correctly measures the striatal uptake; attenuation and triple energy window (TEW) scatter correction (ACSC) gives 65.4% of the ACSCRM count concentration; and attenuation and scatter correction individually give 77.3% and 24.9% of the same count concentration, respectively. TEW scatter correction subtracts counts from the data prior to reconstruction, which explains the low values when

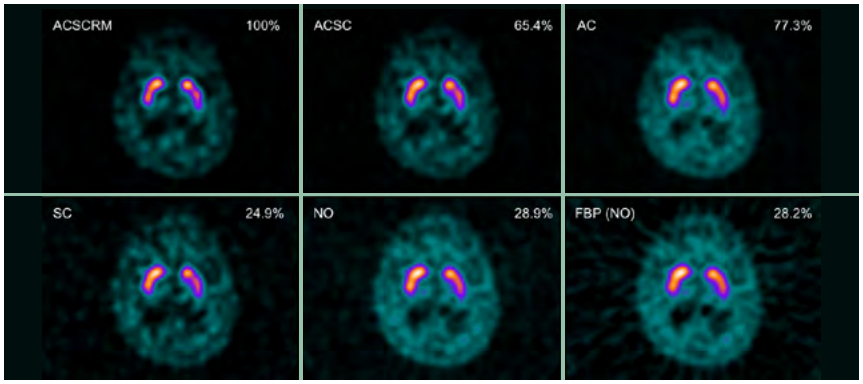

Figure 6. I-123 ioflupane SPECT images reconstructed with iterative reconstruction and: attenuation correction, scatter correction and resolution modelling (ACSCRM); attenuation and scatter correction (ACSC); attenuation correction (AC); scatter correction (SC); and no corrections (NO). Filtered back-projection reconstruction with no corrections (FBP (NO)) and striatal count concentrations normalised to the value from all corrections (ACSCRM) are also shown.

scatter correction is used. The use of no corrections, be it with iterative or filtered back-projection reconstruction, produces low striatal count concentrations. While it might be considered that calibration using matching sets of calibrations would overcome the differences, it is clear from visual interpretation that such a calibration would affect different regions in different ways. This creates considerable challenges in terms of the choice of corrections and calibrations to be used.

A second area where quantitative SPECT can differ between users is in the use of iterative reconstruction. Reconstruction using iterative techniques such as OSEM uses multiple estimates of the image, making comparisons with the projection data that has been acquired (18). With each iteration, the reconstruction updates to a better estimate and provides a more accurate quantitative value in the image. However, the technique gets noisier with increasing number of iterations, so it is normal to stop at a point at which the image is acceptable from a noise and contrast perspective. As a consequence, the value of uptake may not be accurate. Given that the convergence (the rate at which the iterative reconstruction reaches the correct answer) changes from image to image and indeed within the image, stopping the reconstruction early means that the quantitative values are not consistent within the image and between imaging studies. Furthermore, the stopping point may be different at different imaging centres, or with different SPECT systems. Fortunately, these issues can be overcome by having a later stopping point in the reconstruction to ensure that the reconstruction consistently reaches the correct answer in the image, with any excess noise handled by a post- reconstruction smoothing filter. Figure 7 shows how the change in iteration number changes the quantitative value and the noise in the image.

Visual assessment of the data in Figure 7(a) shows the expected progress in the formation of the image with increasing numbers of iterations and subsets. In the central panel which is at 5 iterations and 10 subsets, the image appears to be completely resolved. This is supported by Figure 7(b), where striatal uptake has plateaued. Typically, reconstructions are stopped before this number of iterations and subsets. Figure 7(c) also shows the increasing level of noise in the data, although the use of a post-reconstruction filter controls the increasing levels of noise to a point where it again plateaus just beyond 5 iterations and 10 subsets.

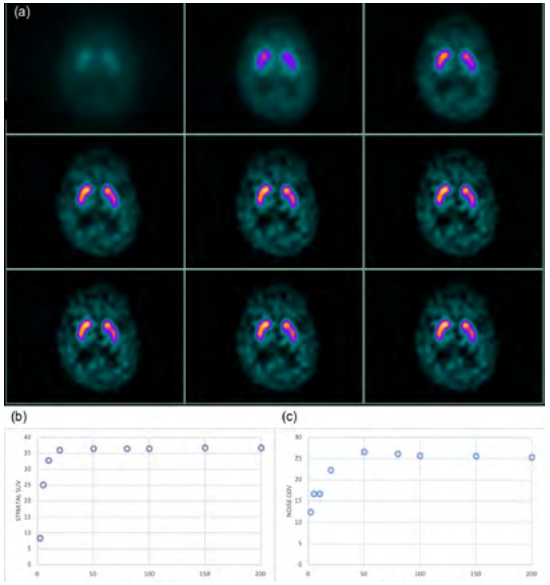

Figure 7 (a). I-123 ioflupane SPECT images reconstructed with increasing number of iterations and subsets in the OSEM reconstruction. Charts showing the change in quantitative value in the lesion (b), and the increasing level of noise in the background (c) with increasing number of EM-equivalent iterations. EM-equivalent iterations is the product of iterations and subsets

Visually, the noise is acceptable throughout the reconstruction series. This shows that it is possible to iterate far enough to reach convergence while keeping image noise to acceptable levels.

One other aspect to be aware of with quantitative SPECT comes as a consequence of the limited spatial resolution available on such systems. For technetium-99m imaging, reconstructed spatial resolution is typically around 8-10mm, although when using medium or high-energy collimators with Lu-177 and I-131 respectively, the spatial resolution can be worse. Using resolution modelling in the tomographic reconstruction can improve the spatial resolution a little. Imaging of features less than 2.5 times the spatial resolution of the system will result in an underestimation of the SUV because of the partial volume effect, as demonstrated in Figure 8a. Taking a profile through a small, medium and large feature represented by the solid box, the effect of spatial resolution represented by the red lines shows that for a large feature, the maximum intensity such as SUV_{max} will be recovered, although the SUV mean will be reduced slightly because of the loss of resolution at the edges. In the medium-sized feature, the maximum value within the region will again be recovered while the mean value in the region is significantly underestimated, and in the small feature both the maximum and mean values are under-represented. This simple example does not demonstrate activity outside the region, where there

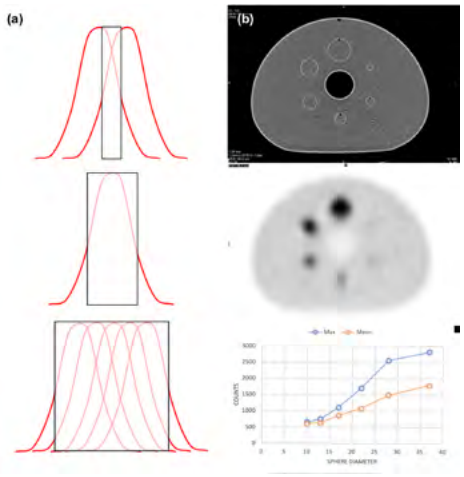

Figure 8 (a) Three rectangular profiles representing small, medium and large features with increased activity. The red lines demonstrate the effect on apparent maximum and mean uptake due to the limited spatial resolution of SPECT (b) A phantom experiment with technetium-99m showing the apparent differences in visual and quantitative uptake in features due to the partial volume effect.

will also be a spill-in of counts from the surrounding area, but it does show the known underestimation of volumes within SPECT, and also why segmentation techniques often define lesion boundaries as around 40% of the maximum count level. Figure 8(b) shows the effect on a NEMA image-quality phantom, where different-sized hot lesions containing the same activity concentration show different visual and quantitative values of uptake. As a consequence, users of quantitative SPECT must be aware that the uptake of small features in an image will be underestimated. Note that because of edge effects, the mean value within the region is always less than the maximum value.

Partial volume correction algorithms are available that help correct for these types of effects (19). Partial volume issues are a challenge in both PET and SPECT, and although correction algorithms have so far been used mostly for PET applications, algorithms are now also being used in SPECT . However, these types of correction are almost exclusively used for research applications. Motion correction is another growing area of research in quantitative SPECT. Respiratory and cardiac motion can cause a significant degradation in the achievable spatial resolution of a system, with the motion blurring out an image taken over multiple respiratory and/or cardiac cycles. Although corrections for motion in PET have been available for some time, solutions are more complex in SPECT because of the rotating detectors used. Nevertheless, algorithms are now starting to appear in this area too (21).

ACCURACY AND PRECISION

Applying various corrections and using an increasing number of iterations during the reconstruction may improve accuracy by reducing the bias in a value, but as a consequence they may reduce the precision, i.e. they can increase the noise/uncertainty in the value. Careful decisions should therefore be made regarding what is needed from the imaging investigation. Figure 9 (a) shows a cross-sectional study where the data has been reconstructed using two methods – one with low bias but low precision, and the second with a larger bias (inaccuracy) but better precision (lower uncertainty). The lower normal range cut-off point for both reconstructions is shown by the dashed lines. The figure demonstrates that a higher precision (lower uncertainty) clearly places the value above the normal value, while with the lower precision result it is unclear whether the value is normal or not. Similarly, in Figure 9(b), which shows repeat longitudinal measurements pre and post intervention, the lower uncertainty makes it clearer whether

there has been a real change in value. Of course, the ideal would be very low bias and very high precision. In SPECT as in PET, however, the incorporation of reconstruction corrections and the use of more iterations brings more uncertainty into the measurement.

STANDARDISATION AND HARMONISATION

Having different values of uptake from different sites and systems is clearly not helpful if normative comparative values are required in cross-sectional studies, nor is it helpful in follow-up studies if the results are acquired on different systems or at different sites. As with PET, there is therefore a clear need for harmonisation. For centres involved in multi-centre trials, or in single-centre research studies, core labs or principal investigators will often stipulate parameters to ensure consistency in data (22). It has also been shown that this approach can work in quantitative SPECT (23). It is hoped that guidelines and/or accreditation such as that defined by EARL for PET applications will result in more consistent and comparable quantification of SPECT data.

A final issue that is hampering the standardisation of quantitative SPECT is beyond the control of users and sites. At the time of writing there is no DICOM definition for quantitative SPECT. As a consequence, quantitative image data is proprietary to the system, and not transferrable to PACS for reporting or review. While some independent software platforms are capable of reading this proprietary data, this issue needs to be resolved for the technology to be a success.

CLINICAL IMPLEMENTATION OF QUANTITATIVE SPECT

At the time of writing there are four general quantitative SPECT platforms, which will be presented in alphabetical order below.

GE Healthcare have their Q.Volumetrix MI suite, which takes injected activity data and body habitus data at the scanner and a planar sensitivity factor for each radionuclide to provide reconstructed data in terms of activity concentration and SUV. The reconstruction uses OSEM iterative reconstruction and applies CT attenuation, dual/triple energy window scatter correction and resolution modelling. Some of these factors can be turned off, but it is recommended that they are all left on for the best quantitative value. This software will only accept projection data from appropriate GE scanners (Figure 10a).

Hermes Medical Solutions offer their Hybrid Recon package, which can create

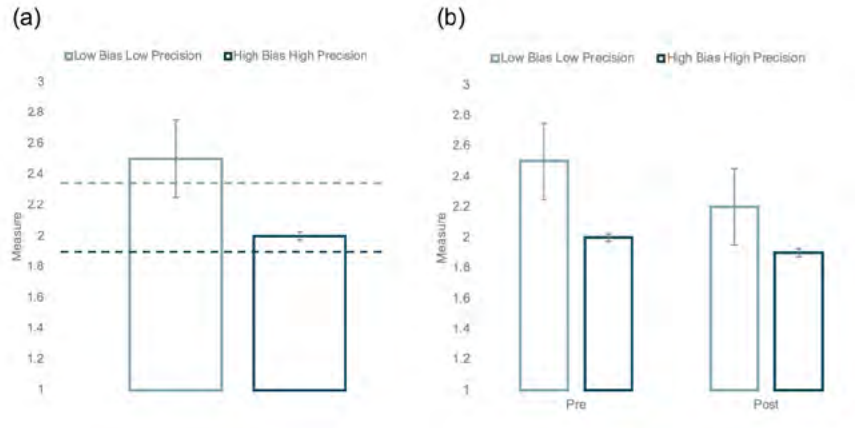

Figure 9 (a) Bar charts showing a cross-sectional measurement using a technique with low bias and low precision (light blue), and high bias and high prevision (dark blue). The normal values for each measurement are shown as a dashed line in each colour. While a low bias may give a more accurate value, low precision gives uncertainty whether the value is normal or abnormal, while higher precision clearly shows the value to be normal. (b) The same low bias low precision and high bias high precision data shown in a longitudinal study, pre and post intervention. Once more the low precision gives uncertainty in how the disease has progressed while the high precision measurements show treatment response.

quantitative SPECT data irrespective of the SPECT manufacturer so long as they have a sensitivity factor for the required radionuclide and collimator information to perform resolution modelling. CT attenuation correction, Monte Carlo scatter correction and motion correction are also available. Here again, patient injection and body habitus information are required to create images of activity concentration and SUV, which in this instance are entered at the processing workstation (Figure 10b).

MIM in their SPECTRA Quant product again offer software that works with all SPECT systems. CT-based attenuation correction, energy window scatter correction, motion correction and resolution modelling are incorporated into the iterative reconstruction, which together with volume sensitivity measurements for each radionuclide produces images of activity concentration or SUV. Operationally, injection information and body habitus information are entered in the software. MIM also extend this concept further to include dosimetry tools in their SurePlan software, which has the capability to produce dose maps and dose-volume histograms for molecular radiotherapy applications (Figure 10c).

Siemens have two products for quantitative SPECT: xSPECT Bone, which is optimised for bone SPECT studies,

and xSPECT Quant which extends the application into theranostics. Once more, reconstructions include corrections for attenuation, scatter correction (TEW) and resolution, although in this instance a conjugate gradient rather than a standard OSEM algorithm is used. The choice of a conjugate gradient algorithm results in quicker convergence than standard OSEM. xSPECT bone also incorporates extra-modal information from the CT in the form of zone maps to give sharper definition and determination of uptake within bone tissue, while xSPECT Quant includes an option for a NIST-traceable calibration source that automatically calibrates the system in terms of activity concentration. An alternative Tc-99m-based protocol is also available for sensitivity calibrations (Figure 10d).

SUMMARY

Absolute quantitative SPECT has the potential to become a powerful tool in nuclear medicine. Its advantages in theranostics are obvious, while its possibilities in bone SPECT and other SPECT applications are growing. There are some challenges, however. At the time of writing, the lack of a DICOM standard for quantitative SPECT is an impediment. The consequential loss of PACS and general compatibility across various workstations for this data is problematic, although it does not prevent reporting on manufacturer-specific or manufacturer-independent workstations. Other issues surrounding reconstruction and harmonisation are similar to those seen in PET, and operational issues are relatively easy to overcome.

SPECT has been a feature of nuclear medicine for some time now. The addition of absolute quantification elevates its usefulness and is generating increased interest in the modality.

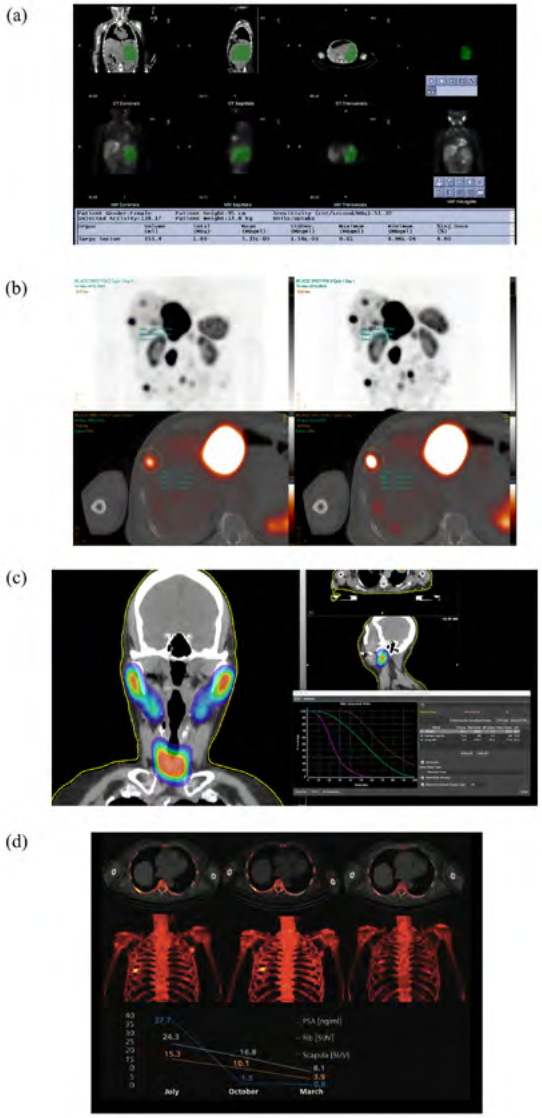

Figure 10 (a) An Iodine-123 mIBG SPECT/CT study showing SUV and tumour volume metrics using GE Q.Metrix. (b) Day 0 and Day 1 Lu-177 DOTATATE SUV SPECT images, quantitative reconstruction performed with Hybrid Recon from Hermes Medical Solutions, images displayed in Affinity Viewer (Image courtesy of Hermes Medical Solutions). (c) Dose contours and dose volume histograms following a radionuclide therapy using MIM Sureplan (Image courtesy of MIM Software Inc.) (d) A longitudinal Tc-99m MDP series showing the change in SUV in Rib and Scapula bone lesions using xSPECT Quant (Image courtesy of Siemens Healthineers).

REFERENCES

1. Ritt P, Vija H, Hornegger J, Kuwert T. Absolute quantification in SPECT. Eur J Nucl Med Mol Imaging. 2011;38(SUPPL. 1):69–77.
2. Kaneta T, Ogawa M, Daisaki H, Nawata S, Yoshida K, Inoue T. SUV measurement of normal vertebrae using SPECT/CT with Tc-99m methylene diphosphonate. Am J Nucl Med Mol Imaging [Internet]. 2016;6(5):262–8. Available from: www.ajnmmi.us
3. Brady SL, Shulkin BL. Analysis of quantitative [I-123] mIBG SPECT/CT in a phantom and in patients with neuroblastoma. EJNMMI Phys. 2019;6(1).
4. Ballinger JR. Theranostics and precision medicine special feature : Review Article Theranostic radiopharmaceuticals : established agents in current use. Br J Radiol. 2018;91(December 2017):20170969.
5. Welsh JS, Kennedy AS, Thomadsen B. Selective internal radiation therapy (SIRT) for liver metastases secondary to colorectal adenocarcinoma. Int J Radiat Oncol Biol Phys. 2006;66(SUPPL. 2):62–73.
6. Siegel JA, Thomas SR, Stubbs JB, Stabin MG, Hays MT, Koral KF, et al. MIRD pamphlet no. 16: Techniques for quantitative radiopharmaceutical biodistribution data acquisition and analysis for use in human radiation dose estimates. J Nucl Med. 1999;40(2):37–62.
7. Dewaraja YK, Frey EC, Sgouros G, Brill AB, Roberson P, Zanzonico PB, et al. MIRD pamphlet no. 23: Quantitative SPECT for patient-specific 3-dimensional dosimetry in internal radionuclide therapy. J Nucl Med. 2012;53(8):1310–25.
8. Suh MS, Lee WW, Kim YK, Yun PY, Kim SE. Maximum standardized uptake value of 99mTc hydroxymethylene diphosphonate spect/ct for the evaluation of temporomandibular joint disorder. Radiology. 2016;280(3):890–6.
9. Duncan I, Ingold N. The clinical value of xSPECT/CT Bone versus SPECT/CT. A prospective comparison of 200 scans. Eur J Hybrid Imaging. 2018;2(1).
10. De Laroche R, Simon E, Suignard N, Williams T, Henry MP, Robin P, et al. Clinical interest of quantitative bone SPECT-CT in the preoperative assessment of knee osteoarthritis. Med (United States). 2018;97(35).
11. Kuji I, Yamane T, Seto A, Yasumizu Y, Shirotake S, Oyama M. Skeletal standardized uptake values obtained by quantitative SPECT/CT as an osteoblastic biomarker for the discrimination of active bone metastasis in prostate cancer. Eur J Hybrid Imaging. 2017;1(1):1–16.
12. Armstrong AJ, Anand A, Edenbrandt L, Bondesson E, Bjartell A, Widmark A, et al. Phase 3 assessment of the automated bone scan index as a prognostic imaging biomarker of overall survival in men with metastatic castration-resistant prostate cancer a secondary analysis of a randomized clinical trial. JAMA Oncol. 2018;4(7):944–51.
13. Umeda T, Koizumi M, Fukai S, Miyaji N, Motegi K, Nakazawa S, et al. Evaluation of bone metastatic burden by bone SPECT/CT in metastatic prostate cancer patients: defining threshold value for total bone uptake and assessment in radium-223 treated patients. Ann Nucl Med [Internet]. 2018;32(2):105–13. Available from: http://dx.doi.org/10.1007/s12149-017-1224-x
14. Bailey DL, Willowson KP. An evidence-based review of quantitative SPECT imaging and potential clinical applications. J Nucl Med. 2013;54(1):83–9.
15. Boellaard R, Delgado-Bolton R, Oyen WJG, Giammarile F, Tatsch K, Eschner W, et al. FDG PET/CT: EANM procedure guidelines for tumour imaging: version 2.0. Eur J Nucl Med Mol Imaging. 2014;42(2):328–54.
16. Rahmim A, Qi J, Sossi V. Resolution modeling in PET imaging: Theory, practice, benefits, and pitfalls. Med Phys. 2013;40(6):1–15.
17. Nuyts J. Unconstrained image reconstruction with resolution modelling does not have a unique solution. EJNMMI Phys. 2014;1:98.
18. Hudson HM, Larkin RS. Ordered Subsets of Projection Data. IEEE Trans Med Imaging. 1994;13(4):601–9.
19. Thomas BA, Cuplov V, Bousse A, Mendes A, Thielemans K, Hutton BF, et al. PETPVC: A toolbox for performing partial volume correction techniques in positron emission tomography. Phys Med Biol. 2016;61(22):7975–93.
20. Erlandsson K, Thomas B, Dickson J, Hutton BF. Evaluation of an OSEM-based PVC method for SPECT with clinical data. IEEE Nucl Sci Symp Med Imaging Conf. 2010;2686–90.
21. Vija A, Cachovan M. Automated Motion Correction in Quantitative SPECT Reconstruction: A Feasibility Study of a Method Framework Applied First to Bone Imaging. J Nucl Med. 2017;58(Supplement 1):703.
22. Dickson JC, Tossici-Bolt L, Sera T, De Nijs R, Booij J, Bagnara MC, et al. Proposal for the standardisation of multi-centre trials in nuclear medicine imaging: Prerequisites for a European 123I-FP-CIT SPECT database. Eur J Nucl Med Mol Imaging. 2012;39(1):188–97.
23. Peters SMB, van der Werf NR, Segbers M, van Velden FHP, Wierts R, Blokland K (J). AK, et al. Towards standardization of absolute SPECT/CT quantification: a multi-center and multi-vendor phantom study. EJNMMI Phys. 2019;6(1).

4

BONE SCINTIGRAPHY

by Vladimir Vukomanovic,
Vesna Ignjatovic,
Marija Jeremic,
Nenad Mijatovic
and Milos Stevic

INTRODUCTION TO RADIONUCLIDE BONE IMAGING

Various bone conditions, whether neoplastic or of other origin, lead to multifactorial and complex processes that involve reciprocal interplay between osseous cells, surrounding tissue and the stroma itself. Early detection of skeletal disorders is crucial for accurate staging and the implementation of adequate therapeutic options, in order to reduce the risk of complications and improve quality of life.

Over the past decades, advances in the understanding of osseous pathology have led to the development of various diagnostic modalities. Among the imaging techniques currently available, the most frequently performed modality for detection of osseous involvement is radionuclide bone scintigraphy.

BONE SCINTIGRAPHY

Skeletal scintigraphy, commonly known as a "bone scan", is a useful and versatile nuclear medicine method, and has been established as a highly sensitive gold standard diagnostic tool for bone pathology. One of the pathognomonic hallmarks of local bone remodelling is increased mineral turnover and the formation of calcium phosphate salts. A bone scan is a special type of procedure that uses technetium-99m-labelled bisphosphonate compounds to pinpoint the pathological condition which is causing increased osteoblastic activity. Although skeletal scintigraphy is not specific (a wide range of pathological abnormalities produce osteoblastic activity), its exceptional sensitivity, relative inexpensiveness and wide availability make it a useful screening tool for many pathological conditions of bones and joints.

Although protocols vary among institutions, a bone scan is typically performed through three phases of imaging:

The 1st (dynamic) phase reflects the radionuclide angiogram and is obtained for 60-90 seconds, immediately after i.v. administration of ^{99m}Tc-labelled bisphosphonates (adults: 8-10 MBq/kg/; children: EANM/SNMMI paediatric protocol).

The 2nd (blood pool) phase is obtained immediately after the flow phase for up to 10 minutes, and reflects tracer activity that has extravasated into the soft tissue.

The 3rd (delayed) phase of imaging is usually performed 2-5 hours after tracer injection and reflects the rate of bone turnover. This delay allows optimal clearance and higher uptake of the tracer, producing an adequate target/non-target ratio.

The most common bone scan indications are primarily imaged using the delayed phase protocol only, which is mainly used in oncology studies.

A bone scan is usually acquired using a gamma camera in whole-body scanner modality. Additionally, the nuclear medicine technologist can obtain planar anterior and posterior spot view images of the skeleton as needed. Single photon emission computed tomography (SPECT) produces cross-sectional images in orthogonal planes, which facilitates both contrast and precise anatomical localisation. Although SPECT is not generally performed as a stand-alone modality, tomographic images are particularly useful for unequivocal imaging of skeletal tracer uptake, especially in anatomically complex structures such as spine and skull. The technologist should repeat the procedure if the images are sub-optimal due to patient movement, urinary contamination, or attenuation from jewellery, clothing or medical devices.

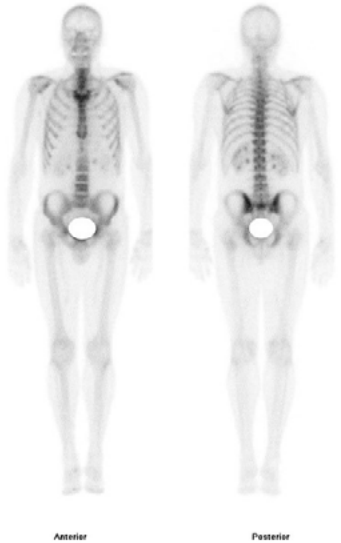

Figure 1. Normal appearance of ^{99m}Tc-labelled bisphosphonate "whole-body" scan

Normal scintigraphic findings

An understanding of the normal physiological distribution of radiolabelled bisphosphonates is important for correct interpretation of skeletal scintigraphy.

Symmetrical and homogeneous tracer distribution throughout the osseous structures is the normal physiological finding in healthy adults, with clear delineation of the ribs and vertebral structures. Furthermore, faint or increased symmetrical areas of benign tracer uptake are present at the paired joints (glenohumeral, acromioclavicular, sternoclavicular, sternomanubrial,

sacroiliac and pubic symphysis, acetabulofemoral, tibiofemoral and patellofemoral, talocrural) and in the calvarial region, which corresponds to hyperostosis frontalis in women (Figure 1). In children, intense symmetric uptake in the physes of the long bones represents the normal growth centres. The accumulation of tracer in the above-mentioned anatomical structures generally decreases with age.

Critical scintigraphic findings

Abnormalities on bone scan are indicated as areas of increased focal tracer uptake which reflect generally increased bone mineral turnover, with higher sensitivity for osteoblastic than for osteolytic bone lesions. Accurate interpretation can be particularly difficult without adequate clinical experience, and should not be confidently assigned to a definite pathology. Bone scans should therefore be performed under the supervision of a physician specialising in nuclear medicine.

The nuclear medicine technologist, however, must take into account the shape and location of the tracer uptake in order to quickly recognise areas of increased activity, so-called "hot spots". Moreover, the technologist can assess the tracer uptake pattern: monostotic vs. polyostotic, axial vs. appendicular, periarticular vs. metaphyseal-diaphyseal, focal vs. linear or spindle-like. Since most bone scans are performed as an integral part of oncological disease staging and management, an experienced technologist can precisely identify patterns of ***osseous*** metastases. The presence of multiple, randomly increased tracer uptake, varying in size, shape and intensity, is highly suggestive of bone metastases and requires no further clarification. Traumatic and degenerative disorders can differ from metastatic disease by virtue of their characteristic distribution and location.

Extraosseous activity can be seen as faint renal and minimal soft-tissue activity. Due to the normal renal tracer excretion, urinary bladder is also normally present on scans. Absence of renal and bladder activity should raise suspicion of a so-called "superscan", which corresponds to diffusely increased osseous uptake throughout much or all of the skeleton due to metastatic disease.

A variety of conditions can often manifest as areas of decreased tracer uptake, such as metastatic osteolytic disease or the late phase of radiation osteitis after radiation therapy. On the other hand, chemotherapy affects bone scan findings by means of increased intensity or the appearance of new foci as a result of bone matrix regeneration responding to treatment ("flare" phenomenon).

Increased soft-tissue and extraosseous tracer uptake of bisphosphonates must be taken into account, since the latter can be seen in various pathological conditions.

Other bone imaging techniques

Although bone scan is highly sensitive for skeletal disorders, the modality itself is not specific and may require further clarification with other imaging modalities.

Compared to conventional radiography, bone scintigraphy is a sensitive technique which enables osseous lesions to be detected up to several months earlier.

Positron emission tomography (PET) is superior to conventional bone scan in terms of providing quantitative standardised uptake value (SUV) and a higher spatial resolution. The radiopharmaceuticals which are most frequently used in PET bone studies are sensitive for osteoblastic and osteolytic bone lesions. PET skeletal imaging continues to evolve, and will almost certainly become increasingly important in the future.

To improve specificity, complementary imaging modalities such as computed tomography (CT) and magnetic resonance (MR) are often performed to provide additional structural anatomical information on bone remodelling. Contrast-enhanced CT enables the visualisation of cortical and trabecular bone with high resolution, while MR imaging can be used to obtain excellent soft-tissue resolution of the marrow cavity and surrounding structures.

Since all bone imaging modalities have strengths and weaknesses, hybrid imaging techniques such as SPECT/CT, PET/CT and PET/MR increase sensitivity, specificity and accuracy. As a result, the technologist can determine if abnormal radionuclide uptake corresponds to suspicious osseous lesion on cross-sectional imaging. The highest diagnostic yield for skeletal pathology can therefore be obtained by using a combination of these imaging modalities.

RADIOPHARMACEUTICALS FOR BONE LESION ASSESSMENT

^{99m}Tc-diphosphonates

^{99m}Tc-labelled diphosphonates are the most widely used radiopharmaceuticals. ^{99m}Tc decays by isomeric transition with a half-life of 6.02 h to ^{99}Tc by emitting one 140.5-keV gamma ray per decay. The molecules most commonly used for performing bone scintigraphy are methylene diphosphonate (MDP), hydroxymethylene diphosphonate (HMDP) or hydroxyethylene diphosphonate (HDP), and 2,3-dicarboxypropane-1,1-diphosphonate (DPD).

Pharmacokinetics: The injected radiolabelled diphosphonates adsorb to the surface of hydroxyapatite crystals in

proportion to local bone vascularisation and osteoblastic activity. After intravenous administration, the clearance from the vascular compartment is fast, with half times of 2–4 min. Peak uptake varies for the different agents, but is usually around 1 h. Four hours after injection, approximately 50 to 60% of the injected amount is fixed in the skeleton, the unbound fraction (34%) is excreted in the urine, and only 6% remains in circulation.

The diphosphonates listed above are commercially available and supplied in a vial containing the diphosphonate, a stannous reducing agent and other excipients in the form of a powder ready for labelling. The radiopharmaceutical is prepared by addition of the required amount of sodium pertechnetate diluted in sterile physiological saline to the vial in accordance with the manufacturer's instructions. Because the radiopharmaceutical is susceptible to oxidation, care should be taken to avoid introducing air into the multidose vial during preparation or removal of doses. The radiopharmaceutical should be used within 6 h of preparation unless allowed otherwise by the manufacturer. For bone scintigraphy in adults, the average activity administered by a single intravenous injection should be 300 – 740 MBq (8 – 20 mCi). The administered activity usually ranges between 8 and 10 MBq/kg for adults, but may be increased to 11–13 MBq/kg. For children, the administered activity is based on body weight according to the guidelines of the European Association of Nuclear Medicine (EANM)/ SNMMI Paediatric Dosage Harmonization Working Group. The typical paediatric dose is 170–210 MBq (~4–6 mCi), with a minimum of 20–40 MBq (0.5–1.0 mCi) and a maximum not exceeding the maximum for a healthy adult.

Optimal imaging is 2–4 h after tracer administration. At this time point about one third of the administered dose is bound to bone, one third is excreted in the urine and the remainder is associated with other tissues. Of the administered activity, approximately 30% is cleared within the first hour, 48% within 2 h and 60% within 6 h. Renal excretion is the primary route for elimination; the renal elimination rate of ^{99m}Tc-diphosphonates depends mainly on glomerular function. Tracer elimination through the gastrointestinal tract is insignificant.

Adverse reactions to the injection of the radiopharmaceutical are virtually non-existent. The reported incidents are usually related to other agents in the kits that are necessary for stabilisation, e.g. pH buffers, reducing agents to keep technetium in the allowed valence state, and/or metabolites.

Interactions:

Bisphosphonates – clodronic acid and etidronic acid: stop 2 weeks before scintigraphy.

Tetracycline antibiotics: stop at least 2 h before scintigraphy.

Medication containing iron: increased extraossal accumulation of the radioisotope has been reported for iron-containing ingredients.

Drugs containing aluminium, notably antacids, may lead to abnormally high accumulation of ^{99m}Tc in the liver, presumably caused by the formation of labelled colloids.

^{18}F-sodium fluoride

The mechanism of uptake of ^{18}F-sodium fluoride is similar to other bone tracers used in nuclear medicine and depends on regional blood flow and osteoblastic activity. It is preferentially deposited by chemisorption onto bone surfaces, exchanging with hydroxyl groups in hydroxyapatite crystal of bone to form fluoroapatite.

$2F^- + Ca\ 10(PO4)\ 6(OH)\ 2 \rightarrow Ca\ 10(PO4)6F2 + 2OH^-$

The skeletal uptake of ^{18}F-sodium fluoride (NaF) is quite high, approximately 70%, and 25% is excreted in the urine by 6 h. As regards imaging time, the fluoride scan can be completed within 2 h of ^{18}F-sodium fluoride administration. Since the plasma protein binding of ^{18}F-NaF is low, fluoride ions are freely filtered in the glomeruli. Fluoride, however, also undergoes tubular reabsorption. As a result, renal clearance of ^{18}F-NaF is dependent on overall urinary flow, because tubular reabsorption of fluoride increases with decreasing glomerular filtration rate. Therefore, it is recommended that patients undergoing ^{18}F-sodium fluoride PET be well hydrated to reduce radiation exposure.

With ^{18}F-sodium fluoride and dynamic PET imaging, certain

RADIONUCLIDE	PHYSICAL HALF- LIFE	CHEMICAL FORM	PRINCIPAL PHOTON ENERGY (KEV)	ADMINISTERED ACTIVITY IN ADULTS (MBQ)
^{18}F	1.8h	Fluoride	511	110-370
^{99m}Tc	6h	MDP, HDP, HMDP	140	600-800

Table 1: Diagnostic radionuclides for bone scintigraphy

physiological and biochemical bone parameters can be measured in vivo. These quantitative indices are the measurement of local bone blood flow and fluoride influx rate. ^{18}F-fluoride is injected intravenously; activity for adults is 185–370 MBq (5–10 mCi). A higher activity may be used in obese patients. Paediatric activity should be weight-based: 2.22 MBq/kg (0.06mCi/kg), using a range of 18.5–185 MBq (0.5–5mCi)

SPECIFIC TECHNIQUES AND THEIR USEFULNESS IN ONCOLOGICAL AND NON-ONCOLOGICAL DIAGNOSIS

List of most common indications for bone scintigraphy

» Oncology: primary bone tumours and bone dysplasia (osteosarcoma, osteoid osteoma, osteoblastoma, fibrous dysplasia, giant cell tumour and osteopoikilosis) and metastatic disease (prostate, breast, lung, renal cancer and paraneoplastic syndromes);

» Orthopaedics, sports & traumatology: periostitis, enthesopathies, spondylolisthesis, stress-related and insufficiency fractures;

» Paediatrics: osteochondritis of the hip (Legg-Calvé-Perthes disease) transient synovitis of the hip, battered child syndrome, bone infarction (sickle cell disease, thalassaemia);

» Rheumatology: rheumatoid arthritis, spondyloarthropathies and related disorders, osteoarthritis, osteonecrosis and bone infarction;

» Diagnosis of infectious lesions, such as osteomyelitis and spondylodiscitis;

» Exploration of unexplained symptoms.

Usefulness of each modality in terms of diagnosis

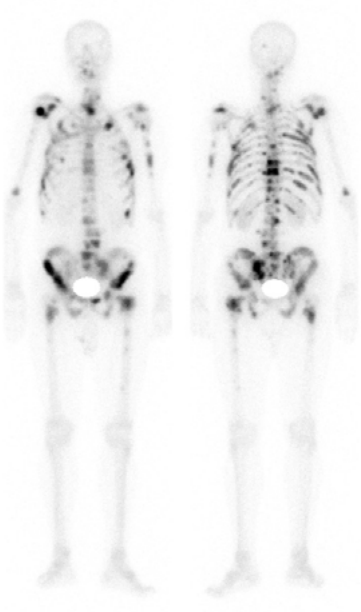

Figure 2. Multiple secondary deposits of prostate adenocarcinoma. The multiple foci of high tracer uptake in the skeleton. "Whole-body" modality

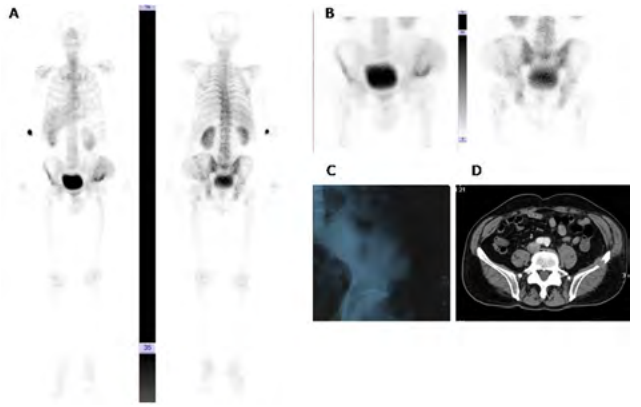

Figure 3. Primary bone tumour of the left iliac bone, from its ridge to the projection of the anterior inferior iliac spine. A. "Whole-body" modality. B. Spot scintigram of the pelvic region. C. RTG of the left iliac bone D. MSCT of the left iliac bone.

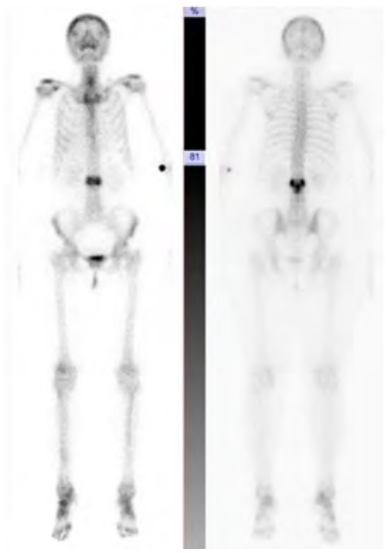

Figure 4. Paget's disease of the second lumbar vertebra (Mickey Mouse Sign). "Whole-body" modality.

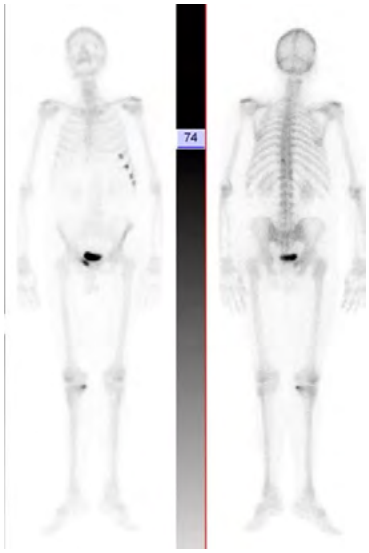

Figure 5. Trauma to the anterior portions of the 7th, 8th, 9th and 10th ribs. "Whole-body" modality.

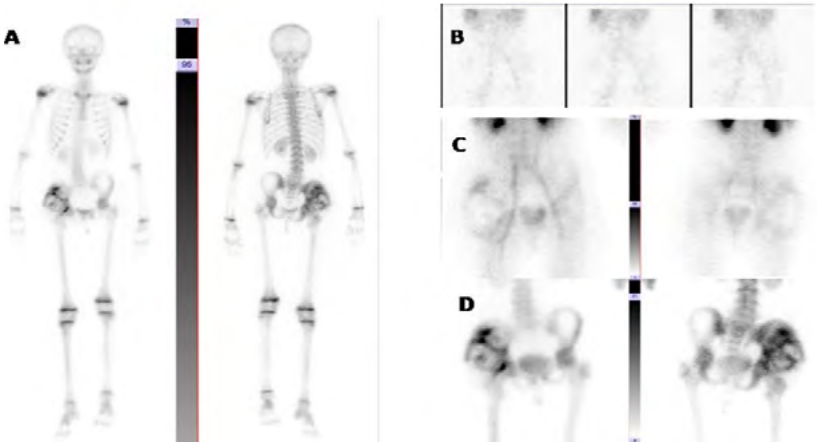

Figure 6. Monostotic fibrosis of the right iliac bone. (Jaffe-Lichtenstein Sy). A. "Whole-body" modality. B, C and D. Three-phase bone scintigraphy

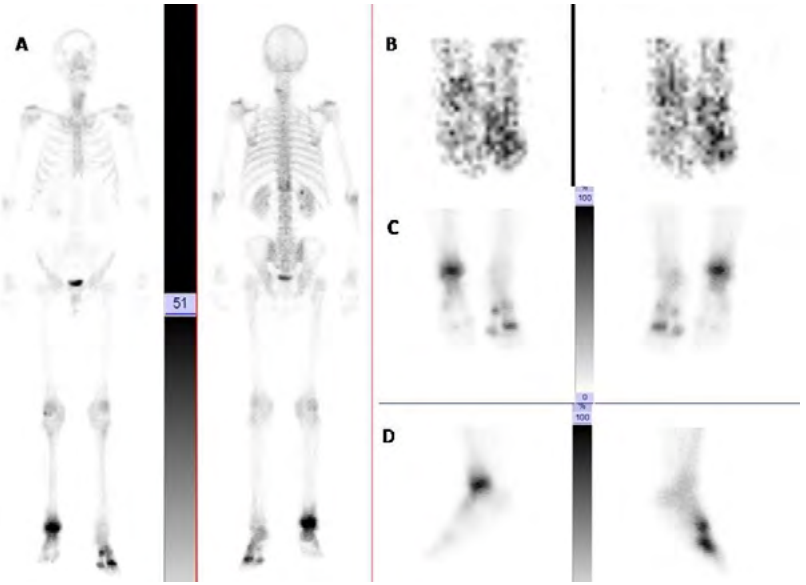

Figure 7. Three-phase bone scintigraphy. Left foot osteomyelitis and right ankle injury. A. "Whole-body" modality. B, C and D. Three-phase bone scintigraphy modality. B, C and D. Three-phase bone scintigraphy

THE SPECIFIC ROLE OF THE NUCLEAR MEDICINE TECHNOLOGIST IN BONE SCINTIGRAPHY

The nuclear medicine technologist performs an important role in skeletal scintigraphy, starting from the patient reporting to the nuclear medicine department in order to confirm the correct diagnosis and the degree of urgency for performing the procedure. After completion of the examination, the technologist obtains from the patient the basic information needed to determine whether the procedure is feasible:

» Does the patient suffer from claustrophobia?;
» Can the patient lie on his/her back for 20 min?;
» Is the patient pregnant or planning a pregnancy, or is she breastfeeding a baby?;
» Check if the patient is allergic to any medicines;
» Blood pressure and body temperature should be measured.

The technologist then explains the procedure to the patient before administering a specific dose of radiopharmaceuticals, based on body weight and patient age. The patient now has to wait in a separate room for a minimum of 2 hours before the scan takes place. During this time the patient is allowed to eat, take his/her regular therapy, preferably drink at least 1L of water, and urinate regularly. After this period, the patient is told to empty the urinary bladder, and is called to a room with a gamma camera where whole-body scintigraphy will be performed.

Prior to scintigraphy, the patient should remove all metal objects such as belt, watch, glasses, jewellery, etc. Then the patient is instructed to lie down on his/her back, with hands next to the body and legs horizontal; he/she must remain motionless and breathe normally. The technologist checks whether the radiopharmaceutical has been administered using shield partition as well as whether the patient has emptied his/her bladder. If the radiopharmaceutical is administered paravenously, the technician covers that part of the arm with lead foil and checks if valid diagnostic information can be obtained. If a valid scintigram cannot be obtained, a re-scan is scheduled. If the patient has not emptied his/her bladder, he/she is asked to urinate again.

Scanning usually takes 20 minutes. If, due to inability to urinate, the bladder has covered a large part of the pelvis, then scintigraphy in SPECT or SPECT/CT modality can be performed; this is decided by a nuclear medicine specialist. After the scintigraphy has been completed, the patient is instructed on further behaviour for the next 24 hours: children and pregnant women should be avoided, keeping a distance of at least 2 metres and

not spending too long in the same room. The toilet should be flushed twice every time. If the patient is breastfeeding, she must be told to delay breastfeeding for at least 4 hours.

RESPONSIBILITIES OF THE NUCLEAR MEDICINE TECHNOLOGIST IN PREPARATION OF THE IMAGING EQUIPMENT

Whole-body scintigraphy

Whole-body (WB) scanning is a routine and common procedure for bone scintigraphy for which low-energy, high-resolution, parallel-hole (or all-purpose) collimators are used. The energy window should be centred at 140 keV with the window width between 15% and 20%. The matrix size should be 1024x256 or 2048x512. A scan speed of 12 cm/min is recommended (although it can range from 8 cm/min to 12 cm/min, depending on the manufacturer and performance of the gamma camera) with the auto-contour option ON. The scan is performed in anterior and posterior projections. Before scanning, the technologist checks whether all criteria are fulfilled and adjusts the scan length to the patient's height. The majority of devices are pre-set to a scan length of 200 cm, but this can be adjusted in order to reduce the time required for scanning.

Planar scintigraphy

Planar scintigraphy has very wide applications in almost all nuclear medicine procedures. Depending on the diagnostic information requested, various collimators can be used. Low-energy, high-resolution parallel-hole collimators are most commonly used in routine work, although other collimator types may be used for lower energies. The matrix size should be 256x256 or 512x512. The nuclear medicine specialist (physician) decides whether or not to switch the zoom option ON. The duration of the scan can be determined by the number of counts registered, or by time. In routine work, the number of counts collected is usually 500 000, but 300 000 counts can be used for arm, hand, foot or some another lateral patient positions. These specifications are for standard single-head or dual-head gamma cameras.

For some small lesions, the nuclear medicine specialist can request a pinhole collimator. These collimators have a high resolution and a small field of view. The following acquisition parameters are recommended: photo peak at 140 keV±10%, matrix size 256x256 or 512x512, and total number of counts 100 000.

Planar images do not require special processing, although contrast and colour can be adjusted according to the nuclear medicine specialist's instructions. The option threshold can be used to adjust the contrast to facilitate the physician's analysis of the images.

Three phase bone scintigraphy

Three phase bone scintigraphy starts with the so-called "angiographic phase", i.e. a fast dynamic scan immediately after intravenous application of the radiopharmaceutical. The technologist places the patient in the correct position on the gamma camera so that the area of interest is in the centre of the detector field of view. The dynamic scan starts at the same moment as administration of the radiopharmaceutical, using the following parameters: photo peak at 140 keV±10%, matrix size 128x128, 32 to 64 frames, duration of frames 2 to 3 s each. This phase is also called the "flow phase".

The second phase is also called the "blood pool phase ". Scanning starts 1 to 10 min after administration of the radiopharmaceutical. The recommended duration of the scintigraphy is 3 to 5 min, with a matrix size of 256x256 or 512x512. Quantification is performed using the region of interest (ROI) method, where uptake in target tissues is compared with uptake in healthy surrounding tissues.

The third phase is the "delayed phase ", which is conducted 2 to 5 hours after initial administration of the radiopharmaceutical. Various imaging methods can be used in this phase, one option being planar scintigrams with matrix size 256x256 or 512x512, the number of counts depending on the region under investigation: at least 700,000 to 1,000,000 counts for the thoraco-abdominal region, 250 000 to 400 000 counts for the large joints and skull, and 150 000 to 250 000 counts for the distal joints, depending on the field of view of the gamma camera. In this phase SPECT or SPECT/CT imaging can also be performed, depending on the type of gamma camera available.

SPECT AND SPECT/CT SCANS

Depending on the requirements of the nuclear medicine specialist and the available options on the gamma camera, acquisition of SPECT or SPECT/CT scans is sometimes necessary on some region of the patient's body. It is difficult to give general recommendations for scanning parameters in this situation. Depending on the kind of camera and its performance/ the area to be scanned, parameters for a typical dual-head camera could be as follows: matrix size 256x256, 64 frames per detector head, each with a duration of 10 to 30 s for each detector position. The duration of frame depends on the size of the region, its anatomical localisation and uptake in the surrounding tissues and organs.

If the nuclear medicine specialist insists on SPECT/CT acquisition, CT should be done immediately after SPECT if the patient is still on the table. The field of view (FOV) of hybrid devices is large, and the default option is the same FOV for CT as for SPECT acquisition. The nuclear medicine specialist should be consulted about the FOV for CT, and if possible, the latter should be reduced to optimise the dose received by the patient during the examination. For SPECT/CT acquisition the following parameters are recommended: matrix size 256x256, 32 or 64 frames per detector head respectively, each with a duration of 10 s to 30 s, with a tube voltage of 80–130 kV and an intensity–time product of 2.5 to 300 mAs, depending on the anatomical region being scanned. Optimisation factors such as small variations in voltage and milliamperes should be examined to assess how they affect the patient dose. Local diagnostic reference levels (DRL) may be applied, if established in the country or hospital in question.

It is recommended that reconstruction be performed with the three-dimensional ordered-subset expectation maximization iterative algorithm (OSEM), including corrections for attenuation and scattering. Typically, three or five iterations are necessary and eight to ten subsets. Reconstructed images are shown as two-dimensional cross-sections in the axial, coronal and sagittal plane together with the cross-section obtained by CT fusion imaging, but they could also be shown separately.

CHAPTER REFERENCES

1. Agrawal K, Marafi F, Gnanasegaran G, Van der Wall H, Fogelman I. Pitfalls and limitations of radionuclide planar and hybrid bone imaging. Semin Nucl Med 2015;45(5):347-72.
2. Bartel TB, Kuruva M, Gnanasegaran G, et al. SNMMI procedure standard for bone scintigraphy 4.0. J Nuc Med Technol 2018;46(4):398-404.
3. Blake GM, Park-Holohan SJ, Cook GJ, Fogelman I. Quantitative studies of bone with the use of 18F-fluoride and 99mTc-methylene diphosphonate. Semin Nucl Med 2001;31:28–49.
4. Beheshti M, Mottaghy FM, Paycha F, et al. (18)F-NaF PET/CT: EANM procedure guidelines for bone imaging. Eur J Nucl Med Mol Imaging 2015;42:1767–77.
5. Even-Sapir E, Metser U, Flusser G, et al. Assessment of malignant skeletal disease: initial experience with18F-fluoride PET/CT and comparison between 18F-fluoride PET and 18F-fluoride PET/CT. J Nucl Med 2004;45:272–8.
6. Fogelman I, Gnanasegaran G, Van der Wall H. Radionuclide and hybrid bone imaging. Berlin: Springer; 2013.
7. Heindel W, Gübitz R, Vieth V, Weckesser M, Schober O, Schäfers M. The diagnostic imaging of bone metastases. Dtsch Ärzteb Int 2014;111(44):741–7.
8. Helyar V, Mohan HK, Barwick T, et al. The added value of multislice SPECT/CT in patients with equivocal bony metastasis from carcinoma of the prostate. Eur J Nucl Med Mol Imaging 2010;37(4):706-13.
9. Horger M, Bares R. The role of single-photon emission computed tomography/computed tomography in benign and malignant bone disease. Semin Nucl Med 2006;36(4):286-94.
10. International Atomic Energy Agency. Safety Standards for protecting people and the environment. Radiation Protection and Safety of Radiation Sources: International Basic Safety Standards. General Safety Requirements Part 3, Viena: IAEA; 2014.
11. International Atomic Energy Agency. IAEA-TECDOC-1782. Good Practice for Introducing Radiopharmaceuticals for Clinical Use. Viena: IAEA; 2016.
12. Love C, Din AS, Tomas MB, Kalapparambath TP, Palestro CJ. Radionuclide bone imaging: an illustrative review. RadioGraphics 2003;23(2):341-58.
13. Mattsson S, Johansson L, Leide Svegborn S, et al. Radiation Dose to Patients from Radiopharmaceuticals: a Compendium of Current Information Related to Frequently Used Substances. ICRP Publication 128. Ann ICRP 2015;44(2 Suppl):7-321.
14. McDougall IR. Skeletal scintigraphy. West J Med 1979;130(6):503–14.
15. Nakamoto Y, OsmanM, Wahl RL. Prevalence and patterns of bone metastases detected with positron emission tomography using F-18 FDG. Clin Nucl Med 2003;28:302–7.
16. O'Sullivan GJ, Carty FL, Cronin CG. Imaging of bone metastasis: an update. World J Radiol 2015;7(8):202-11.
17. Rager O, Nkoulou R, Exquis N, et al. Whole-Body SPECT/CT versus Planar Bone Scan with Targeted SPECT/CT for Metastatic Workup. Biomed Res Int 2017;2017:7039406.
18. Sleiman Y. Naddaf, B. David Collier, Abdelhamid H. Elgazzar, Magdy M. Khalil. Technical Errors in Planar Bone Scanning. J Nucl Med Technol 2004;32:148-53.
19. Talbot JN, Paycha F, Balogova S. Diagnosis of bone metastasis: recent comparative studies of imaging modalities. Q J Nucl Med Mol Imaging 2011;55(4):374-410.
20. Van den Wyngaert T, Strobel K, Kampen WU, et al. The EANM practice guidelines for bone scintigraphy. Eur J Nucl Med Mol Imaging 2016;43(9):1723-38.
21. Yang DC, Ratani RS, Mittal PK, Chua RS, Pate SM. Radionuclide three-phase whole-body bone imaging. Clin Nucl Med 2002;27:419–26.
22. Vaño E, Miller DL, Martin CJ, et al. Diagnostic reference levels in medical imaging. ICRP Publication 135. Ann ICRP 2017;46(1)1-144.
23. Wu Q, Yang R, Zhou F, Hu Y. Comparison of whole-body MRI and skeletal scintigraphy for detection of bone metastatic tumors: a meta-analysis. Surg Oncol 2013;22:261–6.

5

LUNG IMAGING

by Bożena Birkenfeld,
Jacek Iwanowski
and Monika Gawron

INTRODUCTION

The lungs are a pair of organs located in the chest, constituting the human respiratory system. Their primary function is gas exchange, i.e. providing oxygen to the human body and removing carbon dioxide. They are also a filter preventing pollution and other undesirable substances from entering the body. Lungs are necessary for life.
The right lung consists of three lobes: upper, middle and lower, divided by a horizontal and oblique fissure. The left lung is smaller than the right one and consists of two lobes: upper and lower, separated by an oblique fissure. Respiratory airways, the circulatory system and the lymphatic system with lymph nodes are located within the lungs.

The air enters the lungs through the trachea, which subsequently branches into the primary bronchi, lobar, segmental and interlobular bronchi, bronchioles, and alveoli. Blood is transferred to each lung through a large pulmonary blood vessel, the right and left pulmonary artery and vein. These divide into lobar and segmental vessels and subsequently into smaller vessels, which constitute the capillary circulation surrounding the alveoli where gas exchange occurs.

An anatomical unit of the lung smaller than the lobe is the segment, supplied by its own bronchus and artery. The right lung consists of ten segments and the left one has nine.

The borders between segments are not visible under normal conditions. Bronchopulmonary segments are visible in imaging tests when they become airless and/or when blood circulation within them is impaired. This may be due to inflammatory infiltration, cirrhosis, atelectasis, tumour lesions or pulmonary embolism. Pathological changes in the lungs may occur in their individual components, the respiratory tract, blood vessels and in the lymphatic system. Lung lesions can be benign or malignant.

IMAGING MODALITIES FOR THE ASSESSMENT OF PULMONARY DISEASES

Diagnosis of pulmonary diseases is based on clinical examination, laboratory assays, functional tests and imaging modalities. Spirometry is a common pulmonary function test performed to assess the vital capacity of the lungs. Spirometry provides an assessment of the total lung capacity (TLC), which in an adult human is approximately 5 litres. Bronchoscopy and endobronchial ultrasonography (EBUS) are procedures used for direct assessment of the bronchial tree, allowing sampling of abnormal or suspicious lesions for histopathological examination. A similar diagnostic technique is percutaneous lung lesion biopsy.

Additionally, various imaging modalities are used for the diagnostic assessment and subsequent monitoring of lung diseases. These are able to visualise the morphological structure of the organs and/or their metabolism or function. Pulmonary diseases which can be visualised by imaging are usually those affecting the parenchyma, the vascular and/or bronchial tree and the lymph nodes.

The following imaging modalities are applied to diagnose lung diseases:

1. **Lung morphological modalities:** chest x-ray, high-resolution computed tomography, computed tomography angiography, pulmonary angiography, lung ultrasound, magnetic resonance tomography – usually performed for assessment of structural lung disorders.
2. **Lung metabolic/functional planar imaging techniques:** nuclear medicine imaging done with different radiopharmaceuticals: lung perfusion scintigraphy, lung ventilation scintigraphy – usually performed for diagnosis of benign pulmonary pathology, most often for pulmonary embolism.
3. **Lung hybrid imaging techniques. Metabolic/functional and morphological tomographic imaging techniques:** single photon emission computed tomography (SPECT), SPECT combined with CT (SPECT/CT), positron emission tomography combined with CT (PET/CT), positron emission tomography combined with MRI (PET/MRI) done with different radiotracers – usually performed for the diagnosis of focal benign or malignant lung lesions.

Lung morphological modalities

Chest x-ray is a simple diagnostic tool used in detection and diagnosis of lung diseases. It is cheap, widely available and involves low exposure to ionising radiation.

High-resolution computed tomography (HRTK) has revolutionised the imaging of chest and lung lesions and is currently the basic imaging modality. It is done in several variants: high-dose, low-dose, and with or without contrast medium. The technique images the lung parenchyma, vessels, heart, mediastinum, pleura, and chest wall. It has a very good resolution, scan time is short and the image provides detailed data about the size, shape and location of lesions and their anatomical relation to the surrounding organs. It is sometimes performed without contrast due to patient contraindications, mainly impaired renal function, hence it is

obligatory to measure serum creatinine if the use of contrast medium is planned during the procedure.

Computed tomography pulmonary angiography (pulmonary angioCT or CTPA) with contrast shows blood flow in pulmonary vessels and is done to detect pulmonary embolism. It has almost completely replaced the previously applied technique of pulmonary angiography, which is an invasive procedure.

Transthoracic ultrasound (US) of the lungs is a non-invasive procedure used for diagnosis of lesions in the mediastinum, lungs and pleura, fluid in the pleural cavities, pneumothorax, pulmonary oedema, and also to assess pulmonary embolism. It is an alternative to imaging procedures using ionising radiation when diagnosing pregnant women. This technique is very effective in performing targeted biopsies of lung lesions and removing fluid from the pleural cavity.

Magnetic resonance imaging (MRI) is an increasingly popular procedure for the diagnosis of chest pathologies, despite the difficulties of lung imaging due to the air-filled spaces. The advantages of MRI are the lack of exposure to ionising radiation and the high resolution for other chest tissues. It can be useful for assessing lung tumours invading the chest wall, the mediastinum, including the blood vessels and heart, and posterior mediastinal tumours. The disadvantage of the test is its higher cost, relatively long acquisition time, frequent cases of claustrophobia in patients and numerous contraindications, including the presence of bone prostheses, pacemakers and metallic implants.

LUNG METABOLIC/ FUNCTIONAL PLANAR IMAGING TECHNIQUES

Lung perfusion scintigraphy

The test involves intravenous administration of radiopharmaceutical, usually labelled with ^{99m}Tc-macroaggregated human albumin (^{99m}Tc-MAA) with particles 10-100 micrometres in diameter. When the pulmonary circulation is normal the particles are evenly distributed in the pulmonary circulation and stop in the capillary circulation of the lungs, causing temporary microembolism and thus enabling the imaging of lung perfusion. If the circulation is impaired, the scan shows segmental defects in the distribution of the radiopharmaceutical, usually projecting to the lung periphery.

Lung ventilation scintigraphy

Ventilation scintigraphy is based on the administration of a substance which reaches the alveoli through the respiratory tract, allowing the imaging of lung aeration. The substances commonly used are Technegas™, ^{99m}Tc-DTPA radioaerosol or krypton-81 gas.

Technegas™ is most often used for ventilation studies in departments of nuclear medicine. The Technegas™ generator is a specially designed machine which produces an ultrafine suspension of carbon nanoparticles 30-100 nm in diameter, labelled with technetium. This is done by heating ^{99m}Tc-pertechnetate in a graphite crucible in a pure argon atmosphere at very high temperatures of up to 2700°C. The resulting microaerosol is inhaled by the patient in several breaths from a dedicated nebuliser so that the particle suspension is deposited uniformly in the small bronchi and the alveolar region, showing ventilation. In contrast to krypton-81 imaging, there is no rush in visualising its distribution. A ventilation study can be done at any time if a Technegas™ generator and technetium are available.

For ventilation studies performed with ^{99m}Tc-DTPA-labelled aerosol, the latter is obtained from a nebuliser connected to the oxygen, into which ^{99m}Tc-DTPA is injected. Oxygen flowing through the nebuliser causes the liquid to break up and form microparticles about 1-3 micrometres in diameter. The patient inhales radioactive DTPA particles into the bronchi and alveoli. During exhalation, the air entering the atmosphere passes through the filters, which retain the remainder of the radioaerosol. After a few minutes of inhalation with radioaerosol, the image can be obtained with a gamma camera. The disadvantage of this method is that the deposition of aerosol on bronchiole walls is quite frequently seen. Also, due to ciliary movement the aerosol is transported higher, and as a consequence the bronchi and trachea are sometimes visible in the scintigraphy images. Occasionally, the swallowed radioaerosol can also be seen in the oesophagus and stomach.

Krypton-81m is also used for ventilation imaging. It is an inert radioactive gas with a very short half-life of 13 seconds, delivered from a cyclotron-produced ^{81}Rb/^{81m}Kr generator. The imaging procedure can be done simultaneously with or immediately following a perfusion study, because the gamma energy of ^{81m}Kr is higher than that of ^{99m}Tc – 190 keV versus 140 keV. During the test, the patient breathes continuously with a mixture of air and ^{81m}Kr. The limitations of the technique are the short half-life of ^{81m}Kr and the high cost of the generator, which means that its on-shelf availability is low.

Perfusion and ventilation scintigraphy are performed using planar or tomographic imaging techniques. A detailed description of the procedure can be found in the European Nuclear Medicine Guide (1, 2). With the planar

method, scintigraphy is performed in anterior-posterior, posterior-anterior, both lateral, right and left posterior-oblique and right and left anterior-oblique projections.

The main indications for ventilation/perfusion scintigraphy are benign lung disorders:

» diagnosis and follow up of pulmonary thromboembolism;

» quantification of radiotracer uptake before pulmonary resection;

» lung transplant evaluation;

» assessment of the aetiology of pulmonary hypertension;

» assessment of chronic pulmonary parenchymal diseases.

Lung hybrid imaging techniques. Metabolic/functional and morphological tomographic imaging techniques.

Hybrid imaging equipment offers a combination of metabolic and morphological imaging in a single device. It has been shown that a single hybrid imaging study gives more information about a patient's pathology than several studies performed separately. The basic idea in the beginning was to add attenuation correction and localisation information for the metabolic lesions visualised in scintigraphy, hence the morphological image quality was rather poor. Contemporary machines, however, offer a combination of high-quality metabolic and morphological devices, for example a SPECT gamma camera combined with 64/128 row CT. Hybrid imaging

techniques include SPECT/CT, PET/CT and PET/MRI, all of which can be useful in benign and malignant lung disorders.

The benign lung disorders they are most often used for are pulmonary embolism and infection, while the malignant disorder they are most commonly used for is lung cancer. Different radiopharmaceuticals are applied, depending on the suspected lung pathology.

UTILITY OF SPECT/CT, PET/CT AND PET/MRI IN THE EVALUATION OF LUNG LESIONS

SPECT/CT scintigraphy in pulmonary diseases

SPECT and SPECT/CT imaging is increasingly available in nuclear medicine departments. It is gradually becoming the standard technique in metabolic imaging of various organs, including lungs. SPECT imaging is based on coronal, transverse and sagittal slices and analysis of tracer accumulation seen on a segmental map of the lungs.

The use of SPECT perfusion/ventilation images together with low-dose CT morphological images provides valuable

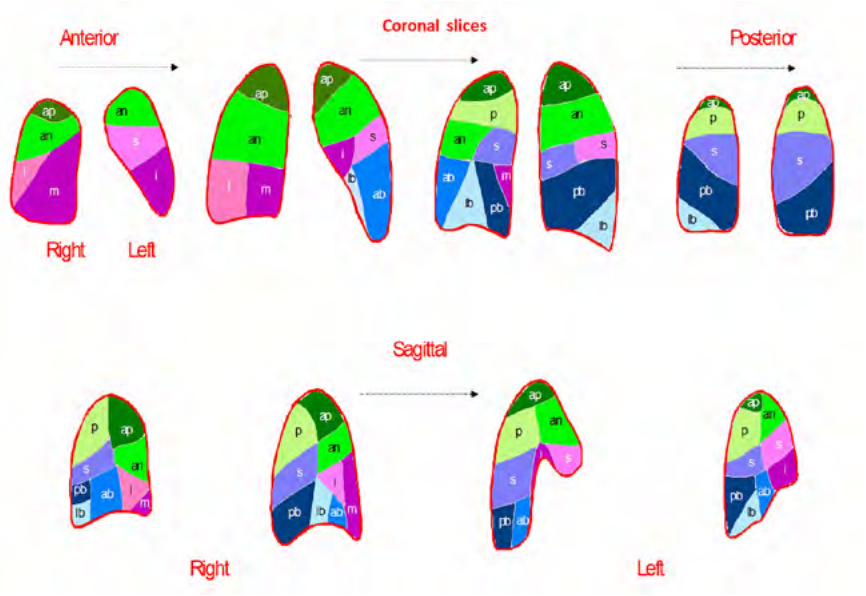

Figure 1: Segmental map of the two lungs in four coronal slices and two sagittal slices for each lung. Courtesy of Prof. Marica Bajc. Bajc M, Schümichen C, Grüning T, Lindqvist A, Le Roux P-Y, Alatri A et al. EANM guideline for ventilation/perfusion single-photon emission computed tomography (SPECT) for diagnosis of pulmonary embolism and beyond. Eur J Nucl Med Mol Imaging 2019; 46(12):2429–51.

Lung segments

Right lung:

Upper lobe: apical ap; posterior p; anterior an

Middle lobe: lateral l; medial m;

Lower lobe: superior s; medial basal mb; anterior basal ab; lateral basal lb; posterior basal pb

Left lung:

Upper lobe: apical ap; posterior p; anterior a; superior lingular sl; lateral l

Lower lobe: superior s; anterior basal ab; lateral basal lb; posterior basal pb

information on lung aeration and allows for more accurate interpretation of lung scintigraphy. It significantly increases the sensitivity of the test, as detailed in the new EANM guideline for diagnosis of pulmonary embolism published in 2019 (3).

Diagnosing pulmonary embolism with a perfusion/ventilation test is the standard procedure currently employed, but may not be possible in some situations. In exceptional situations when a ventilation study cannot be performed due to lack

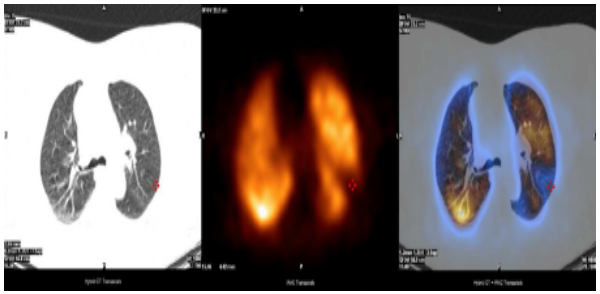

Figure 2: SPECT/CT study with ^{99m}Tc-MAA. Perfusion defect of left lung superior segment seen on transverse slices and corresponding normal density in SPECT/CT lung scintigraphy hybrid imaging: images from left-lung CT, lung perfusion study, lung fusion image. Department of Nuclear Medicine, Pomeranian Medical University, Szczecin

of ventilation agent or lack of patient cooperation during the procedure, CT information interpreted together with the lung perfusion pattern can be helpful.

The SPECT/CT lung scan is also useful in patients with lung neuroendocrine tumours. Somatostatin analogues labelled with ^{99m}Tc SPECT/CT or with ^{68}Ga PET/CT are effective in diagnosing suspected lung neuroendocrine tumours or their metastases. ^{111}In-labelled octreotide is also used, though rather rarely. Depending on their histological type, some neuroendocrine tumours may not accumulate somatostatin analogues but may be visible in an ^{18F}-FDG PET/CT scan.

PET/CT scintigraphy in pulmonary diseases

Imaging with the PET/CT technique, including lung pathology, is most often performed with ^{18F}-FDG. Computed tomography of the lungs is a basic test for diagnosing pulmonary disorders, including tumours of the lung and lymph nodes. However, on the basis of CT only it is very difficult to assess the clinical significance or origin of lung tumours. The high incidence of lung cancer makes it important to recognise malignant lung tumours as early as possible. Lung cancer is the most common cause of death among the neoplastic diseases, and an early diagnosis gives a chance of curing the patient. At present, lung cancer tends to be diagnosed relatively late. In many cases, biopsy from the focal lesion

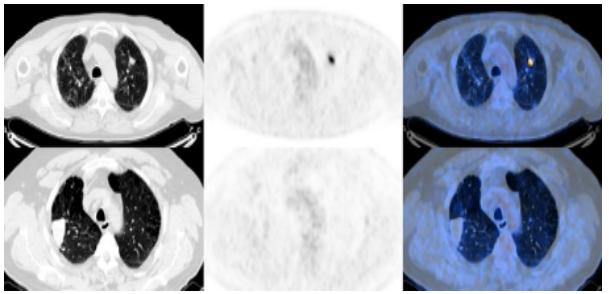

Figure 3: PET/CT study with ^{18F}-FDG – transverse slices. A. Left-lung tumour with increased ^{18F}-FDG accumulation – high probability of malignancy. B. Right-lung tumour with normal ^{18F}-FDG accumulation – low probability of malignancy. Courtesy of PET/CT Center Starmedica, Szczecin

may not be possible or is invasive and highly risky, hence the widespread use of metabolic PET/CT imaging, mostly after administration of ^{18F}-FDG, for assessing the nature of tumours. A focal lesion seen on CT after the administration of ^{18F}-FDG may or may not accumulate it. This tells us whether it is benign or malignant and facilitates decision-making with regard to surgical resection and further histopathological evaluation. More information is included in the EANM procedure guidelines for tumour imaging (4) and in the technologist's guide to principles and practice of PET/CT (5).

PET/MRI scintigraphy in pulmonary diseases

Hybrid PET/MRI imaging is a relatively new technique in clinical practice, but seems to be a promising diagnostic tool. Using MRI instead of CT reduces the radiation dose to the patient, which is especially important in children, young adults, and repeated imaging during follow-up. It does not replace PET/CT, but for some indications like brain, head and neck, cervix and prostate tumours PET/MRI imaging may be done instead or additionally. MRI has limited resolution for lung pathology due to lung aeration. However, recent studies have shown comparable results between PET/CT and PET/MRI in the detection of pulmonary nodules and in lung cancer staging. It is a very promising technique for detection

of mediastinal pleura involvement in lung cancer, diagnosis and assessment of mediastinal tumours, and diagnosis of pleural mesothelioma.

RADIOPHARMACEUTICALS USED FOR MALIGNANT LUNG TUMOUR IMAGING

The main, most widely used radiotracer for lung tumour imaging is ^{18F}-fluorodeoxyglocose (^{18F}-FDG), which is used for differentiation of benign from malignant tumours, lung cancer staging, radiotherapy planning and follow-up. However, one disadvantage of this radiopharmaceutical is that it is not tumour specific and that false positive accumulation may be seen, mainly due to inflammatory processes.

Additionally, there are other radiopharmaceuticals useful for imaging of lung tumours: cellular proliferation markers, amino acid metabolism tracers, tumour hypoxia markers, angiogenesis tracers, and pulmonary neuroendocrine tumour tracers. There are reports that the proliferation marker ^{18F}-fluorothymidine (^{18F}-FLT) can provide more information about the pathophysiology of lung cancer, and it seems to be more specific then ^{18F}-FDG for lung tumour therapy assessment.

A paper published in the JNM in 2019 gives very promising information about ^{68Ga}-FAPI PET/CT tracer (6). The latter is an inhibitor of fibroblast activation protein (FAP), which is highly expressed by tumour cells in various cancer types such as breast, head and neck and pancreatic cancer, but also in non-small-cell lung cancer. It is more specific then ^{18F}-FDG imaging, no diet or fasting preparation is required, imaging can be done a few minutes after injection, and high-quality images are obtained. Perhaps the most interesting finding is that it has potential for targeted therapy treatment when labelled with beta emitters.

SPECIAL PROTOCOLS APPLIED IN LUNG TUMOUR IMAGING

Hybrid PET/CT imaging has become an extremely important technique in cancer staging, prognosis, follow-up and assessment of treatment results. It is also used in the planning of radiation treatment. The CT component of PET/CT imaging, apart from localisation of lesions, also improves the accuracy of attenuation correction and helps to reduce motion artefacts. However, the quality and accuracy of the image may be affected by internal factors from the patient (physiological factors). Respiratory movements and, above all, the movement of the diaphragm, which can move up to 2 cm when breathing calmly in a lying position, significantly affects the accuracy of lung lesion evaluation, especially for rather small lesions localised in the lower lungs. Although computed tomography images are very quickly recorded, only taking a few seconds, the acquisition time for PET imaging, even for a single bed position, rises to a few minutes. As a result, PET images show the average movement of hot spots and SUV values may be misread. In order to eliminate respiratory artefacts during PET/CT examination, several methods have been developed using external devices (respiratory gating) to record the respiratory cycle (7).

Types of respiratory gating system:

» Pressure belt

A belt wrapping the patient at the height of the diaphragm which records the displacement of the abdominal wall in the course of pressure changes during inspiration and exhalation. The system allows image recording in a specific position for full inspiration or exhalation.

» RPM (real-time position management system)

This device uses two infrared sensors located on the patient's chest and synchronised with the camera located at the end of the patient's bed. The camera records the movement of the sensors along with the patient's breathing rhythm.

Correlation of the breathing cycle with PET/CT acquisition data

Several compensation techniques are used, combining acquisition data with information from the respiratory gating system. For this purpose, it is possible to divide the respiratory cycle into several phases or to select a single phase. In addition, time-based (phase-based) or amplitude-based methods can be used. With the time-based method, some acquisition data may be lost due to differing lengths of the breathing cycle. However, a simple solution is to set a range that is acceptable for a breathing cycle in which short and long breath cycles are not recorded. An important factor affecting the image quality is the number of registered respiratory phases, because a small number of intervals can cause image blur and a higher signal-to-noise ratio. On the other hand, a large number of phases yields a clear decrease in noise but can affect the detection of changes, because the number of images determines the number of phases obtained. In addition, the diversity of internal tissues and their movement can affect image noise due to different tissue speeds in different respiratory cycles. It should be taken into account that the respiratory amplitude is not identical in all patients, which may also affect the image noise. The time-based method was introduced by the scanner manufacturers, as it does not require access

to the breathing cycle. Information about the breathing cycle is obtained by devices additionally mounted before acquisition, which are not available at work stations for post-acquisition reconstruction purposes.

The amplitude-based method determines the minimum and maximum thresholds and subdivides the respiratory cycle into "bins" of the amplitude range. However, the method is not very sensitive in terms of the reproducibility of the number of coincidences for each range. The condition for this method is continuous registration by the breathing cycle acquisition station. Although the recording of respiratory amplitudes is a better method than the time method, neither of the methods provides adequate absorption correction. CT images without respiratory gating also produces a large number of motion artefacts, which in turn contributes to errors in both recorded images.

Another method is deep inspiration breath-hold (DIBH), where acquisition data is obtained over a time interval of fifteen seconds on a deep breath for CT and twenty seconds on a deep breath for PET. This results in aggregated images with attenuation correction, reconstructed using a standard conversion algorithm. With this method, all data is obtained for the same tissue position during a deep inspiration breath-hold. This guarantees the accuracy of image fusion as well as accurate reproduction of attenuation correction. However, for patients with shortness of breath or problems with holding their breath, it may cause problems with acquisition. The DIBH method works well in routine lung imaging to detect small nodules and is also useful in abdominal imaging.

REFERENCES

1. Bajc M, Neilly JB, Miniati M, Schuemichen C, Meignan M, Jonson B. EANM guidelines for ventilation/perfusion scintigraphy: Part 1. Pulmonary imaging with ventilation/perfusion single photon emission tomography. Eur J Nucl Med Mol Imaging 2009; 36(8):1356–70.
2. Bajc M, Neilly JB, Miniati M, Schuemichen C, Meignan M, Jonson B. EANM guidelines for ventilation/perfusion scintigraphy. Eur J Nucl Med Mol Imaging 2009; 36(9):1528–38.
3. Bajc M, Schümichen C, Grüning T, Lindqvist A, Le Roux P-Y, Alatri A et al. EANM guideline for ventilation/perfusion single-photon emission computed tomography (SPECT) for diagnosis of pulmonary embolism and beyond. Eur J Nucl Med Mol Imaging 2019; 46(12):2429–51.
4. Boellaard R, Delgado-Bolton R, Oyen WJG, Giammarile F, Tatsch K, Eschner W et al. FDG PET/CT: EANM procedure guidelines for tumour imaging: version 2.0. Eur J Nucl Med Mol Imaging 2015; 42(2):328–54.
5. van der Broek WJM, Testanera G. Principles and practices of PET: A technologist's guide. Vienna: European Association of Nuclear Medicine; 2012. (Technologist's guide).
6. Giesel FL, Kratochwil C, Lindner T, Marschalek MM, Loktev A, Lehnert W et al. 68 Ga-FAPI PET/CT: Biodistribution and Preliminary Dosimetry Estimate of 2 DOTA-Containing FAP-Targeting Agents in Patients with Various Cancers. J Nucl Med 2019; 60(3):386–92.
7. Pépin A, Daouk J, Bailly P, Hapdey S, Meyer M-E. Management of respiratory motion in PET/computed tomography: The state of the art. Nucl Med Commun 2014; 35(2):113–22.

CLINICAL USE OF SPECT/CT: IMAGING OF NEUROENDOCRINE TUMOURS AND SENTINEL NODE IMAGING

by Luka Lezaic

METAIODOBENZYLGUANIDINE IMAGING

Metaiodobenzylguanidine (MIBG) is a structural analogue of noradrenaline, an endogenous catecholamine which is a neurotransmitter of the autonomous nervous system. It is taken up by neuroendocrine cells through the NET transporter and stored in the secretory granules within the cells via the VMAT1 and VMAT2 transporters; alternatively, in specific tumour tissue types (i.e. neuroblastoma), it may be stored in the cytoplasm. It is labelled with ^{123}**I** or ^{131}**I**. While labelling with both isotopes can be used for diagnostic imaging, the former offers superior characteristics for molecular imaging in terms of spatial resolution and dosimetry, while the latter is typically used for therapy using its beta emission (^{123}I/^{131}I-MIBG theranostic pair).

Common indications for imaging with ^{123}I/^{131}I-MIBG are neuroblastoma, neuroendocrine tumours of the autonomous nervous system (pheochromocytoma, paraganglioma), and, less frequently, other neuroendocrine tumours; it is also used for evaluation of autonomic myocardial innervation on suspicion of catecholamine-induced cardiomyopathy and differentiation of parkinsonian syndromes.

Neuroblastoma

Neuroblastoma is a most common solid extracranial malignant paediatric tumour of neuroectodermal origin. In over half of the patients, it is metastatic at diagnosis. Molecular imaging plays a key role in staging, evaluation of response to therapy and follow-up; in addition, it provides prognostic information and is used to select appropriate patients for radionuclide therapy.

^{123}I-MIBG is an essential part of evaluation of neuroblastoma patients. It is typically performed for staging purposes; the number and distribution of lesions are used in validated scoring systems (Curie, SIOPEN) that are used to guide therapy and provide prognostic information. The investigation is highly accurate, with both sensitivity and specificity around 90%. Nevertheless, the use of hybrid (SPECT/CT) imaging has been consistently shown to increase the diagnostic performance in comparison to planar imaging, typically identifying a greater number of lesions (increased lesion contrast, unmasking lesions obscured by physiological uptake – e.g. heart, liver, urinary system) and allowing for differentiation between skeletal and soft-tissue lesions (Figure 1).

Other molecular imaging options in neuroblastoma include PET/CT with ^{18}F-fluorodeoxylucose (FDG), somatostatin receptor imaging with SPECT (^{111}In-DTPA-OC, ^{99m}Tc-HYNIC-TOC) or PET (^{68}Ga-

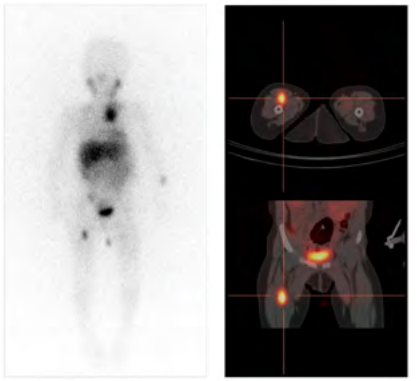

Figure 1. Metastatic neuroblastoma. Planar ^{123}I-MIBG imaging (left panel) demonstrates multiple metastases throughout the body. SPECT/CT (right panel) clearly differentiates between bone marrow and soft tissue lesions.

DOTATATE/TOC/NOC) tracers and PET/CT with ^{18}F-dihydroxyphenylalanine (DOPA). **^{18}F-FDG** PET/CT is typically performed with (suspicion of) ^{123}I-MIBG-negative lesions and/or in poorly differentiated disease; its diagnostic performance is generally lower in comparison to ^{123}I-MIBG. Similarly, the diagnostic performance of somatostatin receptor imaging is inferior to ^{123}I-MIBG due to variable expression of somatostatin receptors, but offers an appropriate selection of patients when peptide receptor radionuclide therapy (PRRT) is contemplated and ^{131}I-MIBG therapy is unavailable. **^{18}F-DOPA** PET/CT is an emerging highly sensitive and specific imaging modality for neuroblastoma; according to available data, it consistently shows superior diagnostic performance in comparison to other molecular imaging methods, including ^{123}I-MIBG, and may be considered an imaging method of choice in the future. Skeletal scintigraphy with ^{99m}Tc-bisphosphonates no longer plays a relevant role in neuroblastoma imaging; a limited indication may exist for potential evaluation of cortical lesions.

Pheochromocytoma/paraganglioma

Pheochromocytoma/paraganglioma (PPGL) are also tumours of neuroectodermal origin, located either in the adrenals (pheochromocytoma, PHEO) or in the ganglia (sympathetic and parasympathetic). Those of sympathetic origin may present clinically with symptoms of catecholamine excess, while those of parasympathetic origin often present as mass/infiltrating lesions. Up to 10% of lesions may be hereditary, and up to 10% of lesions may be malignant. Molecular imaging plays a role in staging and follow-up, less often in diagnosis of the lesion. An increasing indication is patient selection for radionuclide therapy.

^{123}I-MIBG accumulates in the secretory granules of neuroendocrine cells (see above). Its sensitivity and specificity for localising pheochromocytoma is typically high (around 85-100% and 90-100%, respectively). It is lower for paragangliomas

(overall around 50-75%), especially for those of parasympathetic origin (head and neck; around 20-50%).

Another single-photon imaging option for PPGL is somatostatin receptor scintigraphy (**^{111}In-DTPA-OC, ^{99m}Tc-HYNIC-TOC**). Generally, its sensitivity is inferior to ^{123}I-MIBG, except for parasympathetic (head and neck) PGL, where the sensitivity typically exceeds 90% and it represents the single-photon imaging technique of choice for the indication. However, the diagnostic performance of single-photon tracers is inferior to that of newer positron-emitting tracers. **^{68}Ga-DOTA-TATE/TOC/NOC**, the PET variant of somatostatin receptor imaging, detects metastatic pheochromocytoma and primary and/or metastatic paraganglioma in over 90% of cases. **^{18}F-DOPA** exhibits sensitivity of around 80% and **^{18}F-FDG** of around 75% in this context, while the sensitivity of **^{123}I/^{123}I-MIBG** was reported to be around 40% (Figure 2).

Somatostatin receptor scintigraphy with single-photon emitting tracers

Somatostatin is a peptide hormone and neurotransmitter with typically inhibitory action. Somatostatin receptor scintigraphy (SRS) utilises the characteristic of neuroectodermally derived tissues and neoplasms (broadly encompassed under the umbrella term neuroendocrine tumours/neoplasms, NET/NEN) of expression of somatostatin receptors on their surface.

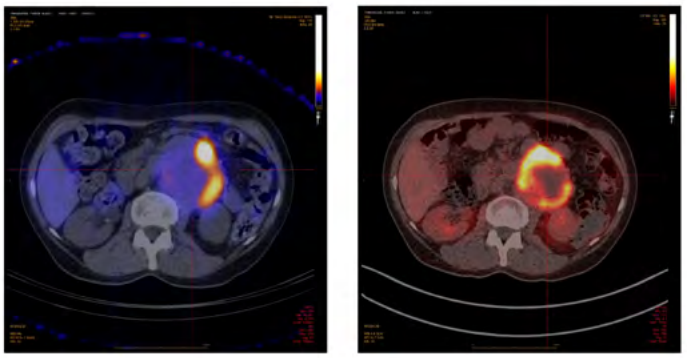

Figure 2. Different metabolic information provided by ^{123}I-MIBG SPECT/CT (left panel) and ^{18}F-FDG PET/CT (right panel) in a paraganglioma. A "flip-flop" phenomenon of heterogeneity of metabolism in a centrally necrotic tumour (areas less active on ^{123}I-MIBG are more active on ^{18}F-FDG and vice versa).

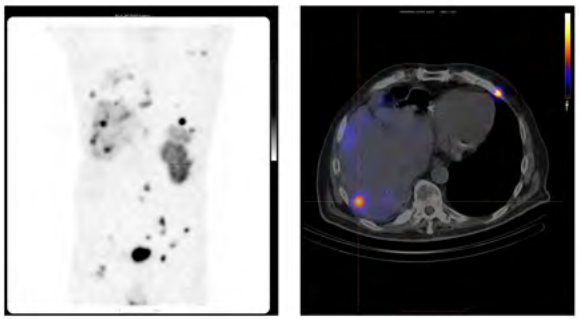

Figure 3. Metastatic neuroendocrine neoplasm, somatostatin receptor imaging with ^{99m}Tc-EDDA/HYNIC-TOC. Multiple metastases are demonstrated throughout the body on the MIP image (left panel); SPECT/CT clearly localises the lesions and differentiates between liver and bone metastases.

Depending on the NEN type, the expression of somatostatin receptors can range from very high and very dense to relatively low and mild (e.g. glucagonoma, gastrinoma, virtually 100%; ileal carcinoid, over 90%; insulinoma and bronchial carcinoid, around 60%). In humans, five subtypes of somatostatin receptors are described. The most commonly and densely expressed somatostatin receptor subtype is type 2 (sstr2), which is also targeted by single-photon-emitting tracers. Two are widely available: the traditionally used indium-111-labelled octreotide (**^{111}In-DTPA-OC**), commercially available as Octreoscan®, targeting sstr2 and sstr5, and technetium-99m-labelled octreotide (**^{99m}Tc-EDDA/HYNIC-TOC**), commercially available as Tektrotyd®, targeting primarily sstr2.

The overall sensitivity of SRS for NEN is generally high (reportedly between 70% and 90%). Somatostatin receptor scintigraphy therefore holds a central position in the diagnostics of NEN due to its proven high sensitivity, specificity and suitability for staging; it is also used for follow-up, evaluation of therapeutic effect and on suspicion of recurrence/residual disease. Another benefit of SRS is the ability to appropriately select patients for radionuclide therapy (peptide receptor radionuclide therapy, PRRT). Tomographic (SPECT) and hybrid (SPECT/CT) imaging exhibits the typical advantages over planar imaging of higher sensitivity, specificity and localisation of lesions (Figure 3); in addition, the increasing utility of quantitative SPECT imaging allows for more accurate

evaluation of therapeutic effect as well as more accurate and elaborate dosimetry assessment when PRRT is utilised. **^{123}I/^{131}I-MIBG** can also be used to image NEN, but in contrast to its sensitivity for entities originating from the autonomous nervous system (pheochromocytoma/paraganglioma; see above), its sensitivity for gastroenteropancreatic neuroendocrine neoplasms (GEPNEN) and bronchial carcinoids is significantly lower (typically around 50%). The tracer is mostly used for imaging of mid-gut GEPNENs, in particular when radionuclide therapy is contemplated and PRRT is not available.

In comparison to single-photon tracers that target somatostatin receptors, the positron-emitting tracers labelled almost exclusively with gallium-68 **(^{68}Ga-DOTATATE/TOC/NOC)** exhibit significantly higher sensitivity (typically around 90-95% vs. 50-60% in direct comparison) with the added benefit of inherent tomographic imaging, superior contrast and spatial resolution; again, the tracer binding is most avid to sstr2 (-TATE), to a lesser extent also to sstr5 (-TOC) and only one tracer (-NOC) also binds significantly to the sstr3 subtype. Clinically, there is no significant difference in the diagnostic performance of the tracers. Another positron-emitting option for NEN imaging is **^{18}F-DOPA**. In contrast to PPGL imaging, the sensitivity for NEN overall is lower (around 65%); it is currently the PET tracer of choice for imaging of biochemical recurrence of a specific NEN – medullary thyroid carcinoma (sensitivity around 65%). **^{18}F-FDG** typically accumulates poorly in well-differentiated neoplasms that represent the majority of NEN; however, it is useful to confirm the suspicion of tumour dedifferentiation and provides important prognostic information in this context (Figure 4).

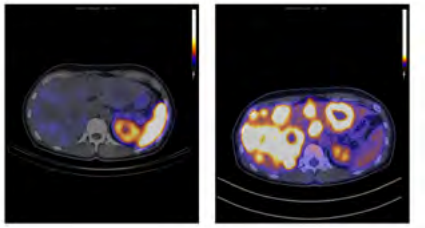

Figure 4. Liver metastases, biopsy-proven neuroendocrine neoplasm (high grade). Liver lesions are completely negative in somatostatin receptor imaging with ^{99m}Tc-EDDA/HYNIC-TOC (left panel). ^{18}F-FDG PET/CT (right panel) demonstrates multiple, partially necrotic, metabolically intensely active liver metastases – poorly differentiated neuroendocrine carcinoma.

Sentinel node scintigraphy with single-photon-emitting tracers

Sentinel node biopsy is a method of staging malignant disease. In many malignancies, the stage of the disease (including lymphatic spread) is the leading factor determining patient prognosis. By definition, the sentinel node(s) is/are the first lymph node(s) draining a specific lymphatic watershed where the offending malignant process is located. Sentinel node scintigraphy reproduces the path of spread of malignant cells and allows the localisation of sentinel node(s), their subsequent removal and histopathological analysis. Confirmation of metastases in the sentinel lymph node(s) typically involves dissection of regional lymph nodes in an attempt to attenuate further spread of the disease.

The radiopharmaceuticals used for sentinel node scintigraphy are technetium-99m-labelled colloids **(^{99m}Tc-colloids)** using particles of different size (3-1000 nm) that spread through the lymphatics and localise passively in the lymph nodes; recently, a tracer that specifically binds to the mannose CD206 receptor on the surface of dendritic cells and macrophages, technetium-99m- labelled tilmanocept **(^{99m}Tc-tilmanocept)**, was introduced into clinical practice. Generally, in studies directly comparing the tracers, no clinically significant differences were found in terms of accuracy; patient tolerance may, however, be higher with the receptor-based tracer. Frequently, sentinel node imaging is a combined procedure using both a radioactive tracer and a conventional (blue) dye with combined depiction of lymphatic vessels and lymph nodes; the combined approach was shown to increase the diagnostic yield.

The clinical entities where sentinel node scintigraphy is most commonly used are breast cancer and malignant melanoma, in which the procedure is integrated into the standard of care; its use in several other malignancies (in particular head and neck cancer; gastrointestinal cancers – oesophagus, stomach, colon; urological cancers – prostate, penis; gynaecological cancers – vulva, cervix, uterus) is evolving into the standard of care.

The overall diagnostic performance of sentinel node scintigraphy is high: for most listed indications, the detection rate (the identification of the sentinel lymph node) is around 90% and above, as is the sensitivity (detection of malignant sentinel lymph nodes) and negative predictive value, in particular when the dual-tracer approach is used; however, somewhat discordant results are reported for colon and uterine cancer (in part likely due to inhomogeneity of studies and techniques). The use of SPECT and SPECT/CT was shown to further increase diagnostic accuracy.

CONCLUSION

For the listed indications and radiopharmaceuticals, the use of SPECT/CT increases the diagnostic performance of imaging studies. When available and technically and logistically feasible, SPECT/CT should be performed in addition to or instead of planar imaging. The added cost and time as well as the additional radiation exposure should also be considered (especially in the paediatric population), but will likely be offset by the significantly enhanced diagnostic information obtained.

LITERATURE

1. Timmers HJ, Chen CC, Carrasquillo JA, et al. Comparison of 18F-fluoro-L-DOPA, 18F-fluoro-deoxyglucose, and 18F-fluorodopamine PET and 123I-MIBG scintigraphy in the localization of pheochromocytoma and paraganglioma. J Clin Endocrinol Metab. 2009;94(12):4757-67.
2. Koopmans KP, Jager PL, Kema IP, Kerstens MN, Albers F, Dullaart RP. 111In-octreotide is superior to 123I-metaiodobenzylguanidine for scintigraphic detection of head and neck paragangliomas. J Nucl Med. 2008;49(8):1232-7.
3. Alrezk R, Suarez A, Tena I, Pacak K. Update of Pheochromocytoma Syndromes: Genetics, Biochemical Evaluation, and Imaging. Front Endocrinol (Lausanne). 2018;9:515.
4. Taïeb D, Hicks RJ, Hindié E, et al. European Association of Nuclear Medicine Practice Guideline/Society of Nuclear Medicine and Molecular Imaging Procedure Standard 2019 for radionuclide imaging of phaeochromocytoma and paraganglioma. Eur J Nucl Med Mol Imaging. 2019;46(10):2112-2137.
5. Brisse HJ, McCarville MB, Granata C, et al.; International Neuroblastoma Risk Group Project. Guidelines for imaging and staging of neuroblastic tumors: consensus report from the International Neuroblastoma Risk Group Project. Radiology. 2011 Oct;261(1):243-57.

Bar-Sever Z, Biassoni L, Shulkin B, et al. Guidelines on nuclear medicine imaging in neuroblastoma. Eur J Nucl Med Mol Imaging. 2018;45(11):2009-2024.

6. Kjaer A, Knigge U. Use of radioactive substances in diagnosis and treatment of neuroendocrine tumors. Scand J Gastroenterol. 2015;50(6):740-7.
7. Sundin A, Arnold R, Baudin E, et al; Antibes Consensus Conference participants. ENETS Consensus Guidelines for the Standards of Care in Neuroendocrine Tumors: Radiological, Nuclear Medicine & Hybrid Imaging. Neuroendocrinology. 2017;105(3):212-244.
8. Moncayo VM, Alazraki AL, Alazraki NP, Aarsvold JN. Sentinel Lymph Node Biopsy Procedures. Semin Nucl Med. 2017;47(6):595-617.

7

MYOCARDIAL PERFUSION HYBRID IMAGING

by MarieClaire Attard
and Hein Verberne

INTRODUCTION AND BACKGROUND

The coronary circulation is a strictly regulated system that matches its blood flow with oxygen requirements through regulation of vascular resistance. In this respect it is important to realise that the vessels of the coronary circulation can be categorised according to their diameter and subsequent related function. The proximal epicardial coronary arteries (conductive arteries) (size range 500 µm to 2–5 mm) mainly act as capacitance vessels. The intermediate pre-arterioles (size range 100–500 µm) act to maintain pressure in response to perfusion pressure or flow change, and the function of the intramural arterioles (size <100 µm) is mainly to match blood supply to the degree of oxygen consumption.

While the conductive arteries and proximal pre-arterioles are responsive to flow-dependent dilation, the distal pre-arterioles are more responsive to perfusion pressure changes. On the other hand, arterioles are highly responsive to metabolic regulation as a result of an increase in oxygen demand. This makes the distal pre-arterioles and arterioles (i.e. resistance vessels) the main site of coronary blood flow autoregulation. Increasing or decreasing vascular resistance by respectively decreasing or increasing the vascular diameter of these resistance vessels results in decreased or increased myocardial blood flow (i.e. higher resistance results in lower flow and vice versa).

The coronary flow reserve (CFR) is a measure of the extent to which coronary blood flow can increase from the resting state to maximal vasodilation (i.e. stress). The CFR is expressed as the ratio of coronary blood flow at maximum stress to coronary blood flow at rest. Since the coronary flow resistance is primarily determined by microvascular autoregulation, CFR is considered a measure of small vessel function.

In the setting of coronary artery disease (CAD), therefore, narrowed conductive arteries activate neuronal and metabolic autoregulation processes leading to lower distal resistance and thereby maintain blood flow at rest. However, this means that some of the CFR has been used to maintain resting conditions. The CFR of a given stenosed epicardial coronary artery may thus fall short under stress, leading to perfusion abnormalities under stress. Perfusion abnormalities are an early sign in the so-called ischaemic cascade, and may lead to angina complaints at later stages of this cascade.

Exercise stress testing (e.g. bicycle or ergometer) provides a direct physiological link between exertional symptoms and coronary ischaemia, therefore dynamic exercise is the first test of choice. However, to allow for an adequate rise in coronary flow patients must be able to exercise to a workload of at least 85% of age-adjusted maximum predicted heart rate (220-age).

It is important to note that not all coronary arteries with a stenosis will cause perfusion abnormalities. Among other factors, this is driven by the geometry of the given stenosis and is almost impossible to deduce from anatomical images only. However, in general it is safe to assume that any stenosis of a coronary artery of more than 80% will most likely cause perfusion abnormalities, and that a stenosis of <20% will have no haemodynamic consequences. This means that a form of functional testing is required to assess the impact on the myocardial flow in lesions with a 20 to 80% stenosis.

There are several ways to image myocardial perfusion non-invasively. Among these techniques, myocardial perfusion imaging with radiotracers is a longstanding, proven and robust modality for (semi-)quantitative assessment of myocardial perfusion.

The addition of ECG-triggered acquisitions (i.e. gated SPECT) allows for the assessment of left ventricle volumes and ejection fraction [2]. The ejection fraction obtained is highly dependent on the regularity of the heart rate. An irregular heart rate or one with several premature ventricular contractions (PVC) will not permit accurate measurement of ventricular volumes, and will therefore result in inaccurate assessment of left ventricular ejection fraction.

Hybrid Imaging

As already stated in the 2015 EANM procedural guidelines for myocardial perfusion imaging, hybrid imaging is defined as the combination and fusion of two datasets by which both modalities significantly contribute to image information [1]. Typically, hybrid imaging is synergistic, i.e. more powerful than the sum of its parts, as it provides information beyond that achievable with either data set alone, leading to improved sensitivity and specificity [2].

The term hybrid imaging does not apply to the combination of nuclear cardiac imaging with X-ray-based attenuation correction (AC), where the (low-dose) CT images do not provide independent information, but only contribute to improving the image quality of the other modality (PET or SPECT) [3].

As there is substantial inter-individual anatomical variability in coronary arteries, the so-called standard distribution of myocardial perfusion territories does not correspond with the patient's individual anatomy in more than half of the patients [4]. Most frequently, left circumflex artery segments are erroneously assigned to the right coronary artery territory, and standard left anterior descending artery segments are erroneously assigned to the

left circumflex territory [5].

Incidental cardiac and extra-cardiac CT findings are not uncommon [6]. Although most such findings are negligible, some may be of clinical relevance. It is thus recommended that images are additionally screened by a physician fully trained in CT readings, including non-contrast-enhanced CT scans for attenuation correction and scouts.

The integration of coronary anatomy through CCTA and (quantitative) documentation of the true ischaemic burden through SPECT/PET allows effective identification of:

1) patients with CAD benefiting from optimal medical therapy versus those who should undergo coronary revascularisation,

2) the culprit stenosis in patients with multiple coronary artery lesions, thereby guiding clinicians to the appropriate method of revascularisation,

3) patients with subclinical coronary atherosclerosis where more aggressive prevention may be indicated, and

4) patients with normal coronary arteries who can safely be deferred from any further cardiac testing.

In summary, the complimentary anatomical and functional information provided by hybrid SPECT/PET-CCTA imaging has been demonstrated to confer added diagnostic value in CAD detection and to effectively stratify risk, predict outcomes, guide patient management, and contribute to optimal downstream resource utilisation.

In general, the primary indications for stress myocardial perfusion imaging are: (1) for diagnostic purposes in patients with suspected CAD; and (2) for prognostic purposes in patients with known CAD or symptoms suggestive of CAD.

The major strength of the technique is its ability to provide powerful prognostic information in a wide range of patient populations, including patients with known CAD, at high risk of CAD, post-myocardial infarction, diabetes, advanced age, obesity, and women.

Clinical Applications of Myocardial Perfusion Imaging

The most appropriate patients for whom this test should be considered include:

(1) patients at intermediate-to-high risk of CAD who have symptoms suggestive of CAD;

(2) patients with known CAD who have new or recurring symptoms that may be attributable to myocardial ischaemia;

(3) patients with prior revascularisation who have recurrent symptoms.

Finally, a less common group of patients that may be eligible for myocardial perfusion imaging are those who have had recent myocardial infarction and did not undergo an early cardiac catheterisation and reperfusion treatment strategy.

Selected lower-risk patients may be candidates for this study as well, particularly if they cannot exercise or if the ECG is not interpretable (left bundle branch block, ventricular pacing, and severe baseline ST segment abnormalities). This study may also be indicated for pre-operative risk stratification prior to high-risk non-cardiac surgery if the results of the study will impact on the peri-operative management of the patient.

The most detailed criteria available to select patients for this procedure are the "Appropriate Use Criteria for Cardiac Radionuclide Imaging" published by the American College of Cardiology and other cardiology or imaging societies.

SPECT/CT

SPECT/CT cardiac imaging is relatively non-invasive, and the technology and method of scanning has advanced in the last couple of years [2]. When performing myocardial perfusion imaging with SPECT/CT, the patient usually undergoes the SPECT first before the CT. One reason for this is that the SPECT examination should first be checked for extra-cardiac activity that might interfere with the interpretation of the perfusion imaging. This way, if the SPECT needs to be repeated, the patient will not be exposed to an additional dose of radiation through an extra CT. When performing the CT, the patient is positioned in the gantry in the same position as during the SPECT acquisition. Generally speaking, the additional CT can be performed to improve image quality (attenuation correction) and/or to acquire anatomical information (i.e. calcium score and coronary artery lesion diameter stenosis). As previously stated, the term hybrid imaging is reserved for the latter indications only. The combined radiation burden associated with SPECT/CT depends strongly on the type of scanner used (CZT vs. more conventional techniques, attenuation correction low-dose CT vs. diagnostic CT, etc.).

In order to improve image quality related to attenuation of the detected SPECT photons, a low-dose CT can be performed. Generally speaking, a CT scan is a reflection of tissue density and thus a reflection of attenuation caused by the different tissue types [7]. The SPECT and CT are usually matched and aligned using dedicated (fully automated) software packages. However, manual correction sometimes remains indispensable and it is the task of the operator to ensure that this is done properly. If manual correction is performed by an inexperienced person, artefactual cardiac defects may occur, leading to an incorrect management of the patient's disease. Image 1 illustrates the software fusion process when the nuclear medicine examination is matched with the CT used for attenuation correction

[2]. Dedicated cardiac scanners usually offer reduced scanning times, allowing for increased patient throughput but also reducing patient discomfort.

It is important to note that the CT-derived attenuation maps do not always have diagnostic quality [2]. Of course, reconstructions performed in the lung setting may reveal incidental findings which prompt further investigation. In addition, and depending primarily on the quality of the CT, the low-dose CT can also be used to obtain a calcium score.

After the CT for attenuation correction, the patient might subsequently undergo an additional CT for calcium scoring. Still in the same position as for the SPECT and CT, a more accurate scout is performed in which the heart is scanned between top and bottom limits (set by the nuclear medicine technologist).

Different cameras are available for the acquisition of myocardial perfusion images. A SPECT camera equipped with multi-pinhole collimators delivers high sensitivity and shortened acquisition times [2].

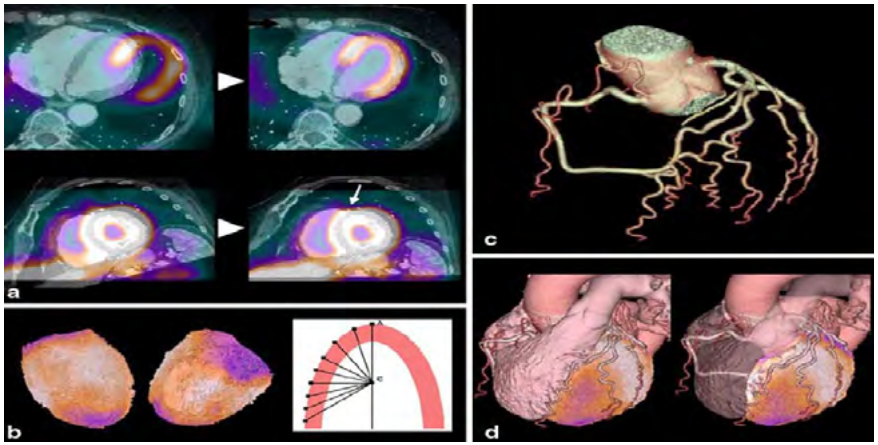

Image 1
[2] Kaufmann P., Springer 23:327

POST-PROCESSING

Advances in processing software have introduced very sensitive methods of visualising myocardial perfusion. Data sets from different imaging modalities can also be matched and processed together, making imaging possible with no need for repetition [2].

RADIATION BURDEN

SPECT/CT is associated with radiation exposure. Hybrid imaging techniques use radiolabelled tracers that enable visualisation of the myocardial perfusion. The addition of CT will increase the radiation exposure for the patient. However, most modern CT scanners are very effective in reducing radiation exposure. The additional radiation exposure of CTCA can be as low as 1 mSv.

Performing SPECT/CT together with CTCA increases the chances of coronary artery disease detection and acquires a full examination using a one-stop approach. The patient does not need to come back for another appointment but continues to follow the trajectory intended for treatment (if any).

DIAGNOSTIC CT

The number of examinations performed by SPECT/CT combined with coronary CTA reduces the number of invasive coronary angiographies [7]. The technique is relatively inexpensive, readily available and non-invasive. It provides good diagnostic information on the presence of stenosis due to calcified or soft plaques.

A CT coronary angiogram requires the administration of intravenous contrast and specific imaging protocols, scanning in step-and-shoot or helical mode. Furthermore, a CT coronary angiogram requires a heart rate that does not interfere with the acquisition of the CT images. By using beta-blockers (such as Metoprolol™ or Bisoprolol™) the heart rate can be controlled, thereby improving image quality. Patients with irregular heart rates should not be scanned for CTCA. In addition, in patients with high grades of calcified lesion the CTCA is less accurate, leading to overestimation of lesion severity. A (nuclear medicine) physician should decide whether to perform a CTCA in patients with a Ca Score >300 [9].

For CTCA, the minimum number of detectors involved in CT is 64 [2]. This is because the spatial and temporal resolution needs to be high in order to diagnose coronary artery disease using CT [2]. CT coronary angiography should only be performed when the potential benefits outweigh the risk involved. It is important

that the patient is well prepared before the CTCA examination, the aim being to scan once only and thus avoid a repeat examination that would increase the patient's radiation dose.

Another type of imaging, such as e.g. rubidium imaging, should be considered in obese patients or in patients with high and/or irregular heart rates [2].

DEVELOPMENTS AND LIMITATIONS

The combination of techniques and modalities reduces the incidence of false positive results. The CT part of the SPECT provides the attenuation correction for the perfusion image but offers no diagnostic quality. The SPECT part of the examination is an excellent detector of perfusion abnormalities. If a CTCA is performed, there is no detection of ischaemia, only an assessment of the anatomy of the coronary arteries and the surrounding anatomy. Together, however, they make detection of coronary artery disease highly sensitive and specific. When performed separately, a normal MPI does not exclude the presence of coronary artery disease [2]. Image 2 shows a clear example of this using polar maps and a volume-rendered CTCA.

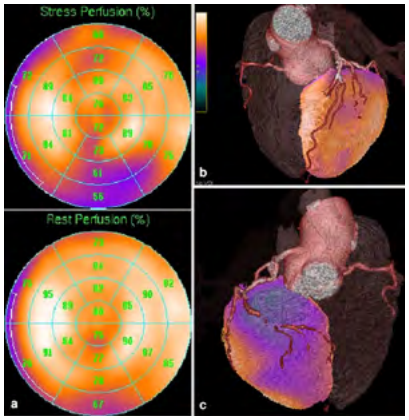

Image 2

[2] Kaufmann P., Springer 23:329

The stress perfusion polar map shows a defect in the basal inferior area which is almost completely resolved during the resting examination (a). However, when a CTCA was performed on the same patient, there was found to be some calcification but no perfusion defects on the anterior wall (b). The posterior volume-rendered image (c) shows an occlusive lesion in the left circumflex artery (LCX) which results in the decrease in perfusion in the basal inferior area.

The reporting nuclear medicine physician must be careful when assessing the images because a normal perfusion SPECT still might not exclude coronary artery disease and the result of the examination might end up being false negative [10].

Motion or breathing artefacts still remain a problem when performing CTCA [10]. Premature ventricular contractions (PVC) during the exact moment of CTCA scanning would result in an inconclusive scan that might need to be repeated.

THE ROLE OF THE NUCLEAR MEDICINE TECHNOLOGIST

Concise and careful planning by the technologist performing the scan is key. Details of the examination and instructions regarding relaxation and breathing need to be explained to the patient prior to the procedure.

The technologist performing the CTCA should be trained to recognise any lesions and report these to the nuclear medicine physician reporting the scan. Detection of a sub-occlusion may prevent the patient suffering a coronary heart attack. A properly trained team and ongoing education enhance performance, patient interpretation and management and improve the accuracy of the examinations performed.

CONCLUSION

Hybrid and multimodal imaging provides detailed information regarding myocardial perfusion studies and coronary artery disease. The results of these examinations influence diagnosis, risk stratification of patients, the treatment involved and patient management.

The whole purpose of performing the appropriate imaging test for a given patient is to improve patient outcome. High-quality images are essential in order to arrive at the proper diagnosis and prognosis.

When seen together side by side, CTCA and myocardial perfusion imaging provide comprehensive information about coronary artery disease, providing the nuclear medicine physician and cardiologist with insight and guidance as to the correct management of the patient.

REFERENCES

1. Verberne H., Acampa W., Anagnostopoulos C., BallingerJ., Bengel F., De Bondt P., Beuchel R., Cuocolo A., van Eck-Smit B., Flotats A., Hacker M., Hindorf C., Kaufmann P., Lindner O., Ljungberg M., Lonsdale M., Manrique A., Minarik D., Scholte A., Slart R., Tragardh E., de Wit T., Hesse B., EANM, EANM Procedural Guidelines for Radionuclide Myocardial Perfusion Imaging With SPECT and SPECT/CT: 2015 Revision, European Journal of Molecular Imaging, (2015), 42(12): 1929-40
2. Kaufmann PA., Cardiac Hybrid Imaging: state-of-the-art, Annals of Nuclear Medicine, (2009), 23(4): 325-31
3. Flotats A., Knuuti J., Gutberlet M., Marcassa C., Bengel F., Kaufmann P., Rees M., Hesse B., Cardiovascular Committee of the EANM the ESCR and the ECNC., Hybrid Cardiac Imaging: SPECT/CT and PET/CT. A Joint Position Statement by the European Association of Nuclear Medicine (EANM), the European Society of Cardiac Radiology (ESCR) and the European Council of Nuclear Cardiology (ECNC), (2011), 38 (1): 201-12
4. Javadi M., Lautamaki R., Merrill J., Voicu C., Epley W., McBride G., Bengel F., Definition of Vascular Territories on Myocardial Perfusion Images by Integration With True Coronary Anatomy: A Hybrid PET/CT Analysis, (2010), 51 (2): 198-203
5. Gaemperli O., Bengel F., Kaufmann P., Cardiac Hybrid Imaging, (2011), 32 (17):2100-8, Eur Heart Journal
6. Husmann L., Tatsugami F., Aepli U., Herzog B., Valenta I., Veit-Haibach P., Buechel R., Pazhenkottil A., Gaemperli O., Burkhard N., Wyss C., Kaufmann P., (2009), Prevalence of Noncardiac Findings on Low Dose 64-slice Computed Tomography Used for Attenuation Correction in Myocardial Perfusion Imaging with SPECT, International Journal Of Cardiovascular Imaging, 25(8):859-65
7. Greulich S., Sechtem U., Multimodality imaging in coronary artery disease – "the more the better?", (2015), Elsevier, Available at www.sciencedirect.com
8. Wann S., Tunio J., Current challenges and future directions in cardiac imaging, (2010), Journal of the Saudi Heart Association, Available at www.sciencedirect.com
9. Gaemperli O., Kaufmann P., Alkadhi H., Cardiac hybrid imaging, (2014), European Journal of Nuclear Medicine, 41 Supp 1, p91-103, Springer.
10. Kauling R., Post M., Rensing B., Verzijlbergen J., Schaap J., Hybrid SPECT.CCTA Imaging in the Work-up of Patients with Suspected Coronary Artery Disease, (2015), Current Cardiovascular Imaging Rep 8:2, Springer Science+Business Media New York.

8

ACCOMPLISHING GOOD DIAGNOSTIC EXAMINATIONS FROM THE PAEDIATRIC POPULATION

by Pietro Zucchetta

Many factors contribute to quality in paediatric nuclear medicine, from a correct referral to a clear and timely report. Scan planning, radiotracer administration, and image acquisition are probably the most relevant aspects involving the nuclear medicine technologist. It is a significant challenge, because standard imaging strategies fall short of the target due to the many differences between adult and child, including disease spectrum.
The technical aspects of most paediatric nuclear medicine examinations are detailed in a number of guidelines and textbooks. Still, there are some general issues worth discussing because they shape the foundations of the approach to the paediatric patient. Moreover, they quite often represent a significant obstacle in setting up a regular paediatric schedule.

The most relevant issue with a large number of paediatric patients is probably the lack of cooperation, with the resulting problems in radiotracer administration, patient positioning, etc. Nevertheless, paediatric nuclear medicine offers invaluable data in many clinical situations and has an established track record as a powerful and safe technique.

The experience of dedicated centres shows that an integrated approach is key to obtaining high-quality nuclear medicine examinations in paediatrics. This integrated strategy relies on careful consideration not only of the technical aspects but also of the complicated emotional and social relationship with the child and his/her parents. The family can be a powerful ally or a significant drawback, and experienced staff will make any attempt to include the parents or other family members in the team in charge of the examination.

Teamwork is a mainstay of paediatric nuclear medicine: a single operator, even if highly skilled and experienced, can seldom manage all the steps. The goal is to create a safe, friendly environment that reduces anxiety, fear, and stress for everyone involved, including the staff. Including the family in the work of the team is of paramount importance, and every effort is required to establish a sound relationship, avoiding barriers and considering doubts and the need for information and reassurance. A gentle, open attitude and a lot of patience can work wonders, even in the most challenging situation.

This approach requires an adequate allotment of time, because rushing the child and his/her parents from the reception area to the scanning table can enhance fear and stress, giving the impression that the patient is being treated like an object. As a rule of thumb, paediatric scans need twice as long as adult ones. Each exam is unique with regard to technical aspects (i.e. venous access, positioning, etc.) and emotional requirements. Therefore, scheduling of paediatric scans needs to be flexible; it is highly preferable to have a dedicated room, and to avoid intermixing adult and child scans or setting a too-tight schedule. A frequent solution is to reserve a room for paediatric activities once or twice a week. Adequate time is probably the most relevant requisite to reduce sedation requirements. Cooperation can be obtained in most cases if the time constraints are adapted to the paediatric environment, from explanations to venepuncture and immobilisation. In most cases a window of opportunity opens at some point, but that point is difficult to identify in advance. On the other hand, however, the window will not remain open indefinitely, because boredom, fear or hunger can swiftly turn cooperation into active opposition.

Scheduling should allow a little extra time and dedicated space for the first encounter: creating the right environment in the preparatory phase will save time and trouble during the scan. It is highly advisable to set up a child-only space, even a small, temporary one, with decorations, games, TV set, etc. Hospitals often seem cold and sometimes downright frightening places for younger children: a couple of pencils and a sheet of paper can work magic.

RADIATION PROTECTION

Radiation protection is a key point in the day-to-day activity of a nuclear medicine department. Ethical and legal constraints require strict control of exposure to radiation for patients, staff, and the general public.

The concern over radiation-related health risk is even higher in children, because data from the population of atomic bomb survivors suggests increased susceptibility with decreasing age. Therefore, paediatric nuclear medicine examinations require rigorous measures to keep radiation exposure to the lowest level compatible with a useful exam.

The activity administered to the adult patient has to be scaled down in children, using body weight or body surface as a reference. The "Paediatric Dose Calculator" (available on the EANMMI website or as a stand-alone app) simplifies the calculation based on the body weight and offers a quick estimate of the radiation dose associated with the proposed activity. It is worth reiterating that the recommended

activity should be adapted to the specific exam, considering e.g. the equipment used (detector technology, collimator, etc.), scan duration (3 vs. 4 minutes per bed position in PET imaging) and sedation time constraints and risks.

The expanding role of hybrid imaging, mainly SPET/CT and PET/CT, has further complicated the issue, because the CT part of the exam requires additional care to avoid unnecessary exposure. The latest scanners and cameras offer dedicated paediatric protocols, which should be used whenever possible because they allow a significant reduction of the dose to the patient.

Every exam should be tailored to the individual patient and the clinical setting, avoiding standardised presets.

Careful observance of the radiation protection rules will also help reassure the parents about the safety of the nuclear medicine examination. Even the most relaxed and trusting parent has some doubts about the radiation-related risks, which must be discussed explicitly before the start of the scan. We do not really know if diagnostic doses increase the risk of developing cancer, but the technologist should clearly state that this risk, if present, is very low and that the information gained from the examination is essential to the clinical management of the child. The explanation is usually straightforward, because most of the functional data gathered from a nuclear medicine exam cannot be obtained easily or with fewer risks using other diagnostic methods.

The level of detail given in the explanation should be adapted to the knowledge level of the parent(s), but reticence and oversimplification should be avoided. A clear description of the balance between potential risks and clinical benefits is essential information and plays a pivotal role in communication between the treatment team and the family.

COMMUNICATION

Communication is the key to obtaining the cooperation of the family and, where possible, the child. Preliminary facts should be provided to the family before the procedure, via leaflets, e-mail, relevant sections on the institutional website, etc. Only a few of the common nuclear medicine procedures in paediatrics require specific preparation (i.e. fasting for some GI studies, avoiding interfering drugs before an MIBG scan or a brain FDG PET/CT). The most relevant exception is probably whole-body FDG PET/CT, where image quality requires fasting, avoidance of physical activity in the day(s) before the scan and prevention of exposure to cold during the hours preceding the injection. The last point is particularly relevant, because temperature-dependent brown-fat activation can interfere heavily with image interpretation, particularly in lymphoma patients.

The patient's information is provided before the scan, covering the indication for the examination, approximate scan duration, injection technique and institutional policy regarding venepuncture attempts, radiation exposure and immobilisation. Open questions are preferable (i.e. "Do you know why/how/…?, Have you been told…? ") because they allow for doubts or practical requirements. The health professional should steer the talk, keeping it to reasonable time limits, but it is essential to focus on the conversation and avoid multitasking. Room preparation, computer set-up, etc. should have been performed already or put off until the end of this critical phase.

Key points should be summarised and repeated to avoid misunderstandings due to emotional pressure or time constraints. It is crucial to deliver a coherent message; therefore the whole staff need to know the relevant details of the procedure.

Parents are not the only object of the information effort. The child is at the centre of the action, and even young children should be involved and informed, adapting the approach to their stage of cognitive and psychosocial development. Children's attention span is often underrated, but they are usually well aware of their situation and want to be reassured.

Infants and babies cannot understand verbal commands, but voices, handling and general attitude can have a profound influence on their reactions. Smiling, a soothing tone, and uninterrupted contact with a cooperative parent can facilitate the most complex procedure. Simple explanations can be given to children starting at about 3 years old, with the child sitting on a parent's lap. Try to keep your eyes at the same level as the child's: it is often difficult to trust a towering white-clad adult. Explanations should be brief and adapted to the child's attention span and level of understanding.

Open, honest communication with parents is essential in order to obtain their cooperation and establish a good technologist–parent relationship, but honesty is also vital in gaining the trust of the child. It is not necessary to underline unpleasant details, but one has to be truthful, if reticent. Crying should not be frowned upon, because it is a normal reaction to stress and pain, particularly when the child is incapable of verbal communication. Recognising stress and fear often helps to reduce weeping and sobbing when pain and discomfort are experienced.

Offering choices helps the child to gain some control over her/his situation: choosing the position of the parent beside

the scanning bed, selecting videos or music on a tablet, etc.

The injection is probably the most significant source of fear for the child, and a proper injection technique is essential to avoid unnecessary distress. Anaesthetic creams can be used to reduce pain and fear, but the most relevant aspect remains a good relationship with the child and the parents. Tactful explanation of the various steps, underlining what is absolutely painless, will keep the negative anticipation to a minimum. Bandages and medication removal are often perceived as unpleasant, so it is useful to ask for the child's cooperation.

The explanations to the child are a good opportunity to reinforce some of the messages to the parents and give them another chance to ask supplementary questions.

The final phase of the conversation should cover instructions for the management of the child after the scan. They usually include free oral hydration and frequent voiding to reduce the radiation dose to the bladder, as well as advice on the proper disposal of radioactive nappies.

SEDATION

It is possible to perform most of the nuclear medicine procedures in paediatric patients without sedation. Many departments sedate only a small proportion of children undergoing standard planar imaging. Lengthy examinations (mostly PET/CT, SPET/CT, PET/MR) usually require sedation, when immobility is essential and repeated acquisitions are contraindicated and cumbersome.

The age range varies slightly, depending on local resources and skills, but the most frequent indication for sedation is between 8-9 months and 4-5 years.

Imaging of babies and small children can often rely on the induction of natural sleep. An earlier wake-up and avoiding naps before the examination are useful strategies, as is feeding before the scan, most often after an IV line has been placed. Dimmed lights and a quiet environment (beware of phones, intercoms, etc.) can facilitate sleep induction.

Sedation should not be a routine option, therefore, because it carries some definite risks, but is reserved for selected cases after careful cost-benefit analysis. Sedation usually requires specialised professionals for administration and monitoring, and all the equipment needed (vital signs monitors, infusion pumps, resuscitation tools) must be available and checked before starting the procedure.

Patient preparation and requirements are subject to local regulations and institutional policies, often including an anaesthesiologic evaluation in the days before the examination. Strict adherence to the preparation protocol and absence of contraindications to sedation (i.e. febrile illness, acute disorders, etc.) need to be verified before injecting the radiotracer.

It is also worth remembering that the occupation time of the scanning room is often longer than for conscious patients, particularly if no recovery room is available.

INJECTION

The injection is the critical step in many paediatric scans, and the time required to identify the optimum site and position a safe access can be as long as 30 minutes, even in a dedicated environment with experienced staff.

The most favourable situation is having an IV line already established on the inpatient's hospital ward. Use of indwelling central catheters or ports may be allowed, and in many oncological patients this is the only available access. In this case, the injection is usually reserved to trained personnel using scrupulous sterile technique. It is highly advisable to use the shortest line available and to flush it before injecting the radiotracer. The acquisition of a dynamic scan (i.e. MAG-3 renography, 3-phase bone scan) has to start before injecting a central line, because the bolus will arrive in the field of view very quickly. After the injection it is essential to flush the line thoroughly to avoid radiopharmaceutical retention, particularly at the tip of the device.

Butterfly needles fitted with a three-way stopcock are preferred when an IV line is not available. A saline syringe or an IV line is connected to one port and the radiopharmaceutical syringe to the remaining one. A first saline flush will verify vein patency, and after the radiotracer injection a second flush will complete dose delivery, leaving the line in place if required (diuretic test, etc.)

At least in smaller children, a second operator should help in immobilising the injection site; parents should mainly try to soothe the child, but they can help control the other limbs if they are willing to do so. This is a critical point in the procedure, because even small children or babies can be difficult to control when they are overwhelmed by fear, particularly if they are surprised by the venepuncture. On the other hand, it is essential to avoid a brute force approach. Careful evaluation and planning are therefore required during the previous phase to identify the role of each team member.

IMAGING ENVIRONMENT

The imaging environment encompasses not only the scanning room but also the reception area, the waiting room, and the corridors. It is important to introduce child-friendly elements such as cartoon posters or wall decorations to make the atmosphere less intimidating. If a dedicated waiting room is available, a TV set or a computer/tablet showing movies or children's shows may help, particularly for longer post-injection waiting times. Toys and games need appropriate cleaning to avoid spreading infection, but the information leaflet can suggest that families bring one favourite toy from home. The toy can participate in the scanning procedure, staying with the child on the imaging table to provide comfort and reduce apprehension.

Child-friendly decorations can also help on the scanning room walls and ceiling, or on the gamma camera and the PET/CT gantry. Needles, syringes, scissors, and other menacing equipment should be kept out of view whenever possible.

The single-head gamma camera is the best solution for imaging of babies and young children. The camera should be configured head face up underneath the imaging table. In some models it is possible to fit an adapter over the collimator surface, allowing the direct positioning of the baby on it. This set-up has the advantage of direct access to the child, with better positioning, supervision, and immobilisation. Moreover, the child will not be frightened by the impending camera and will have unobstructed access to his/her parents and distractions such as videos, phones, etc. when supine.

Some manufacturers offer dedicated cradles, which are mounted on the standard table. These offer some advantages in SPECT imaging, but their practical utility is debated. Different types of vacuum cushion are also used, with good results. Whatever the method, the child cannot be left unattended.

It is advisable to have the parents remove any unnecessary clothing and, where applicable, to change the child's nappy just before positioning the patient. This should happen in a different room, or at least on separate stretcher/bed, to prevent urine contamination of the imaging table or the detector.

When the child lies on the table under the camera head, it is mandatory to reassure him/her and avoid direct contact between the camera and the body of the patient. A parent or member of staff should keep the child under direct and continuous control, to prevent sudden movements and bumping of the head or limbs on the camera. Gentle restraint is necessary for babies and younger children, to avoid movement artefacts and keep the patient safe. Parents should cooperate in keeping the child still, but often they need to be directed and helped by the technician.

Safety straps or some other kind of gentle restraint should always be used, because they guarantee the safety of the child. They are no substitute for careful uninterrupted monitoring, because quiet children can become agitated within a few seconds due to noise or simply boredom, and even sedated children can awake suddenly. Therefore, the technologist should never leave a child unattended on the imaging table, and it is prudent to have a member of staff on hand to help the parent.

The staff should demonstrate the use of the restraints before the examination, both to the parents and to the child, whenever possible. It must be made clear that they are for the child's protection and are not a way of avoiding contact with the child.

At the end of the acquisition, it is better to check the whole scan before allowing the child off the table. It is often a challenge to convince the child to return to the gamma camera or the PET scanner, even for a single one-minute image.

The technologist should anticipate table and detector movement in order to reassure both the child and the parents. Good communication must continue for the whole duration of the scan, maintaining empathy and preventing anxiety. Encouragement and praise can motivate older children and are often appreciated by adolescents as well. Stickers, bravery awards, etc., presented to the patient before discharge, can help reduce any negative feelings. The child and his/her parents should always be reassured, even in difficult and prolonged examinations.

Finally, it is useful to point out that follow-up examinations will also run more smoothly if they can build on an established good relationship between the technologist, the child, and the parents.

IMAGE ACQUISITION

As a general rule, the acquisition protocol should be adapted to each patient, not only with regard to the obvious parameters related to body habitus, weight, etc. (i.e. acquisition zoom or pixel dimensions), but to the general approach. The goal is not to achieve the best image quality possible, but to acquire the image(s) needed to resolve the clinical question. This goal should be achieved in the shortest time possible, keeping stress to a minimum for the child and for the parents.

Motion correction software can help in reducing motion artefacts, particularly in SPET/CT acquisition. However, it cannot substitute for careful positioning, clever use of mild restraint and meticulous

watching throughout the entire scan.

Many distraction techniques have proven useful, from reading stories to DVD players, smartphones, and tablets. The parents can usually identify the best solution and should be warmly encouraged to deploy their skills in this crucial task. As a positive side effect, they will also feel more in control of the situation.

CONCLUSION

Paediatric nuclear medicine poses many challenges to the nuclear medicine team, and the technologist is deeply involved in most steps of the procedure. Obtaining quality images while keeping physical and emotional discomfort to a minimum requires sounds technical knowledge, empathy, flexibility, and a lot of patience. On the other hand, this can be one of the most rewarding professional activities because the patients and their parents feel the engagement and are usually very grateful. At the end of the day, smiles usually overcome tears and whining.

SUGGESTED READING

1. Gordon I. Issues surrounding preparation, information and handling the child and parent in nuclear medicine. J Nucl Med. 1998;39(3):490–494.
2. Pintelon H, Jonckheer MH, Piepsz A. Paediatric nuclear medicine procedures: routine sedation or management of anxiety? Nucl Med Commun. 1994;15(8):664–666.
3. Ljung B. The child in diagnostic nuclear medicine. Eur J Nucl Med. 1997 Jun;24(6):683-90.
4. Borgwardt L, Larsen HJ, Pedersen K, Højgaard L. Practical use and implementation of PET in children in a hospital PET centre. Eur J Nucl Med Mol Imaging. 2003;30(10):1389–1397
5. Gelfand MJ, Clements C, MacLean JR. Nuclear Medicine Procedures in Children: Special Considerations. Semin Nucl Med. 2017;47(2):110–117.
6. Lassmann M, Treves ST; EANM/SNMMI Paediatric Dosage Harmonization Working Group. Paediatric radiopharmaceutical administration: harmonization of the 2007 EANM paediatric dosage card (version 1.5.2008) and the 2010 North American consensus guidelines. Eur J Nucl Med Mol Imaging. 2014;41(5):1036–1041
7. Parisi MT, Bermo MS, Alessio AM, Sharp SE, Gelfand MJ, Shulkin BL. Optimization of Pediatric PET/CT. Semin Nucl Med. 2017;47(3):258–274.

9

INFLAMMATION AND INFECTION STUDIES

by Andor W.J.M. Glaudemans

INTRODUCTION

Molecular imaging of infections and inflammatory diseases has seen a dramatic growth in interest in the last decade due to improvements in our knowledge of the pathophysiology of infections and inflammatory diseases, as well as to recent development in imaging modalities. Nuclear medicine imaging offers unique possibilities to differentiate between infections and sterile inflammation and between infections and tumours, but it has also important added value in defining the extent of an infection, in selecting the best location for biopsy, and in monitoring treatment efficacy. Hybrid camera systems allowing combinations of pathophysiology and anatomy have led to better diagnostic accuracy. Nuclear medicine has positioned itself as a key player in the field of infections and inflammatory diseases.

Different nuclear medicine imaging techniques and radiopharmaceuticals are available for imaging infection and inflammation. However, all of them have their pros and cons, not all techniques are available in every centre, and there is widespread variation in how the scans are acquired and the results interpreted. Over the last decade, the EANM Committee on Inflammation and Infection has worked hard on three main goals: [1] the standardisation of nuclear medicine techniques for the diagnosis of infection and inflammation and their interpretation criteria, [2] the dissemination of these techniques amongst nuclear medicine practitioners, and [3[the publication of joint diagnostic guidelines with clinicians [1].

The following guidelines are available now for those with an interest in a particular topic: [1] guidelines on how to label autologous white blood cells [2,3], [2] guideline on the correct acquisition and interpretation criteria for white blood cell imaging [4], [3] guideline on the use of FDG in infection/inflammation [5], [4] guideline on multimodality imaging for infective endocarditis [6], [5] guideline for vasculitis and polymyalgia rheumatica [7], [6] guideline for cardiac sarcoidosis [8], [7] guideline on peripheral bone infection [9], [8] guideline on prosthetic joint infection [10], [9] guideline on spinal infections [11], [10] guideline on vascular graft infections [12], and [11] guideline on cardiac amyloidosis [13]. Many of these guidelines focus on FDG-PET/CT imaging as the nuclear medicine imaging technique of choice, but some of them also still include conventional nuclear medicine imaging (gamma-camera imaging).

In this chapter, the most commonly used radiopharmaceuticals and imaging techniques for gamma-camera imaging of infection and inflammation will be discussed, with a focus on the correct acquisition and interpretation of the scans. The most often used technique is white blood cell scintigraphy. The other commonly used conventional imaging techniques (bone scan, bone marrow scintigraphy, ^{67}Ga-citrate) only play a minor role these days, but will also be discussed.

In the second part of this chapter, an overview will be given of all available radiopharmaceuticals for conventional nuclear medicine imaging and some experimental radiopharmaceuticals will be discussed. Finally, some clinical examples will be shown.

RADIOPHARMACEUTICALS FOR GAMMA-CAMERA IMAGING

Bone scintigraphy

The bone scan is one of the oldest existing nuclear medicine techniques and is still one of the cornerstones of nuclear medicine practice in many centres, despite the increasing use of the PET bone scan (NaF-PET) in some hospitals. Gamma-camera bone scintigraphy is performed by intravenous administration of diphosphonates labelled with ^{99m}Tc. Generally, the bone scan consists of three phases (perfusion, blood pool, and late phase with incorporation of the radiopharmaceutical into the bone matrix) and all phases are necessary when a bone infection is suspected. Recently, a procedural guideline was published on how to perform bone scintigraphy correctly [14].

The three phase bone scintigraphy can be used as an initial screening method to exclude the presence of peripheral bone infection in case of negativity, because of its good availability (it can mostly be performed within 24 hours of the request from the referring clinician), relatively low costs and high negative predictive value. After recent fracture and/or surgery and if there is high suspicion of an infection the role of bone scintigraphy is negligible, since the specificity is rather low, and uptake can be seen in all sites of increased bone metabolism irrespective of the underlying disease. Furthermore, in a low-grade infection the first two phases can even be negative, so the late phase is essential and when positive it may be the only indication of an existing infection.

The time frame in which the bone scan is confirmed positive after fracture and/or surgery is not known, but increased osteoblastic activity probably remains visible within the first 2 years of the trauma or surgery. During this time period there is no role for bone scintigraphy. There

might be a role in chronic latent bone infections, but even then, a positive bone scintigraphy must be interpreted with caution and when positive other imaging methods are necessary to better differentiate between real infection and other causes of increased osteoblastic activity.

Indications for the use of bone scintigraphy in infections and inflammatory diseases are: (1) To exclude the presence of an infection in the musculoskeletal system, and (2) to look for viability of the involved bone or to see if there are sequestra. When this is the only question from the referring trauma or orthopaedic surgeon, then a three-phase bone scintigraphy is required. When performing a conventional bone scan, all three phases are necessary to see if there is perfusion and osteoblastic activity of the involved bone. When looking for a sequester (which can be rather small) SPECT/CT is required for exact location and in order to see a small "cold" spot in the case of a sequester. This is really the only question for which bone scan is the absolute best option in patients after trauma and/or bone surgery. However, since the spatial resolution in conventional bone scintigraphy is rather limited (to approximately 8 mm), smaller sequestra may be missed.

White blood cell scintigraphy

Scintigraphy with labelled autologous white blood cells (WBC scintigraphy) is another of the oldest existing nuclear medicine imaging techniques (developed back in the 1970s), though thanks to better and hybrid imaging systems and improved acquisition and interpretation criteria it is still the gold standard in nuclear medicine techniques for several infections.

Scintigraphy with autologous leukocytes is characterised by high specificity, because the latter only accumulate as a consequence of active migration into inflamed tissues. After injection, radiolabelled WBCs show rapid clearance from the lungs and blood pool, with progressive migration into the spleen, liver, bone marrow and sites of infection where a neutrophilic infiltrate predominates.

Radiolabelled WBCs first adhere to the vascular endothelium and then migrate toward the infected area through the endothelium and basal membrane. Thus, radiolabelled WBCs are a specific indicator for leukocytic infiltration [15].

The white blood cells can be labelled with either ^{99m}Tc-exametazine (HMPAO) or ^{111}In-oxine. ^{99m}Tc-labelled white blood cells have replaced ^{111}In-labelled white blood cells for most indications, because of their more suitable radiation characteristics. ^{111}In has a long half-life of 67 h and radiation energy of 173 and 247 keV that increases the radiation burden, whereas ^{99m}Tc has a short half-life of 6 h and ideal radiation energy of 140 keV.

Due to the different biodistribution and kinetics of white blood cells (WBC) in blood, bone marrow, inflammation and infection, 3 sets of images should preferably be acquired: "early" images (between 30 minutes and 1 hour after injection), "delayed" images (2-4 h after injection) and "late" images (20-24 h after injection) (Figure 1). In order to reduce operator dependence in image display and final interpretation, image acquisition times should be corrected for isotope decay. If early images are acquired for a set number of counts or a set period of time, delayed and late images should be corrected for the isotope half-life. With this acquisition modality, different images can be compared on the same intensity scale, in absolute counts (and not in % of maximum activity), thus avoiding any operator bias. This method also allows correct detection of a true increase in uptake in suspected regions over time, an important criterion of positivity for bone infections and most soft tissue infections [4].

A scan should be considered positive for an infection when there is an increase in size or intensity over time. When there is a decrease in size or intensity over time, or when the uptake is stable over time, then the scan should be considered negative. If the correct acquisition protocols and interpretation criteria are used, this technique yields excellent overall diagnostic accuracy. Guidelines regarding indications, acquisition and interpretation of WBC scintigraphy were recently published [4].

WBC scintigraphy has a high diagnostic accuracy for infections in the musculoskeletal system (except in spondylodiscitis) [9,10]. However, the procedure itself has several limitations: the full analysis requires several scans over 2 days, blood manipulation is necessary, the labelling procedure takes time (2-3 hours) and the technique is not available in every nuclear medicine department. WBC

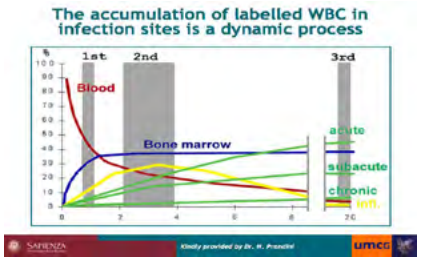

Figure 1. Accumulation of white blood cells is a dynamic process. In infections, uptake increases over time, while in inflammation there is uptake in the 1st (early) and 2nd (delayed) phase, but a decrease in the 3rd (late) phase. Bone marrow uptake remains stable over time. Due to this dynamic process, imaging at several time points is necessary. The diagram is adapted from [17].

scintigraphy can already be performed at an early stage after the trauma and/or surgery. Furthermore, use of antibiotics does not influence the results of WBC scintigraphy [16].

Currently, radiolabelled white blood cell scintigraphy is the gold standard nuclear medicine imaging technique for infections in the musculoskeletal system (peripheral bone infection, prosthetic joint infection, diabetic foot infection), but can also be used as a good alternative for FDG-PET/CT in endocarditis and vascular graft infections.

Anti-granulocyte antibody scintigraphy

As an alternative to WBC scintigraphy, labelled anti-granulocyte antibodies (AGA) can be used. The advantages of using radiolabelled antibodies against surface antigens present on granulocytes are that they are easier to use than radiolabelled autologous WBCs and do not require the handling of potentially hazardous biological specimens. Disadvantages, on the other hand, include the high molecular weight (resulting in slow diffusion into sites of inflammation), a long plasma half-life, slow concentration

in the affected site, uptake in the liver due to clearance by the reticuloendothelial system, and in some cases the induction of human antimurine antibodies, a host response to foreign antigens.

There are two antibodies commercially available: a Fab fragment, Sulesomab (Leukoscan®) and a whole murine IgG, Besilesomab (Scintimun®). Image protocols differ between complete and fragmented antibodies. Images with complete antibody (Besilesomab) should be performed 2-4 h and 16-24 h post injection. Planar images can be performed with the same acquisition protocol as WBC. Images with the fragmented antibody (Sulesomab) should be performed 1-3 and 6-8 h post injection. Guidelines regarding indications, acquisition and interpretation of AGA scintigraphy were recently published [4].

Bone marrow scintigraphy

Bone marrow (BM) scintigraphy can be used in patients with suspected infection of the musculoskeletal system when WBC (or AGA) scans are doubtful. ^{99m}Tc-colloids (colloids larger than 500 nm are recommended) are injected intravenously and images of the region of interest are acquired after a minimum of 30 minutes and a maximum time of 6 h post injection. When there is concordance between WBC and BM scan (uptake in the same region) this is probably due to physiological bone marrow activity; discordant findings (positive on WBC scan, negative on BM scan) point to an infection. However, if the correct acquisition and interpretation criteria are used for WBC/AGA imaging, only a minority of patients still require a BM scan.

^{67}Gallium-citrate scintigraphy

^{67}Ga-citrate binds in ionic form to circulating transferrin as an analogue of iron. It uses transferrin receptors (CD71) to access the cell and then becomes highly stable within the cells. Increased blood flow and increased vascular membrane permeability result in increased delivery and accumulation

of transferrin-bound ^{67}Ga in infected areas. ^{67}Ga also binds to lactoferrin, which is present in high concentrations in infected foci. Some ^{67}Ga may be transported bound to leukocytes. Direct uptake by certain bacteria has also been observed, due to the high affinity of siderophores and low-molecular- weight chelates produced by bacteria for ^{67}Ga. The siderophore–^{67}Ga complex is presumably

transported into the bacterium, where it remains until phagocytosed by macrophages. Approximately 25% of the total injected dose is excreted through the urinary system, whereas the rest is retained in the bone, bone marrow, liver and soft tissues. The best target-to-background

ratio is normally achieved after 48–72 h. ^{67}Ga-citrate has a very low specificity, and its long physical half-life (78 h) and high-energy radiation are unfavourable characteristics for scintigraphic imaging [15]. Although still used in some countries, ^{67}Ga-citrate scintigraphy is becoming obsolete and has been replaced by FDG-PET/CT. However, it may still find applications in fever of unknown origin, sarcoidosis or spondylodiscitis in centres that are lacking a PET-CT scanner.

Role of hybrid imaging

The advent of hybrid imaging technologies combining molecular/functional and anatomical information has significantly increased the diagnostic accuracy of conventional nuclear imaging examinations by increasing sensitivity and specificity and reducing the number of equivocal lesions. This hybrid technology has redefined the diagnostic work-up of patients and influenced patient management. Hybrid imaging techniques have improved image properties because of (1) advances in detector designs and collimator modelling inherent to newer devices, (2) incorporation of CT data into SPECT reconstruction, and (3) fusion of anatomic and functional data, allowing more accurate localisation and assessment of disease extent. SPECT/CT should be an integral part of a conventional scintigraphy, the main aim being to better distinguish bone infections from soft tissue infections and to more accurately assess the extent of the infectious or inflammatory process.

Other available radiopharmaceuticals for conventional infection and inflammation imaging

Many efforts have been made in the past to develop other, more specific, radiopharmaceuticals. Most of them, however, were not successful. Most attempts were made to radiolabel antibiotics, such as ^{99m}Tc-ciprofloxacin, which was the first radiolabelled antibiotic tested in humans to image infections. The first studies were promising, showing fast renal clearance with low hepatic, bone marrow or gastrointestinal uptake. The results obtained were controversial, however, which may have been the result of different bacterial strains imaged, ongoing antibiotic therapy, and a lack of standardisation in acquisition and interpretation. Other compound groups that were radiolabelled included antifungal agents, antimicrobial peptides, vitamins, endothelial cell components, antibodies, cytokines, peptides, etc. In recent years, radiolabelled interleukin-2 (^{99m}Tc-IL2) showed good results in vulnerable atherosclerotic plaques [18], for rejection after lung transplantation [19] and to visualise the lymphocytic infiltration in metastatic melanoma [20]. A PET variant is now under investigation [21]. A complete overview of available radiopharmaceuticals is shown in Figures 2 and 3.

Imaging bacteria and other micro-organisms

Antibiotics
- ^{99m}Tc/^{18}F-Ciproflaxicin (Infecton®)
- ^{99m}Tc-Alafosfalin
- ^{99m}Tc-Cefepime
- ^{99m}Tc-Cefoperazone
- ^{99m}Tc-Ceftixozime
- ^{99m}Tc-Ceftriaxone
- ^{99m}Tc-Cefuroxime
- ^{99m}Tc-Gatifloxacin
- ^{99m}Tc-Kanamycin
- ^{99m}Tc-Isoniazid
- ^{99m}Tc-Lomefloxacin
- ^{99m}Tc-Ofloxacin
- ^{99m}Tc-Moxifloxacin
- ^{99m}Tc-Nitrofurantoin
- ^{99m}Tc-Norfloxacin
- ^{99m}Tc-Pefloxacin
- ^{99m}Tc-Rifampicin
- ^{99m}Tc-Sitafloxacin
- ^{99m}Tc-Sparafloxacin

Antifungal agents
- ^{99m}Tc-Fluconazole
- ^{123}I-Chitinase
- ^{99m}Tc-CBP21
- ^{99m}Tc-hLF 1-11

Antimicrobial peptides
- ^{99m}Tc/^{18}F-Ubiquitidin 29-41
- ^{99m}Tc-human neutrophil peptide 1-3
- ^{99m}Tc-bacteriophage

Vitamins
- ^{99m}Tc/^{111}In-biotin
- ^{99m}Tc-PAMA4 (vitamin B12)

Imaging endothelial cell activation
- ^{99m}Tc-anti-E-selectin
- ^{111}In-intercellular adhesion molecule-1 (ICAM-1)
- ^{99m}Tc/^{111}In-vascular cell adhesion molecule-1 (VCAM-1)

Imaging increased extravasation
- ^{99m}Tc/^{111}In-Human Immunoglobulin-G (HIG)
- ^{99m}Tc-Albumin Nanocolloids
- ^{99m}Tc/^{111}In-biotin

Imaging infiltration of polymorphonuclear cells

Labelled white blood cells (WBC)
- ^{99m}Tc-HMPAO-WBC
- ^{111}In-oxine-WBC
- ^{99m}Tc-sulphur colloids-WBC
- ^{18}F-FDG-WBC
- ^{64}Cu-WBC

Labelled monoclonal antibodies (MoAb)
- ^{99m}Tc-antigranulocyte IgG1 murine antibody BW250/183 (Besilesomab, Scintimun®)
- ^{99m}Tc-anti-stage specific embryonic antigen-1 murine antibody (anti-SSEA-1) (fanolesomab, LeuTech®)
- ^{99m}Tc-anti NCA-90 murine antibody Fab' fragment (sulesomab, Leukoscan®)

Others
- ^{18}F-Fluorodeoxyglucose (FDG)
- ^{123}I-Interleukin-1 receptor antagonist (IL1ra)
- ^{99m}Tc-Interleukin-8 (IL8)
- ^{99m}Tc-P483H (against platelet factor 4)
- ^{99m}Tc-EP1-HNE2 (neutrophil elastase inhibitor)

Other available radiopharmaceuticals
- $^{67-68}$Ga-citrate

Figure 2. Available radiopharmaceuticals for infection imaging.

Source: Signore A, Glaudemans AW. The molecular imaging approach to image infections and inflammation by nuclear medicine techniques. Ann Nucl Med 2011; 25(10):681-700.

Imaging apoptosis
- ^{99m}Tc-Annexin-V

Imaging mononuclear cells involved in chronic inflammation
- ^{99m}Tc-HMPAO/^{111}In-oxine-Lymphocytes
- ^{111}In-Macrophages
- ^{99m}Tc-HMPAO-Monocytes

Monoclonal antibodies
- ^{99m}Tc-anti-TNFα monoclonal antibody
- ^{99m}Tc-anti-CD4 monoclonal antibody
- ^{99m}Tc-anti-CD20 monoclonal antibody
- ^{99m}Tc-anti-CD3 monoclonal antibody

Peptides
- ^{111}In-Substance P
- ^{99m}Tc-J001X
- ^{125}I-Fas peptides
- ^{99m}Tc/^{111}In-Octreotide

Cytokines
- ^{99m}Tc/^{111}In/^{123}I/^{18}F-Interleukin-2 (IL2)
- ^{123}I-Interleukin-12p40

Others
- ^{18}F-fluorodeoxyglucose (FDG)
- ^{99m}Tc/^{111}In-Human Immunoglobulin-G (HIG)
- ^{11}C-PK11195 (microglia activation)

Figure 3. Available radiopharmaceuticals for inflammation imaging.

Source: Signore A, Glaudemans AW. The molecular imaging approach to image infections and inflammation by nuclear medicine techniques. Ann Nucl Med 2011; 25(10):681-700.

CLINICAL EXAMPLES

47-year-old male patient. Pain complaints several years after surgery for a tibia fracture. CT scan was inconclusive. Because of suspected infection WBC scintigraphy was performed.

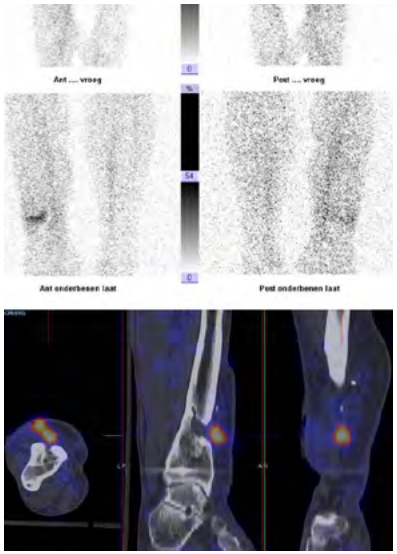

Figure 4: WBC scintigraphy (upper row: delayed images (4 h after injection of the radiolabelled cells) anterior and posterior view, middle row: late images (22 h after injection) anterior and posterior view, lower row: SPECT/CT images at the delayed time point). The planar images (corrected for decay and showed in counts intensity) show increased uptake in size over time, suspected infection. SPECT/CT reveals that the infection is located outside the bone. Scan conclusion: soft tissue infection, no bone involvement.

36-year-old male patient. Several surgical operations in the past for distal tibia fracture and pseudoarthrosis. Now wound complaints. Because of suspected infection WBC scintigraphy was performed.

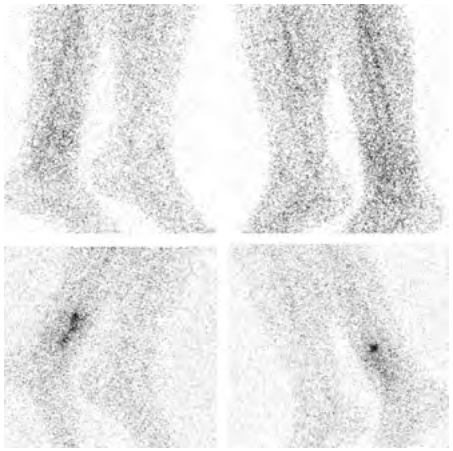

Figure 5: WBC scintigraphy (upper row: delayed images (4 h after injection of the radiolabelled cells) lateral views, lower row: late images (24 h after injection) lateral views. The planar images (corrected for decay and showed in counts intensity) show only physiological uptake in the delayed images, but increased uptake in the late images, so increase in size over time, suspected infection.

46-year-old female patient. Several surgical operations in the past for distal tibia fracture and pseudoarthrosis. Because of suspected infection WBC scintigraphy was performed.

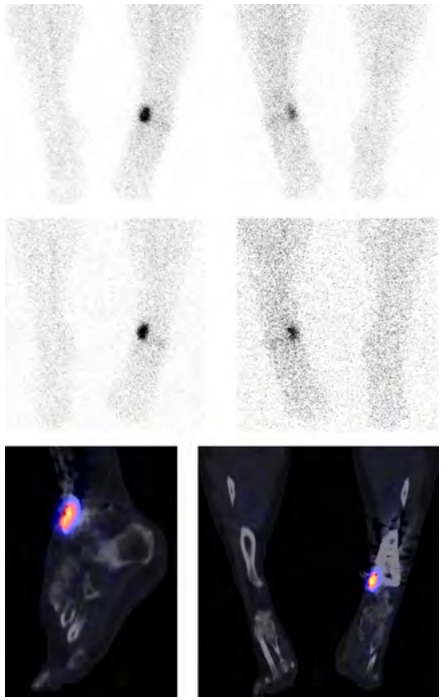

Figure 6: WBC scintigraphy (upper row: delayed images (4 h after injection of the radiolabelled cells) anterior and posterior views, middle row: late images (24 h after injection) anterior and posterior views, lower row: fused SPECT/CT images. The planar images (corrected for decay and showed in counts intensity) show high focal uptake, increasing over time, suspected infection. The SPECT-CT images show that the infection is located at the metallic implant in the medial malleolus.

CONCLUSIONS

In conclusion, nuclear medicine modalities play a very important role in patients with suspected infection or inflammation. For most infectious or inflammatory diseases FDG-PET/CT is the preferred nuclear imaging technique, but there is still a role for conventional nuclear medicine in several infectious diseases, and particularly for white blood cell scintigraphy in peripheral bone infections and prosthetic joint infections. When performing nuclear medicine imaging, practitioners should be aware of existing guidelines on how to correctly acquire and interpret the images and existing diagnostic flowcharts showing when to use which technique for which indication. Fortunately, several guidelines and diagnostic flowcharts for infections and inflammatory diseases are now available and technicians, nuclear medicine specialists and clinicians should be aware of these new guidelines and adhere to them in practice.

REFERENCES

1. Signore A, Lazzeri E, Glaudemans AW. Infection and inflammation imaging standardization: the EANM guidelines. Clin and Transl Imaging 2018; 6(4):253-255.
2. De Vries EF, Roca M, Jamar F, Israel O, Signore A. Guidelines for the labelling of leucocytes with (99m)Tc-HMPAO. Eur J Nucl Med Mol Imaging 2010; 37(4):842–848.
3. Roca M, de Vries EF, Jamar F, Israel O, Signore A. Guidelines for the labelling of leucocytes with (111)In-oxine. Eur J Nucl Med Mol Imaging 2010; 37(4):835–841.
4. Signore A, Jamar F, Israel O, Buscombe J, Martin-Comin J, Lazzeri E. Clinical indications, image acquisition and data interpretation for white blood cells and anti-granulocyte monoclonal antibody scintigraphy: an EANM procedural guideline. Eur J Nucl Med Mol
5. Imaging 2018; 45(10):1816-1831.
6. Jamar F, Buscombe J, Chiti A, Christian PE, Delbeke D, Donohoe KJ, et al. EANM/SNMMI guideline for 18F-FDG use in inflammation and infection. J Nucl Med 2013; 54(4):647-658.
7. Erba PA, Lancellotti P, Vilacosta I, Gaemperli O, Rouzet F, Hacker M, Signore A, Slart RH, Habib G Recommendations on nuclear and multimodality imaging in IE and CIED infections. Eur J Nucl Med Mol Imaging 2018; 45(10):1795-1815.
8. Slart RH, Glaudemans AW, Chareonthaitawee P, Treglia G, Besson, TL, Bley TA, et al. FDG-PET/CT(A) imaging in large vessel vasculitis and polymyalgia rheumatica: joint procedural recommendation of the EANM, SNMMI, the PET Interest Group (PIG), and endorsed by the ASNC. Eur J Nucl Med Mol Imaging 2018; 45:1250–1269.
9. Slart RH, Glaudemans AW, Lancelotti P, Hyafil F, Blankstein R, Schwartz R, et al. A joint procedural position statement on imaging in cardiac sarcoidosis: from the cardiovascular and inflammation and infection committees of the European Association of Nuclear Medicine (EANM), the European Association of Cardiovascular Imaging (EACVI), and the American Society of Nuclear Cardiology (ASNC). Eur Heart J Cardiovasc Imaging 2017; 18(10):1073–1089.
10. Glaudemans AW, Jutte PC, Cataldo MA, Cassar-Pullicino V, Gheysens O, Borens O, Trampuz A, Wörtler K, Petrosillo N, Winkler H, Signore A, Sconfienza LM. Consensus document for the diagnosis of peripheral bone infection in adults: a joint paper by the EANM, EBJIS, and ESR (with ESCMID endorsement). Eur J Nucl Med Mol Imaging 2019; 46(4):957-970.
11. Signore A, Sconfienza LM, Borens O, Glaudemans AW, Cassar-Pullicino V, Trampuz A, Winkler H, Gheysens O, Vanhoenacker FMHM, Petrosillo N, Jutte PC. Consensus document for the diagnosis of prosthetic joint infections: a joint paper by the EANM, EBJIS, and ESR (with ESCMID endorsement). Eur J Nucl Med Mol Imaging 2019; 46(4):971-988.
12. Lazzeri E, Bozzao A, Cataldo MA, Petrosillo N, Manfre L, Trampuz A, Signore A, Muto M. Joint EANM/ESCR and ESCMID-endorsed consensus document for the diagnosis of spine infection (spondylodiscitis) in adults. Eur J Nucl Med Mol Imaging 2019; 46(12):2464-2487.
13. Chakfe N, Diener H, Lejay A, Assadian O, Berard X, Caillon J, Fourneau I, Glaudemans AW, Koncar I, Lindholt J, Melissano G, Saleem B, Senneville E, Slart RH, Szeberin Z, Teebken O, Venermo M, Vermassen F, Wyss TR. European Society for Vascular Surgery (ESVS) 2020 Clinical practice guidelines on the management of vascular graft and stent graft infections with the endorsement of the European Association of Nuclear Medicine (EANM). Eur J Vasc Endovasc Surg 2020, in press.
14. Dorbala S, Ando Y, Bokhari S, Dispenzieri A, Falk RH, Ferrari VA, Fontana M, Gheysens O, Gillmore JD, Glaudemans AW, Hanna MA, Hazenberg BP, Kristen AV, Kwong RY, Maurer MS, Merlini G, Miller EJ, Moon JC, Murthy VL, Quarta CC, Rapezzi C, Ruberg FL, Shah SJ, Slart RH, Verberne HJ, Bourgque JM. J Card Fail 2019; 25(11):e1-e39.
15. Van den Wyngaert T, Strobel K, Kampen WU, Kuwert T, van der Bruggen W, Mohan Hk, et al. The EANM practice guideline for bone scintigraphy. Eur J Nucl Med Mol Imaging 2016; 43:1732-1738.
16. Signore A, Glaudemans AW. The molecular imaging approach to image infections and inflammation by nuclear medicine techniques. Ann Nucl Med 2011; 25(10):681-700.
17. Glaudemans AW, Israel O, Slart RH. Pitfalls and limitations of radionuclide and hybrid imaging in infection and inflammation. Semin Nucl Med 2015; 45(6):500-512.
18. Glaudemans AW, Galli F, Pacilio M, Signore A. Leukocyte and bacteria imaging in prosthetic joint infections. Eur Cell Mater 2013; 25:61-77.
19. Glaudemans AW, Bonanno E, Galli F, Zeebregts CJ, de Vries EF, Koole M, Luurtsema G, Boersma HH, Tuarino M, Slart RH, Signore A. In vivo and in vitro evidence that 99mTc-HYNIC-interleukin-2 is able to detect T lymphocytes in vulnerable atherosclerotic plaques of the carotid artery. Eur J Nucl Med Mol Imaging 2014; 41(9):1710-1719.
20. Telenga ED, van der Bij W, de Vries EF, Verschuuren EA, Timens W, Luurtsema G, Slart RH, Signore A, Glaudemans AW. 99mTc-HYNIC-IL-2 scintigraphy to detect acute rejection in lung transplantation patients: a proof-of-concept study. EJNMMI Res 2019; 9(1): 41.
21. Markovic SN, Galli F, Suman VJ, Nevala WK, Paulsen AM, Hung JC, Gansen DN, Erickson LA, Marchetti P, Wiseman GA, Signore A. Non-invasive visualization of tumor infiltrating lymphocytes in patients with metastatic melanoma undergoing immune checkpoint inhibitor therapy: a pilot study. Oncotarget 2018; 9(54):30268-30278,
22. Di Gialleonardo V, Signore A, Glaudemans AW, Dierckx RA, de Vries EF. N-(4-18F-fluorobenzoyl)interleukin-2 for PET of human-activated T lymphocytes. J Nucl Med 2012; 53(5):679-686.

10

PARATHYROID AND THYROID IMAGING

by Martin Gotthardt

INTRODUCTION

Nuclear medicine plays a relevant role in imaging of thyroid and parathyroid disease. Ever since the principle of radionuclide imaging was introduced by Nobel laureate George de Hevesy, nuclear medicine has used radionuclides to track physiological and pathophysiological metabolic processes in the human body. I-131 was first used for therapy of Grave's disease in 1941. The isotope was used to determine iodine uptake in the thyroid, and calculation of therapeutic doses via the thyroid uptake was already described back in 1948. Although imaging/uptake measurements of the thyroid with radioactive isotopes of iodine thus has a long tradition, the role of nuclear medicine for diagnosis of thyroid disease varies between countries throughout Europe and is often determined by medical traditions that have developed over the last century.

Factors influencing the role of nuclear medicine include the incidence of thyroid disease as well as how actively nuclear medicine has acquired patients with thyroid diseases. Diagnosis and treatment of thyroid disease may be fully in the hands of nuclear medicine (as in Germany or Austria, obviously excluding surgical treatment) but can also be limited to diagnosis and I-131 treatment on behalf of endocrinologists (as in many parts of the Netherlands). Also, the view on diagnosis and treatment may vary in countries with traditional iodine deficiency leading to high incidence of enlarged thyroids, so-called goitres (as, for example, in the regions around the Alps), as compared to regions where high amounts of iodine-containing sea fish were available as food and thus iodine-deficient goitres were not common. Based on such traditions, we see considerable differences across Europe in the role that thyroid diseases play in the perception of healthcare professionals and the general population, although the regional differences in iodine supply are much reduced compared to 50 years ago. However, in many countries the average daily uptake of 200 micrograms of iodine as advised by the WHO has not yet been reached (WHO 2004). This results in a moderate iodine deficiency in parts of the population, so that nodular goitres (enlarged thyroids with thyroid nodules) are still common. As we will see later in this chapter, this has a considerable influence on diagnosis and localisation of thyroid nodules and hyperplastic parathyroid glands. In this context, ultrasound can play a major role alongside scintigraphic imaging techniques for validation of scintigraphic findings, adding to the specificity of image diagnosis. Still, the approach to image interpretation, treatment and follow-up of patients with thyroid nodules and/or parathyroid adenoma may depend on the presence of multinodular goitre.

Here, a concise overview will be given of anatomy/physiology, diseases and diagnostic imaging of the thyroid and parathyroid glands. The aim is not to replace guidelines or deliver protocols but to give an overview of the current state of the art in thyroid and parathyroid imaging. However, some general recommendations for imaging protocols are given.

ANATOMY AND PHYSIOLOGY OF THE THYROID AND THE PARATHYROIDS

The thyroid is a gland consisting of two lobes lying on the left and right side of the trachea with the so-called isthmus in between, a relatively thin layer of thyroid tissue connecting both lobes. The thyroid is located just above the sternum and below the larynx. Behind the thyroid lobes, the four parathyroid glands are found – normally one each behind the upper and lower poles of each thyroid lobe. While the location of the thyroid itself does not usually vary, the location of the parathyroid glands is less reproducible. They can sometimes be found in an intrathyroidal location, in the (most often upper anterior) mediastinum, in the thymus or, if they have not migrated properly during embryological development, clearly above the thyroid. In addition, the lower parathyroids can also be located in the middle behind the thyroid lobes or at the upper poles. Normally, they are the size of a grain of rice, and although the spatial resolution of ultrasound, for example, is sufficient to visualise such small structures, they usually cannot be distinguished from surrounding tissue by imaging. Incidentally, one parathyroid gland may be missing or an additional gland may be present, mostly in the thymus.

The role of the thyroid is production of the three thyroid hormones, triiodothyronine (T3), thyroxine (T4), and calcitonin. T3 and T4, produced in the thyroid cells (thyrocytes), are responsible for the metabolic rate of the body and are also essential for growth and development during childhood. For production of thyroid hormones, iodine is required. Lack of thyroid hormones during childhood (as a result of severe iodine deficiency or because the thyroid has not developed in the embryo) leads to so-called cretinism, characterised by retardation of development, small size and low cognitive function. Calcitonin is produced in the C-cells in the thyroid and is responsible for

calcium metabolism. In the parathyroid glands, parathyroid hormone (PTH) is produced. The latter also plays a major role in the calcium metabolism of the human body, as well as influencing vitamin D and phosphate levels. Calcitonin is responsible for lowering calcium levels in the blood, while PTH increases blood calcium levels.

Secretion of T3 and T4 is stimulated by the thyroid-stimulating hormone (TSH) secreted from the anterior pituitary gland. TSH is regulated by the thyrotropin-releasing hormone (TRH) produced by the hypothalamus, and high levels of thyroid hormone in the blood suppress TRH production via a feedback loop.

THYROID DISEASES

Thyroid diseases can be classified into diseases leading to enlargement of the thyroid gland or formation of nodules (adenomas), changes in function with hyper- or hypofunction, combinations thereof, and malignant diseases. Thus, the size of the thyroid and its function do not necessarily correlate: a large goitre may have a normal function, while hyperproduction of thyroid hormones may occur in a small thyroid.

Anatomical changes in the thyroid gland: As a consequence of insufficient iodine supply, the thyroid can be enlarged while the function is normal. The individual daily iodine requirement may vary, so that different individuals, although having an identical daily iodine supply, may develop a goitre or not. The maximal normal volume of a thyroid gland is 18 grams for women and 25 grams for men. In enlarged thyroids, nodules develop frequently and nodules resulting from iodine deficiency may also develop in thyroids of normal size. Nodules that have grown as a result of iodine deficiency may become cystic, in which case they can grow rapidly or even become acute within a couple of days as a result of bleeding into the cystic nodule. Such patients may be afraid of having cancer, which frequently can be excluded if a cystic nodule is present. Enlargement of the thyroid or growth of nodules tends to start during puberty or pregnancy/breastfeeding.

Diseases changing the function of the thyroid gland: Hyperthyroidism may occur as a consequence of autonomous function of one or more thyroid nodules, which is usually caused by iodine deficiency. This is more common in countries with low iodine supply, while in countries with high average iodine intake, Graves' disease is a more common cause of hyperthyroidism. Graves' disease is an autoimmune disorder in which autoantibodies against the TSH receptor expressed in the thyrocytes are produced. This antibody is able to stimulate the TSH receptor, resulting in continuous overproduction of thyroid hormones. Another autoimmune disease leading to hyperthyroidism is Hashimoto's disease, in which the thyrocytes are destroyed by the autoimmune process. Thus, hyperthyroidism in this case is not caused by overproduction of thyroid hormones, but by release of thyroid hormones that were stored in the thyroid. Medication reducing thyroid hormone production (thyrostatic medication) is therefore not efficient in this case, while it works very well if autonomous nodules or Graves' disease are present.

Thyroid malignancies: The most common thyroid carcinomas derived from the thyrocytes are papillary and follicular thyroid carcinoma. Papillary thyroid carcinoma preferably metastasises to the lymph nodes, whereas follicular carcinomas have a tendency to spread via the bloodstream. Both tumours have a high rate of cure, and both 5-year and 10-year survival rates are among the highest for all malignancies. Nearly all early-stage patients are cured, and most patients can still be cured even if lymph node metastases are present; even if metastasised to the lungs, cure is still possible. Thyroid carcinoma may also occur in childhood, especially after exposure to ionising radiation, as was the case, for example, after the nuclear accident in Chernobyl in 1986. Although thyroid carcinoma is more aggressive during childhood, the tumours respond very well to therapy and cure rates are high, even in the case of lung metastases. Therapy consists of surgical removal of the thyroid (as well as cervical lymph nodes in case of metastases) followed by therapy with I-131, which is given for ablation of thyroid remnants as well as tumorous tissue. Although uptake of I-131 in thyroid carcinoma is lower than in healthy thyroid tissue with an efficient uptake of iodine from the bloodstream, it is usually still sufficient to achieve a cure. Only in poorly differentiated thyroid carcinoma or Hürthle cell carcinoma (a subtype of follicular carcinoma) there is no iodine uptake in most cases, so that adjuvant therapy with I-131 is not effective; cure rates and 5- and 10-year survival rates here are thus significantly reduced.

A particularly aggressive subtype of thyroid carcinoma is anaplastic thyroid carcinoma, which despite extensive surgery and external beam radiation of the cervical area leads to death within months in most cases.

Medullary thyroid carcinoma is derived from the C-cells and produces calcitonin, which together with carcinoembryonic antigen (CEA) serves as a tumour marker after therapy. Radical surgery with extensive removal of metastatic lymph nodes is the treatment of choice. As C-cells do not take up iodine, adjuvant therapy with I-131 is not an option. External beam irradiation may be considered in selected cases, also for reducing lymphogenic spread.

PARATHYROID DISEASES

Parathyroid disease (hyperparathyroidism, HPT) is usually characterised by an overproduction of PTH, leading to increased calcium levels in blood and urine. As a result, nephrocalcinosis, urolithiasis, bone disease, gastrointestinal and neuromuscular symptoms may occur. Nowadays, the diagnosis is usually made based on elevated calcium levels in the blood, diagnosed when laboratory tests are performed. Therefore, the diagnosis is often made in a subclinical state (Gotthardt et al 2013). If not diagnosed early, clinical symptoms may include urolithiasis, bone or stomach pain, but there are also cases with neuropsychiatric symptoms (ranging from slight behavioural changes to severe cases with coma).

There are three forms of this so-called hyperparathyroidism: a primary, a secondary and a tertiary form. Primary hyperparathyroidism (pHPT) is usually caused by one enlarged hyperfunctioning parathyroid, a so-called adenoma. In about 10-15% of cases, two parathyroid adenomas may be found. Parathyroid carcinoma is usually also associated with hyperparathyroidism, but is very rare (fewer than 1% of cases).

Secondary hyperparathyroidism (sHPT) is the result of chronically low calcium levels, most often caused by renal failure but they can also result from the use of certain drugs. In sHPT, the parathyroids are enlarged as a result of overproduction of PTH in an attempt to normalise blood calcium levels, thus usually more than one or all parathyroids are enlarged. Chronic sHPT will lead to autonomous overfunction of the enlarged (hyperplastic) parathyroids, so-called tertiary hyperparathyroidism (tHPT).

Primary hyperparathyroidism may also occur as part of multiple neuroendocrine neoplasia (MEN) syndrome (MEN1 or MEN2A), leading to a combination of endocrine tumours, usually of pancreas, thyroid and parathyroids (Hindie et al 2009, Greenspan et al 2012; Gotthardt et al 2013).

THYROID AND PARATHYROID IMAGING

The indications for imaging of the thyroid differ significantly from those for the parathyroids. The aim of thyroid imaging is usually not to localise a particular lesion, but to characterise it or to determine the metabolic activity of the thyroid or nodules. Parathyroid imaging is used to localise an adenoma or hyperplastic glands, e.g. in preparation for surgery.

Thyroid imaging – indications

Imaging of the thyroid can be performed for several reasons: to diagnose anatomical pathology, such as goitre or thyroid nodules; to define the metabolic activity of a lesion or the thyroid as a whole; and to characterise lesions, i.e. identification of malignancy. All these indications require different approaches.

Anatomical pathology can most easily be diagnosed by ultrasound, which allows measurement of the size of the whole thyroid, identification of nodules and also determination of the size of the nodules for further follow-up. Thyroid scintigraphy was formerly used for this purpose, but this indication is obsolete when ultrasound is available. In the case of very large goitres, CT scanning may be required for complete imaging of the entire gland, especially if part of the thyroid is located in the retrosternal compartment, or if compression of the trachea is suspected.

Scintigraphic imaging of the thyroid is usually performed to determine the metabolic activity of either the whole thyroid or individual nodules. For this purpose, I-131 or I-123 may be used, or as an alternative, Tc-99m. For diagnosis of autonomous thyroid nodules, scintigraphy is usually performed with suppressed TSH, meaning that the thyroid is not stimulated. Under such conditions, high uptake indicates autonomously functioning thyroid tissues, which can be one or more nodules causing hyperthyroidism. Differentiation between Hashimoto's disease and Graves' disease is also possible, because in Hashimoto's disease the thyroid is not stimulated and hyperthyroidism is caused by thyroid hormone release from the progressively destroyed thyroid, thus uptake is low. In the case of Graves' disease, TSH receptor- stimulating antibodies cause hyperthyroidism, leading to high uptake. Thyroid scintigraphy is sometimes used if thyroid nodules are detected, to measure whether uptake of the radionuclides in the lesion is normal or not. If so, the lesion is considered to be benign while in case of missing uptake, malignancy should be ruled out by fine needle aspiration cytology. Thyroid scintigraphy is not generally used for this indication in Europe, but it is in some countries. The same is true for determination of thyroid nodule uptake with radiopharmaceuticals such as ^{99m}Tc-labelled MIBI, which in case of high uptake may indicate malignancy. However, the specificity of such scans is limited and further work-up with ultrasound or fine needle aspiration may be required, so that the added value of such examinations is often limited.

Parathyroid imaging – indications

As mentioned above, parathyroid scintigraphy is performed for localisation of diseased parathyroids, thus the diagnosis of HPT should be confirmed biochemically prior to imaging. Elevated levels of PTH and calcium usually point towards a diagnosis of HPT (Hindie et al 2009; Greenspan et al 2012).

The indication for parathyroid scintigraphy and its combination with other imaging modalities may again vary between countries, but also between hospitals in the same country. Usually, it depends on the preferences of the surgeon and the experience of the nuclear medicine physician. If bilateral neck exploration is performed, in which the surgeon looks for enlarged parathyroids in the usual locations and also explores areas where ectopic parathyroids may occur, localisation diagnosis prior to operation may not be required. However, minimally invasive surgery is commonly used nowadays as it results in lower morbidity and shorter operation times, and in this case the value of preoperative imaging in HPT is evident. If no parathyroid adenoma can be identified by imaging, bilateral neck exploration may be required. Another indication for imaging is patients with persistent or recurrent HPT, who have been operated on previously. Surgery in such patients is more complex and associated with higher morbidity, thus preoperative localisation diagnostics help to reduce operation time and complication rates. Parathyroid scintigraphy should therefore be performed in all patients before minimally invasive or unilateral neck exploration, and in all patients undergoing reoperation for persistent or recurrent HPT. However, parathyroid scintigraphy is less sensitive in the case of sHPT caused by hyperplastic parathyroids, where the surgeon may prefer bilateral neck exploration and the potential contribution of imaging may be limited. On the other hand, the combination of preoperative imaging with an intraoperative PTH assay may help to determine the need for further exploration after removal of lesions identified by imaging prior to operation (Hindie et al 2009).

RADIOTRACERS AND IMAGING PROCEDURES

The radiotracers used for thyroid imaging are radioactive iodine isotopes (^{123}I and ^{131}I) or ^{99m}Tc. The choice of radiotracer depends on the indication for the procedure. For scintigraphic imaging aimed at diagnosis of thyroid disease and simultaneous uptake measurement, ^{99m}Tc can be used. ^{99m}Tc is taken up by the thyroid via the sodium-iodine symporter, the same molecule that is also responsible for iodine uptake in the thyrocytes. Unlike iodine, ^{99m}Tc is not stored inside the thyrocytes, so it is washed out of the thyroid – scintigraphy is therefore performed 20 minutes after injection. Normal thyroid uptake for ^{99m}Tc if TSH is suppressed (i.e. the thyroid is not stimulated by TSH) is up to 1% with a grey zone between 1% and 2%, and uptake values above 2% are considered suspicious for autonomously functioning tissue. In Graves' disease, uptake values of 3-5% are commonly reached. In Hashimoto's disease, the uptake in the thyroid usually remains below 0.2%. Also, after exposure of the thyroid to a larger amount of iodine (as is the case after application of contrast agents containing iodine), uptake of ^{99m}Tc in the thyroid may be blocked, producing results resembling those found in Hashimoto's disease. If ^{123}I is used, images are usually obtained after 3h. Normal uptake values with suppressed TSH are below 10%, while autonomy is present if values are >20-30%. For scintigraphic imaging, activities of 10MBq for ^{123}I and 37MBq for ^{99m}Tc will usually suffice.

In preparation for I-131 therapy, a 24h uptake measurement is usually obtained. Measurement of 24h uptake values requires a radionuclide with a longer half-life, and in this case a low amount of I-131 should be used. The quality of scintigraphic images obtained with I-131 with a high-energy collimator is usually limited, but probe measurement is sufficient for determination of uptake, so lower activities can be applied.

^{99m}Tc- labelled tetrofosmin or sestamibi are used for parathyroid scintigraphy, and both accumulate in thyroid tissue as well as in parathyroid adenomas. Dual-phase imaging relies on higher retention of the radiotracer in parathyroid adenomas as compared to the thyroid, hence images are obtained 10 and 120 minutes after injection of the radiotracer. In this setting, sestamibi has the advantage of quicker washout from thyroid tissue and longer retention in parathyroid adenomas, while tetrofosmin has a slow washout from both, which may mask parathyroid adenomas (Fjeld et al 1997). Sestamibi should therefore be preferred over tetrofosmin. However, if dual-tracer imaging is performed, tetrofosmin is an option. It should also be borne in mind that hyperplastic parathyroid glands in sHPT have a quicker washout than parathyroid adenomas in pHPT. These differences can be observed in larger cohorts of patients. However, it should be mentioned that parathyroid adenomas and thyroid can have the same sestamibi washout, so that no retention of sestamibi in parathyroid adenomas is observed. Therefore, SPECT images should always be obtained early (45-60 minutes p.i.) to achieve a good sensitivity. Usually, 500-700MBq of ^{99m}Tc sestamibi or tetrofosmin are administered, which results in adequate image quality (Gotthardt et al 2016).

The principle of dual-tracer imaging is based on planar imaging of the thyroid and the parathyroids with different tracers. The thyroid is imaged with ^{123}I or ^{99m}Tc (as described above) and the resulting images are subtracted from sestamibi or tetrofosmin images. The remaining

activity will then represent the parathyroid adenoma. The activity recommended for ^{99m}Tc is 35-75 MBq, whereas around 10MBq may be used for ^{123}I with its higher target-to-background ratios. Officially, higher activities may be used (recommendations in the guidelines mention a maximum of 370MBq for ^{99m}Tc and around 20MBq for ^{123}I), but the image quality obtained with the activities mentioned here usually suffices.

For an activity of 500MBq, the resulting effective radiation doses will be approx. 4.5mSv for sestamibi and 3.8mSv for tetrofosmin in men, while the effective doses for women are 20-30% higher. For 10MBq of ^{123}I and 37MBq of ^{99m}Tc, the effective doses are 2.2mSv and 0.5mSv, respectively (Valentin 1998, Hindie et al 2009, Greenspan et al 2012).

PATIENT PREPARATION

For thyroid imaging, patients under thyrostatic treatment should discontinue this medication (thiamazole, methimazole or propylthiouracil) for 3 days. As contrast media containing iodine suppress the uptake in the thyroid, administration should be at least 6 weeks ago, or even longer if possible. This also applies for parathyroid imaging if a dual-tracer protocol is used.

For parathyroid imaging in sHPT, vitamin D as well as calcimimetics should be discontinued. It has been recommended that active vitamin D be discontinued for 1 week and native vitamin D for 3-4 weeks. Calcimimetics should be discontinued for 2 weeks. In addition, consider discontinuing any drugs that may suppress parathyroid (hyper)function for a few days before scintigraphy (Hindie et al 2009, Greenspan et al 2012).

IMAGE ACQUISITION AND PROCESSING

Thyroid scintigraphy:

If ^{99m}Tc is used, planar images of the thyroid should be obtained 20 minutes after injection, usually covering the area from the salivary glands to the upper thorax. An external source with a defined amount of ^{99m}Tc can be used for quantification of thyroid uptake, in which case the syringe should be measured before and after injection to determine the exact activity injected. In principle, the same protocol can be used with ^{123}I, but image acquisition should take place later, around 3h after administration. A low-energy parallel-hole collimator should be used, with a matrix size of 256x256. A calibrated probe measurement can be performed for uptake measurement, as this avoids calculation of uptake based on camera measurements.

Dual-phase parathyroid scintigraphy:

In dual-phase scintigraphy, early and late planar images are obtained (~10 and 120 minutes post injection) with the patient in supine position. The gamma camera should be equipped with a low-energy, high-resolution parallel-hole or cone-beam collimator with a 128x128 or 256x256 matrix. It is important that the field of view is large enough to cover the area where parathyroid adenomas can usually be found, including ectopic adenomas (i.e. from the salivary glands to the myocardium). SPECT images should be obtained from the same area starting 45-60 minutes after injection of the radiopharmaceutical. Use of a low-energy, high-resolution parallel-hole collimator with a 128x128 matrix is recommended. In many cases, higher matrix sizes do not add to image quality as reconstruction software packages will reduce larger matrix sizes to 128x128 – it is advisable to check with the vendor whether 256x256 is supported. Acquisition of 120 views of 20-30 seconds each is recommended. SPECT/CT is highly recommended to enable optimum anatomical localisation (Gotthardt et al 2016).

Subtraction parathyroid scintigraphy:

Combined ^{123}I/^{99m}Tc-sestamibi/tetrofosmin scintigraphy can be performed as a simultaneous planar imaging procedure. Sestamibi/tetrofosmin is injected 2-3 hours after administration of the ^{123}I. Again, the patient is placed in supine position. Five to fifteen minutes after ^{99m}Tc-sestamibi/tetrofosmin injection, planar images of the head and neck are obtained in analogy to what has been described above. Because this examination is done as a simultaneous dual-tracer acquisition, symmetrical 10% energy windows (140 keV±5% for ^{99m}Tc and 159 keV±5% for ^{123}I) are used. A low-energy, high-resolution parallel-hole collimator is recommended, with a 256x256 matrix. Although pinhole images may improve spatial resolution, SPECT/CT images may be preferred for improved anatomical localisation. For reduction of cross-talk, the planar images may be acquired using a 14% energy window instead of 10% (140 keV-10%/+4% for ^{99m}Tc and 159 keV+10%/-4% for ^{123}I)

If ^{99m}Tc is used for delineation of the thyroid, dual-isotope imaging is not possible. Sequential protocols are used instead, which may differ in details but generally follow the recommendations put forward here. First, the thyroid is imaged with ^{99m}Tc approx. 20 minutes after injection, followed by application of 400mg of potassium chloride to induce washout of the ^{99m}Tc from the thyroid. The patient lies in a supine position and may not move during the procedure. Then, ^{99m}Tc-sestamibi/tetrofosmin is injected and image acquisition starts 5-15 minutes later (Hindie et al 2009, Gotthardt et al 2016).

Processing of parathyroid scintigraphy:

It is important to avoid oversubtraction, which leads to white areas in the images. Also, if the patient has moved, artefacts may occur, including false positive results. As interpretation of parathyroid SPECT images requires highly sensitive reading, the interpretation of the images is prone to reconstruction artefacts that may vary between reconstruction software packages. Practitioners should therefore be aware that the choice of optimum reconstruction settings and differences between the software packages have a significant impact on sensitivity and specificity of the method (van Hoorn et al 2014).

IMAGE INTERPRETATION

Thyroid scintigraphy

The thyroid should be symmetrical in shape. Size differences between the lobes may occur, but are more common if goitre is present. If autonomously functioning nodules are present and TSH is suppressed, the thyroid will not be visible but only the autonomous nodule(s). If the whole thyroid shows a high uptake of the tracer while TSH is suppressed, Graves' disease should be considered. If thyroid scintigraphy is complemented by ultrasound, misinterpretation of scintigraphic images due to differences in thryoid lobe size, unusual uptake patterns caused by anatomical factors and unexpected hot or cold areas can be avoided.

Parathyroid scintigraphy

Parathyroid scintigraphy should be read in an "over-sensitive" manner. Compared to other types of scintigraphy, the target-to-noise ratios are often lower and the lesions visualised are often below the spatial resolution of the SPECT technique, leading to partial volume effects. Therefore, correct interpretation of parathyroid scintigraphy is highly dependent on expertise and experience. Here too, its combination with ultrasound will help to improve results (see below, parathyroid ultrasound) (Gotthardt 2016).

For all imaging protocols (dual-phase, dual-tracer, different imaging time points), all sites of sestamibi/tetrofosmin uptake either in unusual locations or protruding from the contour of the thyroid (even if uptake is lower than in the thyroid, cf. partial volume effects!) are suspicious for parathyroid adenoma. Also, it should be borne in mind that ectopic adenomas may be present. Focal areas of high uptake which are located in blood vessels (retention in veins) or in tumours (head and neck or breast carcinoma) can lead to false positive findings. SPECT/CT imaging allows correct interpretation of such lesions, which may be clinically relevant. Also, parathyroid adenomas located high in the neck may be misinterpreted as salivary gland uptake, which can be correctly identified by SPET/CT imaging.

In dual-phase scintigraphy, parathyroid adenomas may show up on early planar images as inhomogeneities in the uptake of the thyroid, while on the late images they should be characterised by higher retention of radioactivity. As stated above, especially when tetrofosmin is used, parathyroid adenomas may show the same retention/washout characteristics as thyroid tissue. Therefore, sensitive interpretation of the images is required. Most parathyroid adenomas are located behind the thyroid gland in the lower half of the lobes and thus may appear as slightly darker areas on either early or late images, or both. In contrast to SPECT imaging, they most often lie inside the contour of the thyroid. An increased uptake, even if minor, in the upper or lower part of a thyroid lobe can potentially represent a parathyroid adenoma. However, they can also be located clearly above or below the thyroid lobes.

As stated above, early SPECT images are advised to allow for detection of parathyroid adenomas with quick washout. Furthermore, detection of parathyroid adenomas may be complicated by the activity in the thyroid gland. Therefore, all inconsistencies in the contour of the thyroid gland are potential parathyroid adenomas, especially if located in the dorsal contour. Parathyroid adenomas can thus be visualised as small protrusions. Changing the scaling of the images during interpretation will help to correctly identify lesions (Hindie et al 2009, Gotthardt 2016).

On dual-tracer scintigraphy images, the thyroid-specific (^{99m}Tc or ^{123}I) scan is compared to the scan with uptake in both thyroid and parathyroid (tetrofosmin or sestamibi). Discrepancies between the two scans indicate the presence of a parathyroid adenoma, which may be seen clearly on subtraction images. However, a very slight increase in uptake of ^{99m}Tc or ^{123}I can sometimes be seen in parathyroid adenomas, which can lead to incorrect interpretation of the scans. Also, one needs to be aware that suboptimal fusion

of the ^{99m}Tc/^{123}I and sestamibi/tetrofosmin images may result in false positive or false negative findings caused by over-/undersubtraction or patient movement. If fusion is done correctly, the uptake in the thyroid region of the fusion images should be comparable to background uptake in the neck, and critical assessment of the quality of the image fusion is essential (Hindie et al 2009, Gotthardt et al 2016).

PET IMAGING OF THYROID AND PARATHYROID ADENOMAS

FDG-PET is able to identify malignant nodules in the thyroid. When FDG-PET is performed for other indications, FDG-positive nodules may be found incidentally in the thyroid. Such nodules may be sent for further work-up using ultrasound and fine needle aspiration cytology. A possible alternative indication for FDG imaging in thyroid nodules may be distinguishing between malignant and benign nodules. If FNA delivers indeterminate results normally requiring diagnostic hemythyroidectomy, FDG-PET may be able to identify the malignant nodules and avoid unnecessary diagnostic surgery. The question of the utility of FDG-PET for identifying malignant lesions is not yet answered (Castellana et al 2019), but it should be borne in mind that follow-up of lesions using ultrasound may enable detection of growing lesions as well as being more cost effective.

Although successful localisation of parathyroid adenomas with FDG-PET has been described, it does not seem to be an appropriate procedure for standard parathyroid imaging due to its lower sensitivity and higher cost compared to parathyroid scintigraphy. An alternative may be C-11-methionine imaging, as it seems to enable localisation of adenomas that have not been identified by parathyroid scintigraphy and ultrasound. The use of C-11 is limited to centres that have a cyclotron available and produce this tracer regularly (Chicklore et al 2014).

ULTRASOUND IMAGING

Ultrasound imaging is a fast and safe method for obtaining anatomical information about the thyroid, thyroid nodules, parathyroid adenomas, lymph nodes or other structures in the cervical area. Thyroid ultrasound aims to identify thyroid size, shape and nodules but also allows assessment of the character of nodules based on their echogenicity and ultrasound features. In addition, diseases such as Hashimoto's or Graves' disease display typical patterns which, in the context of clinical symptoms, often allow a diagnosis to be made. Parathyroid ultrasound aims to localise parathyroid adenomas or hyperplastic glands, and in combination with parathyroid scintigraphy it allows us to differentiate thyroid nodules with sestamibi/tetrofosmin uptake or other cervical structures from parathyroid adenomas (deFeo et al 2000).

Thyroid ultrasound:

In the assessment of thyroid disease, ultrasound is more reliable than palpation and scintigraphy for the assessment of anatomical thyroid pathology. For assessment of function, however, scintigraphy is preferable, thus these methods are complementary. When ultrasound of the thyroid is performed, the patient is in a supine position with a pillow beneath her/his shoulders and neck and the head in a reclined position. This position may not be very comfortable for the patient, but it allows assessment of the lower poles of the thyroid, which may, at least in part, be located behind the sternum. In addition, paratracheal or retroclavicular lymph nodes may be missed if the head is not reclined.

The thyroid is imaged in axial and sagittal view, with thickness and width being measured in the axial plane and length in the sagittal plane. Nodules in the thyroid are measured accordingly and are documented with respect to shape, echogenicity (hypo-, hyper-, normal, echo free), delineation, presence of a halo (a black rim around the nodule), cystic areas, calcifications and, if deemed useful, blood flow by Doppler measurements. The patient is then asked to turn his/her head to the left and the right cervical area is examined from mandible to clavicle with respect to presence of enlarged lymph nodes and other findings. The patient then turns his/her head to the right and the same procedure is repeated on the left side of the neck. It is helpful to follow a standardised procedure, and also to have clear protocols for the exact determination of the size of lesions in order to achieve high reproducibility. Lymph nodes should also be assessed based on their ultrasound features: if they are oval in shape, hypoechogenic and a hilum is present, they are usually benign. The size is not a very sensitive or specific predictor of malignancy, except if lymph nodes are very small. A small axis diameter of up to 5mm is considered normal. If a slightly larger lymph node is found but it has benign features, malignancy is unlikely. Submandibular lymph nodes may be much larger in size, hence their echographic features are more important to assess. The lymph node findings should also be documented.

Based on ultrasound patterns, the character of nodules in the thyroid can be determined according to the TI-RADS classification (Tessler et al 2017). This classification also gives advice with respect to which nodules require fine

needle aspiration (FNA). FNA is performed under ultrasound guidance: a fine needle is inserted in a thyroid nodule (23 or 25 gauge give the best results), moved gently back and forth, and if no material becomes visible in the plastic conus of the aspiration needle, vacuum may be applied with a syringe attached to the needle. If blood is aspired, interpretation of the findings by the pathologist may become more difficult. The acquired material is then fixated and prepared for examination by the pathologist. The aim of the procedure is not to acquire histological samples, but to acquire cells that will allow the pathologist to classify them according to the Bethesda classification as benign, malignant or suspicious. The advised therapy will depend on the findings, the options being no follow-up, repeat FNA, follow-up by ultrasound, diagnostic hemithyroidectomy, and total thyroidectomy.

It should be borne in mind that most thyroid malignancies have an excellent prognosis and (except for dedifferentiated/anaplastic carcinomas, which can usually be diagnosed based on clinical features, palpation and ultrasound) grow very slowly. In countries with suboptimal iodine supply, the TI-RADS classification (developed in the US, which has optimum iodine supply and thus low incidence of multinodular goitres) may thus be applied more conservatively, as regressive nodules in multinodular goitres resulting from iodine deficiency may have features of malignancy. As a result, in countries with widespread iodine deficiency, strict adherence to the TI-RADS classification may result in over-aggressive therapy. In such cases, and perhaps if FNA results are equivocal, an experienced (!) ultrasonographer may advise ultrasound follow-up of nodules and perform FNA or operate only if they grow.

Hashimoto's and Graves' disease show a typical pattern of multiple hypoechoic lesions which may be located in a part of the thyroid or found throughout the gland. In the late stages of Hashimoto's disease, when patients are hypothyroid as a consequence of autoimmune destruction of the thyroid, the thyroid is mostly hypoechoic, sometimes with hyperechoic stripe-like patterns of fibrosis.

Parathyroid ultrasound:

In a perfect scenario, parathyroid scintigraphy and ultrasound are performed simultaneously by the same experienced person. Physicians with a lot of experience in performing both procedures together will be considerably better at correctly identifying lesions. If there is no physician experienced in reading both examinations, joint examinations by the nuclear medicine specialist and the ultrasonographer are a preferred solution. Suspicious findings on parathyroid scans can easily be verified by ultrasound in such a setting. The results of the procedure will, however, always depend on the presence of physicians experienced in imaging of parathyroid pathology.

Parathyroid adenomas can have different shapes (oval, lobular, etc.) and are in most cases hypoechogenic, though they can also be echo free (black) or have ultrasound patterns comparable to thyroid nodules in multinodular goitres. In most cases, they are located at the lower pole of the thyroid or in a dorsal position behind the lower half of the thyroid. If located behind the trachea, they can be difficult to visualise, and it is essential to let the patient turn his/her head in order to assess the space between the vertebrae and the trachea. Many parathyroid adenomas have an artery originating from the inferior or superior thyroid artery that can be visualised by Doppler imaging. If a parathyroid adenoma is echo free and located alongside the inferior thyroid artery (which does not happen often but can be the case), it may be missed because it is taken for a blood vessel. However, on Doppler imaging the blood flow in the artery is much higher, allowing correct identification of the lesion, and parathyroid scintigraphy will help to identify such lesions. Furthermore, parathyroid adenomas located behind the thyroid may impress the thyroid contour and thus appear as if located in the thyroid. However, in such cases the thyroid capsule can often be identified as a white rim of connective tissue separating the parathyroid adenoma from thyroid tissue. As such a lesion may be identified as a thyroid nodule on the scintigraphic images, ultrasound can be very helpful in order to correctly differentiate between thyroid nodules and parathyroid adenoma if there are (multiple) suspicious findings in the SPECT images (Gotthardt et al 2013).

CONCLUSION

Imaging of thyroid and parathyroid pathology is optimised when anatomical and functional imaging are combined, and scintigraphy and ultrasound are highly efficient in this context. The addition of ultrasound data about echographic patterns provides valuable information about characteristics of thyroid nodules and helps to increase the specificity of parathyroid scintigraphy. In the optimum scenario, the same experienced physician will perform and/or interpret scintigraphic and ultrasonographic images.

REFERENCES

1. Castellana M, Trimboli P, Piccardo A, Giovanella L, Treglia G. Performance of 18 F-FDG PET/CT in Selecting Thyroid Nodules With Indeterminate Fine-Needle Aspiration Cytology for Surgery. A Systematic Review and a Meta-Analysis. J Clin Med 2019;8(9):1333-1344
2. Chicklore S, Schulte KM, Talat N, Hubbard JG, O'Doherty M, Cook GJ. 18F-FDG PET rarely provides additional information to 11C-methionine PET imaging in hyperparathyroidism. Clin Nucl Med. Mar 2014;39(3):237-242.
3. De Feo ML, Colagrande S, Biagini C, Tonarelli A, Bisi G, Vaggelli L, Borrelli D, Cicchi P, Tonelli F, Amorosi A, Serio M, Brandi ML. Parathyroid glands: combination of (99m)Tc MIBI scintigraphy and US for demonstration of parathyroid glands and nodules. Radiology 2000;214(2):393-402
4. Fjeld JG, Erichsen K, Pfeffer PF, Clausen OP, Rootwelt K. Technetium-99m-tetrofosmin for parathyroid scintigraphy: a comparison with sestamibi. J Nucl Med. Jun 1997;38(6):831-834.
5. Gotthardt M, Franzius C, Zielke A, Rothmund M. Primärer Hyperparathyreoidismus: Lokalisationsdiangostik beim Hyperparathyreoidismus. In: Rothmund, ed. Praxis der Viszeralchirurgie. Vol 2. 3 ed. Heidelberg, Germany Springer; 2013:266-276.
6. Gotthardt M. Parathyroid gland scintigraohy. In Esser/van den Heuvel/van Dalen (edts). Procedure Guideline Nuclear Medicine. Dutch Society of Nuclear Medicine. Kloosterhof, Neer, The Netherlands, 2016; 52-58
7. Greenspan BS, Dillehay G, Intenzo C, Lavely WC, O'Doherty M, Palestro CJ, Scheve W, Stabin MG, Sylvestros D, Tulchinsky M. SNM practice guideline for parathyroid scintigraphy 4.0. J Nuclk Med Technol 2012;40(2):111-118.
8. Hindie E, Ugur O, Fuster D, O'Doherty M, Grassetto G, Ureña P, Kettle A, Gulec SA, Pons F, Rubello D.al. 2009 EANM parathyroid guidelines. Eur J Nucl Med Mol Imag. 2009;36(7):1201-1216
9. Tessler NT, Middleton WD, Grant EG, Hoang JK, Berland LL, Teefey SA, Cronan JJ, Beland MD, Desser TS, Frates MC, Hammers LW, Hamper UM, Langer JE, Reading CC, Scoutt LM, Stavros AT. ACR Thyroid Imaging, Reporting and Data System (TI-RADS): White Paper of the ACR TI-RADS Committee. J Am Coll Radiol 2014;17(5):587-595
10. Valentin D. recalculated dose data for 19 frequently used radiopharmaceuticals from icrp publication 53. Radiation dose to patients from radiopharmaceuticals (Addendum 2 to ICRP Publication 53) ICRP 801997; 1998
11. van Hoorn RA, Vriens D, Postema JW, Arens A, Pfestroff A, Oyen WJG, Gotthardt M. The influence of SPECT reconstruction algorithms on image quality and diagnostic accuracy in phantom measurements and 99mTc-sestamibi parathyroid scintigraphy. Nucl Med Com 2014;35(1):64-72
12. WHO - Iodine status worldwide. WHO Global Database on Iodine Deficiency. de Benoist B, Andersson M, Egli I, Takkouche B, Allen H. 2004. https://apps.who.int/iris/bitstream/handle/10665/43010/9241592001.pdf;jsessionid=47150107A7320ABDF69F575AB8B834B7?sequence=1 (URL accessed April 20th 2020)

1

THE CONTRIBUTION OF HYBRID IMAGING TO RADIONUCLIDE THERAPY

by Paul Gape, Carla Abreu, Glenn Flux and Jan Taprogge

INTRODUCTION

The combination of functional imaging in nuclear medicine (SPECT, PET) with anatomical imaging in CT, in what is referred to as hybrid imaging, provides undoubted diagnostic value. Many of these benefits can also be appreciated in the application of hybrid imaging to radionuclide therapy. Recent developments in radiopharmaceutical production have increased the scope of radionuclide therapy, and implementation of a multidisciplinary approach in the clinic has facilitated improvements in therapeutic efficacy, patient comfort and radiation safety. These factors have contributed to efforts to move towards personalised treatment.

HOW DOES RADIONUCLIDE THERAPY WORK?

Radionuclide therapy involves the process of administering radioactive substances that mimic naturally occurring substances in the body to target disease. These radioactive substances are often delivered to the target (i.e. malignant or benign disease) via the blood circulation. In the case of malignant disease, the ionising radiation emitted by the radionuclide has the aim of killing cancer cells. This is primarily achieved via interaction between the radiation and the DNA, causing irreparable damage which ultimately means the cell is no longer able to reproduce itself [1].

Radionuclides used for therapy emit Auger electrons, beta particles or alpha particles and therefore differ from the radionuclides usually used for imaging. Various targeting agents can be bound to the same radionuclide, enabling a range of applications in the clinic. Examples of radiopharmaceuticals used for therapy, along with some of their properties which make them suitable candidates, are given in Table 1. Auger-electron emitters have shorter ranges in tissues of several nm [2].

The action of radiation on tissue is often characterised using the linear energy transfer (LET) which describes the amount of energy deposited into the tissue per unit length the particle travels through tissue. A higher LET is usually associated with more severe damage to tissue. Beta emitters have a lower LET when compared to Auger-electron or alpha emitters. Alpha particle emitters are associated with the highest LET [3].

Radiation damage to tissue is caused by indirect or direct damage to DNA [4]. Direct damage results from single or double strand breaks of the DNA caused by the radiation, whereas indirect damage is caused when the radiation interacts with the surrounding medium (primarily cellular fluid) to produce free radical ions. These free radicals are highly reactive and can in turn damage the DNA. Double strand breaks are considered more likely to lead to cell death as they are more difficult for the cell to repair. As such, alpha emitters, which have a higher LET than beta or Auger-electron emitters, cause more double strand breaks and thus have a greater cell killing effect.

RADIO-PHARMACEUTICAL	INDICATION	HALF-LIFE	THERAPEUTIC EMISSION	AVERAGE RANGE IN TISSUE (MM)
I-131 NaI	Benign thyroid disease Thyroid cancer	8.1 days	β^- (E_{max} = 0.61 MeV, E_{av} = 0.192 MeV)	0.4
I-131 MiBG	Neuroendocrine tumours			
Y-90 DOTA-	Neuroendocrine tumours	64 hours	β^- (E_{max} = 2.28 MeV, E_{av} = 0.934 MeV)	3.9
Y-90 microspheres	Non-resectable hepatoma Liver metastases			
Lu-177 DOTA-	Neuroendocrine tumours	162 hours	β^- (E_{max} = 0.498 MeV, E_{av} = 0.133 MeV)	0.23
Lu-177 PSMA	Metastatic castration-resistant prostate cancer			
Ra-223 Cl_2	Metastatic castration-resistant prostate cancer	11.43 days	α (E = 5–7.5 MeV)	0.04 – 0.05

Table 1: Common radiopharmaceuticals used clinically for therapy [22],[23], [24].

WHAT IS THE RATIONALE FOR COMBINING IMAGING AND THERAPY?

There is growing interest in the nuclear medicine community in what has come to be known as the 'theragnostic principle'. Underpinning this principle is the concept that diagnostic imaging can be used to inform, guide and evaluate therapeutic treatment [5]. In practice, this is achieved by using the same radiopharmaceutical, or two radiopharmaceuticals with very similar uptake, for both imaging and therapy [6].

The distribution of the radiopharmaceutical within the patient depends on the specific biokinetics of

the individual. In order to investigate this distribution, pre-therapy and post-therapy imaging is necessary.

In pre-therapy imaging, a tracer amount of either the therapy radiopharmaceutical or a diagnostic tracer with (ideally) identical uptake can be imaged quantitatively and used to inform the therapeutic administration. In post-therapy imaging, the therapeutic radiopharmaceutical or a diagnostic radionuclide attached to the therapeutic radiopharmaceutical is imaged and can be used for dosimetry. This allows the absorbed dose to target and non-target tissues to be calculated and compared to a prescribed dose.

HOW CAN WE IMAGE THE THERAPY?

The most applicable imaging method depends on the radionuclide. Radiopharmaceuticals used for therapy may emit characteristic secondary radiation in the form of gamma photons in addition to the emissions responsible for the majority of the cell killing effect. These secondary emissions penetrate the patient's body and can thus be detected with a scintillation camera or an external counter.

If a diagnostic radionuclide is attached to the therapeutic radiopharmaceutical, the primary photons emitted by the diagnostic companion show the uptake of the therapeutic radiopharmaceutical in tissue. An image of the patient can therefore be created in which the number of counts in each region of the image relates to the activity in that anatomical region.

The scope for theragnostic imaging has increased rapidly, and an imaging option is available for most therapies. The possibilities for imaging the radiopharmaceuticals listed in Table 1 are given in Table 2.

Planar images acquired using a conventional gamma camera can characterise the activity distribution. This enables the whole body to be included in the image within an acceptably short duration. However, as a 2D representation of a 3D activity distribution within the patient, planar imaging is not always the most appropriate method for imaging post therapy [7]. Tissues which overlie the imaging plane are not distinguishable, so that it is impossible to determine whether counts in a region of interest have arisen from tissues above or below the ROI. Attenuation correction can be applied when using simultaneous anterior/posterior imaging by application of the conjugate view method [8].

Tomographic imaging enables 3D visualisation of the activity distribution, thereby avoiding the problem of overlying tissues. However, for the counts in the image to accurately represent the activity in the tissue, corrections must be applied for photon attenuation, scatter as the emissions interact with the patient and the imaging equipment, and several other effects which degrade image quality and affect quantification. Conventionally, a CT scan is used to create a voxel attenuation map to indicate the degree of attenuation from the various tissues within the body. The attenuation map is necessary for several of the corrections required in hybrid imaging.

RADIO-PHARMACEUTICAL	OPTIONS FOR PRE-THERAPY IMAGING	OPTIONS FOR POST-THERAPY IMAGING
I-131 NaI	I-131 NaI I-124 NaI I-123 NaI	Gamma-camera imaging of I-131 364 keV γ emission
I-131 MiBG	I-131 MiBG I-124 MiBG I-123 MiBG	
Y-90 DOTA-	Ga-68 DOTA- [26] Y-86 DOTA- In-111 DOTATATE	SPECT/CT of Y-90 Bremsstrahlung Gamma-camera imaging of In-111 173 and 247 keV γ emissions (administered simultaneously)
Y-90 microspheres	Tc-99m MAA	SPECT/CT of Y-90 Bremsstrahlung Y-90 PET [27]
Lu-177 DOTA-	Radio-labelled somatostatin analogues, e.g. Ga-68, In-111	Gamma-camera imaging of Lu-177 113 and 208 keV γ emissions
Lu-177 PSMA	Lu-177 PSMA [28] Ga-68 PSMA	
Ra-223 Cl_2	Tc-99m MDP F-18 fluoride [29]	Gamma-camera imaging of Ra-223 82, 154 and 270 keV γ emissions [30]

Table 2: Pre- and post-therapy imaging options for commonly used radionuclides [25].

QUANTITATIVE UPTAKE MEASUREMENTS

Quantitative pre-therapy imaging at a single time point may be used to inform a subsequent therapy. An example of this is the acquisition of a pre-therapy radioiodine uptake scan to personalise radioiodine treatment of benign thyroid disease [9]. Marinelli et al [10] developed a formula to deliver a prescribed absorbed dose to the thyroid, which is routinely used in many centres around the world to calculate the activity to be administered, as:

$$A_A = C \cdot \frac{D \cdot m_T}{U_{24h} \cdot T_{eff}} \qquad [1]$$

Where C is a unit conversion factor, A_A is the activity to be administered (MBq), D is the prescribed radiation dose to the thyroid (Gy), m_T is the mass of the thyroid (g), U_{24h} is the percentage uptake of radioiodine in the thyroid at 24 hours (%), and T_{eff} is the effective half-life of radioiodine in the thyroid (days) (accounting for both physical decay and biological clearance).

If only a single scan is acquired, the same effective half-life in the thyroid is assumed for all patients. Such assumptions can produce clinically useful information, but the associated large inaccuracies should be considered when applying them to individual patients.

EXTENDING QUANTITATIVE IMAGING TO DOSIMETRY

Whilst a single quantitative image is a useful indicator of the distribution of the radionuclide, dosimetry is required to determine the absorbed dose delivered to tumours and to normal organs.

Absorbed dose is defined as the energy deposited in a tissue, divided by the mass of the tissue. Calculation of patient-specific absorbed doses is essential, with the assumption that treatment outcome is dependent on the absorbed doses delivered to target volumes and to healthy organs [11]. Treatment optimisation and personalisation may be achieved using pre-treatment dosimetry or by adapting the treatment based on dosimetry during treatment. Post-treatment dosimetry may be used to verify the dose delivered and to inform the associated risk, as required under recent EU legislation [12].

Dosimetry – Key Points

- The energy absorbed from ionising radiation per unit mass of material is called the absorbed dose
- Dosimetry = estimating the absorbed dose to normal organs and tumours.
- The dose calculation requires knowledge of the cumulated activity, $\tilde{A}$, and the S-factor, S. Quantitative imaging at multiple time points allows these to be calculated.
- Pre-treatment dosimetry allows the therapy to be planned based on a pre-therapy estimation of absorbed dose, to maximise effect of treatment or ensure safety.
- Post-treatment dosimetry is used to confirm doses to tumours and assess doses to organs at risk.

Figure 1: Key points to understand in dosimetry.

WHAT DO WE NEED FOR DOSIMETRY?

The MIRD scheme [13] provides a framework for calculating the radiation dose from a source volume to a specific target volume. The source and target volumes can be at the organ, sub-organ or voxel scale. The calculation requires accurate knowledge of:

1. The 'cumulated activity' within the source, which represents the total number of radioactive decay events over the course of the therapy.
2. The 'S-factor', which represents the mean dose to the target volume per unit activity in the source volume. This is dependent on the energy of the radionuclide emissions, the 'absorbed fraction', which is the fraction of energy emitted in the source volume and subsequently absorbed in the target region, and the mass of the target volume. The absorbed fraction depends on the size, shape and separation of the source and target volumes.

The product of these two quantities gives the absorbed dose to the target region from the source region in units of Joules per kg. Mathematically, this is described by the basic MIRD equation:

$$D(r_T \leftarrow r_S) = \tilde{A}(r_S) \times S(r_T \leftarrow r_S) \qquad [2]$$

Where D = Absorbed Dose, $\tilde{A}$ = Cumulated Activity, S = S-factor and $r_{S,T}$ = source and target region, respectively.

The total dose to the target region is the sum from each of the separate source regions. Figure 2 shows one method of combining the various elements required to determine the cumulated activity and the S-factor, and is discussed below.

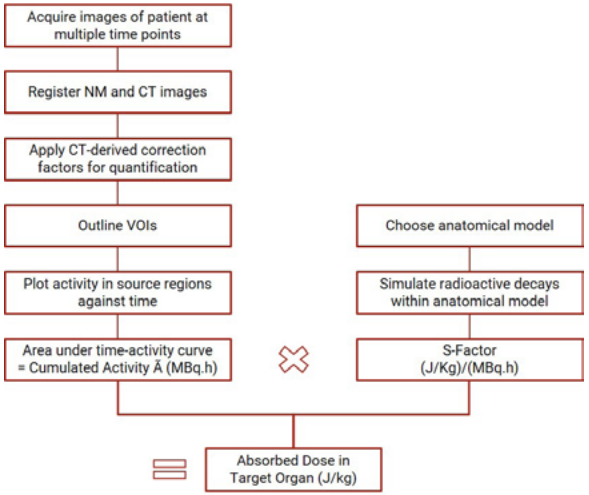

Figure 2: Schematic representation of the various steps in the dosimetry chain allowing cumulated activity and S-factor to be calculated.

Steps to determine cumulated activity using hybrid imaging:

Hybrid imaging at multiple time points

Nuclear medicine (NM) images, e.g. SPECT or PET, are acquired at several time points following administration of the radionuclide, as well as a CT scan to provide anatomical information. These images give a snapshot of the distribution of the radionuclide within the patient at the time of image acquisition. Extending NM imaging to hybrid imaging by incorporating the CT improves visualisation and the accuracy with which the images can be quantified. The accuracy with which the biokinetics within the patient are known is dependent on the number of images acquired.

Image registration

The NM data is registered to the CT data. Image registration refers to the process by which two images are aligned such that the corresponding pixel in each image represents the same anatomy, thereby allowing the anatomical information from CT and the functional information from NM to be viewed simultaneously.

Correction factors for quantification

To convert from counts per second to units of activity (MBq) in the image, several corrections are required.

An attenuation correction is applied to account for the fact that some of the photons originating within the patient will be attenuated before reaching the detector, resulting in fewer counts than would have been obtained if the activity were in air. A CT scan can be used to produce a map of tissue density within the patient. This makes it possible to estimate the specific amount of attenuation for radiation arising at any point within the patient. Attenuation correction implies correcting for this loss of signal due to tissue attenuation.

A scatter correction may also be applied to correct for photons that have changed energy and trajectory due to interactions within the patient, but which are still detected by the scanner. If unaccounted for, these photons will be misplaced in the reconstructed image. There are several methods to correct for scatter. Traditionally, this is achieved with the Triple Energy Window (TEW) method [14], but modern systems may model the expected contribution from scatter based on an attenuation map from CT and by including this estimate in the reconstruction process.

The partial volume effect causes the activity of objects that are of the order of the spatial resolution of the imaging system or smaller to be underestimated [15]. A correction may be applied to account for this.

It may also be necessary to apply a dead time correction if imaging of high activities is required.

PET imaging specifically requires a correction for random coincidences. There is no analogous correction for this in SPECT.

Outlining volumes of interest (VOIs)

Source and target volumes must be delineated on CT, which gives an 'anatomical' volume, or on the NM image, guided by the CT. Outlining requires good knowledge of the relevant anatomy and a multi-professional approach to ensure that inter-operator variability in volumes is kept to a minimum.

If the scans at different time points are registered, it is possible to copy the regions from one image to another. However, the user should take care to adjust the VOIs to account for misalignment, patient motion, or any other effect.

Time – activity curve

Once the necessary corrections have been applied, activity in the source organ can be plotted against time. These points together produce the time–activity curve. The amount of activity in the regions over time depends on both the radioactive decay and the biological clearance of the radiopharmaceutical. Therefore if enough time points are collected, this curve describes the pharmacokinetics of the radiopharmaceutical within an individual patient.

Area under TAC

The activity measured in the image represents the activity in the source region at a single time point. The total number of decays in the source organ over the entire duration of the treatment, which is the quantity we require to calculate absorbed dose, is obtained from the area under the TAC, as shown in Figure 3. This is the cumulated activity, or time-integrated activity. This is calculated by fitting a curve representing the activity as a function of time to the observed data points in the TAC, then calculating the integral of this function from $t = 0$ to $t = \infty$.

Since biological clearance in many processes has been shown to be approximated by exponential patterns, it is common to fit combinations of exponential functions to the observed data [7].

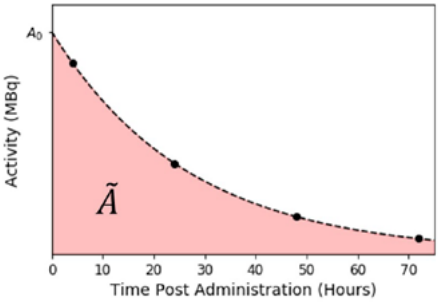

Figure 3: Sample time-activity curve showing activity in source region at a series of 4 time points. An exponential function is fitted to the data to estimate A(t) at all time points, and the area under this curve = cumulated activity.

STEPS TO DETERMINE THE S-FACTOR:

Anatomical model

The gold standard method for S-factor determination is to use a simulation to estimate the energy deposited in the target organ by emissions originating within the source organs, based on the size, shape and separation of the specific patient's organs. However, this is computationally intensive and generally not practical for clinical dosimetry [16]. Therefore, S-factors for nuclear medicine are generally pre-calculated based on a 'mathematical phantom'. This is a reference patient, with organ mass and geometry based on population reference data [17]. However, for research studies the gold standard method may be preferred, in which case a CT of the patient is required to create the anatomical model on which to base the simulation.

Simulation of radioactive decays

Once the anatomical model has been defined, the effect of the radiation can be simulated based on the mathematics describing the interaction of the radiation with the tissues within the patient. The result gives the S-factor, which has units of absorbed dose per MBq of activity. This value is the total energy deposited in the target region from the source region for 1 MBq of activity, divided by the mass of the target region.

However, as discussed above, pre-calculated S-factors will be based on a reference anatomical model. The mass of the target organs for the specific patient can be determined from CT, allowing the pre-calculated S-factors to be scaled to the patient-specific tissue weight.

Once the cumulated activity and the S-factor have been determined, absorbed doses are calculated simply by applying Equation.

PRE- OR POST-TREATMENT DOSIMETRY USING IMAGING

Pre-therapy dosimetry describes the process by which the activity to be administered in the therapy is planned based on a pre-therapy estimation of the absorbed doses to either lesions, to maximise the therapeutic effect, or to healthy organs, to ensure safety limits are not exceeded. Furthermore, pre-treatment dosimetry may be used to decide if a patient is suitable for radionuclide therapy based on the estimated absorbed doses delivered to lesions. Pre-treatment dosimetry requires a good estimate of the mass of the target, and it must be assumed that the distribution during the pre-treatment scan is comparable to the therapy administration, where higher activities and sometimes other radionuclides and tracers are used.

The only therapy for which pre-therapy dosimetry is routinely performed in some countries is still I-131 NaI for benign thyroid diseases. The EANM Dosimetry Committee has published standard operational procedures for pre-therapy dosimetry of benign thyroid diseases [9]. The process often involves a tracer amount of I-131 NaI and single or multiple uptake measurements to assess the biological retention of I-131 NaI in the thyroid. Based on the estimated absorbed dose to the thyroid gland from the tracer amount, the therapeutic activity required to deliver the prescribed radiation dose to the thyroid gland can be estimated. Another example of pre-treatment dosimetry is the SELIMETRY clinical trial, a UK based multi-centre study to investigate the potential of the MEK inhibitor Selumetinib to allow further treatments with radioiodine in advanced radioiodine refractory thyroid cancer patients, when radioiodine is no longer taken up by lesions [18], [19]. Patients in this study are given 4 weeks of Selumetinib before I-123 NaI SPECT/CT imaging is used to assess lesion uptake of radioiodine. Sequential hybrid images at 4, 24, 48 and 72 hours are used to estimate lesion absorbed doses for the subsequent treatment with I-131 NaI. The CT component of the imaging is used throughout in order to apply corrections, for visualisation and to aid outlining of volumes of interest. Pre-treatment I-123 NaI dosimetry is validated in the clinical trial against post-therapy I-131 NaI dosimetry.

A different approach is inter-cycle or post-therapy dosimetry. In many cases radionuclide therapy involves multiple therapy cycles with intervals of several weeks between the cycles. Dosimetry after the first or after each cycle can be used to estimate normal tissue absorbed doses. Subsequent cycles of the treatment can then be planned to ensure healthy organs are not irradiated over a certain threshold limit. Post-therapy dosimetry can be used to confirm lesion absorbed doses and assess doses received by organs at risk.

An example is I-131 MIBG for the treatment of neuroblastoma. The treatment is performed using two administrations given two weeks apart, whereby the activity administered for the second cycle is adjusted based on the whole-body absorbed dose measured during the first administration [20]. A further example of inter-cycle dosimetry is ILUMINET, a multi-centre clinical trial in Lund, Sweden involving Lu-177 Dotatate for neuroendocrine tumours (EudraCT No. 2011-000240-16) [21]. Dosimetry is performed after each cycle to determine the absorbed dose to the kidneys, the major organ at risk. The subsequent treatment cycle is only performed if a pre-defined limit for renal toxicity has not been reached.

CONCLUSION

Increasingly, the theragnostic principle and dosimetry are being applied to radionuclide therapy treatments. The additional information provided by hybrid imaging can significantly impact the patient pathway and should be utilised as much as possible. To achieve this will require a coordinated effort from technologists, physicists and clinicians working towards a shared objective, with common techniques and standard operating procedures between centres. This should provide the basis for personalised treatments, resulting in improved outcomes for patients.

Hybrid Imaging for Radionuclide Therapy – Key Aspects:

- Theragnostics: using imaging to inform, guide and evaluate the therapy.
- Dosimetry: estimating absorbed dose to normal organs and tumours.
- Hybrid imaging offers multiple advantages through combining anatomical and functional information in the image, enabling correction factors to be applied in order improve image quality and allowing for quantitative imaging.
- As we move towards personalised treatments, imaging data will prove increasingly important, requiring a fully integrated and a multidisciplinary approach.

Figure 4: Summary points for the chapter.

REFERENCES

1. Pouget, J.-P., et al., ***Introduction to Radiobiology of Targeted Radionuclide Therapy.*** Frontiers in Medicine, 2015. 2(12).
2. O'Donoghue, J.A. and T.E. Wheldon, ***Targeted radiotherapy using Auger electron emitters.*** Physics in medicine and biology, 1996. 41(10): p. 1973-1992.
3. Sgouros, G., et al., ***MIRD Pamphlet No. 22 (abridged): radiobiology and dosimetry of alpha-particle emitters for targeted radionuclide therapy.*** Journal of nuclear medicine : official publication, Society of Nuclear Medicine, 2010. 51(2): p. 311-328.
4. Hubenak, J.R., et al., ***Mechanisms of injury to normal tissue after radiotherapy: a review.*** Plastic and reconstructive surgery, 2014. 133(1): p. 49e-56e.
5. Pene, F., et al., ***Toward theragnostics.*** Critical Care Medicine, 2009. 37(1): p. S50-S58.
6. Yordanova, A., et al., ***Theranostics in nuclear medicine practice.*** OncoTargets and therapy, 2017. 10: p. 4821-4828.
7. Ljungberg, M. and K.S. Gleisner, ***Hybrid Imaging for Patient-Specific Dosimetry in Radionuclide Therapy.*** Diagnostics (Basel, Switzerland), 2015. 5(3): p. 296-317.
8. Minarik, D., K. Sjögreen, and M. Ljungberg, ***A new method to obtain transmission images for planar whole-body activity quantification.*** Cancer biotherapy & radiopharmaceuticals, 2005. 20(1): p. 72-76.
9. Hänscheid, H., et al., ***EANM Dosimetry Committee series on standard operational procedures for pre-therapeutic dosimetry II. Dosimetry prior to radioiodine therapy of benign thyroid diseases.*** European journal of nuclear medicine and molecular imaging, 2013. 40(7): p. 1126-1134.
10. Marinelli, L.D., ***Dosage determination in the use of radioactive isotopes.*** The Journal of clinical investigation, 1949. 28(6 Pt 1): p. 1271-1280.
11. Strigari, L., et al., ***The evidence base for the use of internal dosimetry in the clinical practice of molecular radiotherapy.*** European Journal of Nuclear Medicine and Molecular Imaging, 2014. 41(10): p. 1976-1988.
12. ***European Council Directive 2013/59/Euratom on basic safety standards for protection against the dangers arising from exposure to ionising radiation and repealing Directives 89/618/Euratom, 90/641/Euratom, 96/29/Euratom, 97/43/Euratom and 2003/122/Euratom. .*** OJ of the EU, 2014. L13(57): p. 1 - 73.
13. Bolch, W.E., et al., ***MIRD pamphlet No. 21: a generalized schema for radiopharmaceutical dosimetry--standardization of nomenclature.*** Journal of nuclear medicine : official publication, Society of Nuclear Medicine, 2009. 50(3): p. 477-484.
14. Ogawa, K., ***Simulation study of triple-energy-window scatter correction in combined Tl-201, Tc-99m SPECT.*** Annals of Nuclear Medicine, 1994. 8(4): p. 277-281.
15. He, B., et al., ***Evaluation of quantitative imaging methods for organ activity and residence time estimation using a population of phantoms having realistic variations in anatomy and uptake.*** Medical physics, 2009. 36(2): p. 612-619.
16. Huizing, D.M.V., et al., ***Dosimetry methods and clinical applications in peptide receptor radionuclide therapy for neuroendocrine tumours: a literature review.*** EJNMMI research, 2018. 8(1): p. 89-89.
17. Stabin, M.G., R.B. Sparks, and E. Crowe, ***OLINDA/EXM: The Second-Generation Personal Computer Software for Internal Dose Assessment in Nuclear Medicine.*** Journal of Nuclear Medicine, 2005. 46(6): p. 1023-1027.
18. Wadsley, J., et al., ***SELIMETRY-a multicentre I-131 dosimetry trial: a clinical perspective.*** The British journal of radiology, 2017. 90(1073): p. 20160637-20160637.
19. Gregory, R.A., et al., ***Standardised quantitative radioiodine SPECT/CT Imaging for multicentre dosimetry trials in molecular radiotherapy.*** Physics in medicine and biology, 2019. 64(24): p. 245013-245013.
20. Buckley, S.E., et al., ***Whole-body dosimetry for individualized treatment planning of 131I-MIBG radionuclide therapy for neuroblastoma.*** Journal of nuclear medicine : official publication, Society of Nuclear Medicine, 2009. 50(9): p. 1518-1524.
21. Sundlov, A., et al., ***Individualised (177) Lu-DOTATATE treatment of neuroendocrine tumours based on kidney dosimetry.*** Eur J Nucl Med Mol Imaging, 2017. 44(9): p. 1480-1489.
22. Stokkel, M.P.M., et al., ***EANM procedure***

guidelines for therapy of benign thyroid disease. European journal of nuclear medicine and molecular imaging, 2010. 37(11): p. 2218-2228.

23. Zaknun, J.J., et al., ***The joint IAEA, EANM, and SNMMI practical guidance on peptide receptor radionuclide therapy (PRRNT) in neuroendocrine tumours.*** European Journal of Nuclear Medicine and Molecular Imaging, 2013. 40(5): p. 800-816.

24. Poeppel, T.D., et al., ***EANM guideline for radionuclide therapy with radium-223 of metastatic castration-resistant prostate cancer.*** European Journal of Nuclear Medicine and Molecular Imaging, 2018. 45(5): p. 824-845.

25. Stokke, C., et al., ***Dosimetry-based treatment planning for molecular radiotherapy: a summary of the 2017 report from the Internal Dosimetry Task Force.*** EJNMMI physics, 2017. 4(1): p. 27-27.

26. Baum, R.P. and H.R. Kulkarni, ***THERANOSTICS: From Molecular Imaging Using Ga-68 Labeled Tracers and PET/CT to Personalized Radionuclide Therapy - The Bad Berka Experience.*** Theranostics, 2012. 2(5): p. 437-447.

27. Kao, Y.-H., et al., ***Post-radioembolization yttrium-90 PET/CT - part 1: diagnostic reporting.*** EJNMMI research, 2013. 3(1): p. 56-56.

28. Kabasakal, L., et al., ***Pre-therapeutic dosimetry of normal organs and tissues of (177)Lu-PSMA-617 prostate-specific membrane antigen (PSMA) inhibitor in patients with castration-resistant prostate cancer.*** European journal of nuclear medicine and molecular imaging, 2015. 42(13): p. 1976-1983.

29. Murray, I., et al., ***The potential of 223Ra and 18F-fluoride imaging to predict bone lesion response to treatment with 223Ra-dichloride in castration-resistant prostate cancer.*** European Journal of Nuclear Medicine and Molecular Imaging, 2017. 44(11): p. 1832-1844.

30. Hindorf, C., et al., ***Quantitative imaging of 223Ra-chloride (Alpharadin) for targeted alpha-emitting radionuclide therapy of bone metastases.*** Nuclear Medicine Communications, 2012. 33(7): p. 726-732.

DOI: https://doi.org/10.52717/ETGD4467

Publisher:
European Association of Nuclear Medicine Schmalzhofgasse 26, 1060 Vienna, Austria
Phone: +43 1 890 44 27 | +43 1 890 44 27-9
Email: office@eanm.org | URL: www.eanm.org

Main-Editor:
Marius Mada

Co-Editors:
MarieClaire Attard
Agata Pietrzak

English Language Editing:
Angela Parker

Project Management:
Banin Hosseini, EANM Executive Office

Layout & Design
Olga Dogadina, EANM Executive Office

FIND MORE EANM TECHNOLOGIST'S GUIDES HERE
http://www.eanm.org/publications/technologists-guide/